

University of Southampton Research Repository

Copyright © and Moral Rights for this thesis and, where applicable, any accompanying data are retained by the author and/or other copyright owners. A copy can be downloaded for personal non-commercial research or study, without prior permission or charge. This thesis and the accompanying data cannot be reproduced or quoted extensively from without first obtaining permission in writing from the copyright holder/s. The content of the thesis and accompanying research data (where applicable) must not be changed in any way or sold commercially in any format or medium without the formal permission of the copyright holder/s.

When referring to this thesis and any accompanying data, full bibliographic details must be given, e.g.

Thesis: Author (Year of Submission) "Full thesis title", University of Southampton, name of the University Faculty or School or Department, PhD Thesis, pagination.

Data: Author (Year) Title. URI [dataset]











Faculty of Earth and Life Sciences

School of Ocean and Earth Science

Mixed sand and gravel beach morphodynamics:

observations and modelling across the nearshore

by

Dominique Townsend MSc

ORCID ID <u>0000-0002-0502-6061</u>

Thesis for the degree of Doctor of Philosophy

January 2025

University of Southampton

Abstract

Faculty of Earth and Life Sciences School of Ocean and Earth Science

Doctor of Philosophy

Mixed Sand and Gravel Beach Morphodynamics: Observations and Modelling Across the Nearshore

by

Dominique Townsend

The nearshore zones of mixed sediment beaches have received relatively little attention until now. This is surprising considering that mixed sediment beaches have a widespread global distribution, intrinsic ecological value and increasingly an important role in flood protection. This thesis set out to expand the existing body of knowledge on mixed sediment beaches by examining, both observations from and modelling of, a mixed composite beach study site located on the South East coast of the UK (Pevensey Bay, East Sussex). The overarching aim of the research was to build a conceptual model of a mixed sediment beach system with a focus on nearshore behaviour which had previously been neglected. Taking a holistic approach, three research questions were posed to achieve this: 1) What is the cross-shore extent of the geomorphologically active zone within a mixed sediment environment? 2) How does sediment move through and within a mixed sediment system contribute to short-term and long-term change? 3) How does cross-shore sediment exchange vary under a variety of hydrodynamic, morphodynamic and sedimentological conditions?

To answer these questions, novel techniques, namely the use of X-band radar and Autonomous Surface Vessels, were used to capture field data at both high frequency temporal and spatial resolution. The depth of closure was examined for a mixed sediment coast and a conceptual model was developed to assist with the interpretation of local variations in the geomorphological active zone. A series of transverse finger bars were found in the shallow nearshore, and their mobility was linked to wave driven processes. Modelling was carried out in the process-based XBeach-X which used Pevensey as a test bed for mixed sediment beach responses to storm conditions, under varying hydrodynamic, bed slope and sediment composition scenarios. Together, the results showed that the nearshore was a highly dynamic zone, and that long-term losses of sediment in the subaerial beach were also being seen below the waterline at a larger scale. It is thought that this ongoing loss is the result of both human intervention and natural processes. Whilst the gravel-rich upper beach and sandy foreshore seem distinct from each other, notably from the discovery of a null point of change between them, the volume of the nearshore ultimately controls the amount of wave power that reaches the shore. The study paves the way for future research, opening the floor for numerous questions, such as 'how resilient are these systems to climate change and ongoing human intervention?'

Tabl	e of Contents	3
Tabl	e of Tables	7
Tabl	e of Figures	8
Rese	earch Thesis: Declaration of Authorship	13
Ackr	owledgements	14
Cha	oter 1 Introduction	16
1.1	Overview and motivation	16
1.2	Research questions	19
1.3	Thesis outline	19
1.4	Study site	21
	1.4.1 Why Pevensey?	21
	1.4.2 Geological & sedimentary setting	22
Cha	oter 2 Exploring nearshore bed dynamics of a mixed beach u	sing the
	depth of closure conceptual model	26
2.1	Abstract	26
2.2	Introduction	26
	2.2.1 Study site	
2.3	Methods	
	2.3.1 Depth of closure – wave energy approach	3∠
	2.2.2. Donth of alacura, abcomusticatel approach	
	2.3.2 Depth of closure – observational approach	33
	2.3.2.1 Data collection	33
		33
	2.3.2.1 Data collection	33 33
	2.3.2.1 Data collection	33 33 35
	2.3.2.1 Data collection	33 35 36

		2.3.5.2 Nearsnore cross-sectional area	
2.4	Res	sults	.37
	2.4.1	Depth of closure – wave energy approach	. 37
	2.4.2	Depth of closure – observational approach	. 38
	2.4.3	Depth of closure – wave energy vs observational approach	42
	2.4.4	Nearshore transport estimation	44
	2.4.5	Sediment analysis	45
	2.4.6	Sediment balance	46
2.5	Disc	cussion	.47
2.6	6 Con	nclusions	.51
2.7	7 Dec	claration of Competing Interest	.52
2.8	B Ack	nowledgements	.52
Ol-	1 6		
Cna	ipter 3	3 Seasonal mobility of transverse finger bars within a mixed sa	ına
		gravel have processed value V hand Daday	E 2
		gravel bay measured using X-band Radar	.53
3.1	Abs	gravel bay measured using X-band Radarstract	
3.1 3.2			.53
	! Intr	stract	.53 .54
	2 Intr	oduction	.53 .54
3.2	2 Intr 3.2.1 3 Met	oduction	.53 .54 .57
3.2	3.2.1 3.3.1	oduction	. 53 . 54 .57 . 60
3.2	3.2.1 3.4 3.3.1 3.3.2	oduction Study site thods Bar characteristics measured using MBES	.53 .54 .57 .60
3.2	3.2.1 3.3.1 3.3.2 3.3.3	Stract oduction Study site thods Bar characteristics measured using MBES Sedimentology	.53 .54 .57 .60 .61
3.2	3.2.1 3.3.1 3.3.2 3.3.3	oduction Study site thods Bar characteristics measured using MBES Sedimentology Bar movement	.53 .54 .57 .60 .61
3.2	3.2.1 3.3.1 3.3.2 3.3.3 3	Study site thods Bar characteristics measured using MBES Sedimentology Bar movement 3.3.3.1 X-Band Radar & sea surface roughness	.53 .54 .57 .60 .60 .61 .61
3.2	3.2.1 3.2.1 3.3.1 3.3.2 3.3.3 3 3.3.4	Study site thods Bar characteristics measured using MBES Sedimentology Bar movement 3.3.3.1 X-Band Radar & sea surface roughness 3.3.3.2 Sea surface roughness to detect bedforms	.53 .54 .57 .60 .61 .61 .62
3.2	3.2.1 3.3.1 3.3.2 3.3.3 3 3.3.4 3.3.5	Study site	.53 .54 .57 .60 .61 .61 .61 .62 .65
3.3	3.2.1 3.2.1 3.3.1 3.3.2 3.3.3 3 3.3.4 3.3.5 Res	oduction Study site thods Bar characteristics measured using MBES Sedimentology Bar movement 3.3.3.1 X-Band Radar & sea surface roughness Hydrodynamic analysis Upper beach volumetric analysis	.53 .54 .57 .60 .61 .61 .62 .65

(3.4.3 Bar movement	70
;	3.4.4 Hydrodynamic analysis	71
;	3.4.5 Upper beach volumetric analysis	75
3.5	Discussion	76
3.6	Conclusions	81
3.7	Acknowledgements	81
Chap	oter 4 Morphology and sediment sorting of a mixed sediment beach	in
	response to storm conditions	83
4.1	Abstract	83
4.2	Introduction	84
4.3	Methods	87
4	4.3.1 Model description	87
	4.3.1.1 Overview	87
	4.3.1.2 Multiple sediment fraction modelling	89
4	4.3.2 Model set-up	90
	4.3.2.1 Model Grid	90
	4.3.2.2 Boundary conditions	91
	4.3.2.3 Model run configurations	91
4.4	Results	92
4	4.4.1 Hydrodynamics	92
4	4.4.2 Bed slope	98
4	4.4.3 Sediment composition	99
4	4.4.4 Bed level change overview1	00
4.5	Discussion 1	01
4.6	Conclusion1	03
4.7	Acknowledgements1	04
Chap	oter 5 Synthesis and Conclusion1	05
5.1	Synthesis 1	05

	5.1.1	Research Question I	.105
	5.1.2	Research Question II	.107
	5.1.3	Research Question III	.111
	5.1.4	From swash to the depth of closure; a conceptual model for a mixed	
		sediment beach	.114
5.2	Furt	ther research	. 117
5.3	Con	nclusion	. 119
Αрр	endix	A Paper 1; Supplementary information	120
5.4	Wav	ve transformation	. 120
5.5	Sed	liment transport	. 121
Арр	endix	B Paper 2; Supplementary information	125
Арр	endix	CPaper 3; Supplementary information	126
ic+	of Pot	ferences	129

Table of Tables

Table 2.1 – Suili	mary of extended profile survey dates and source. Note. N-NINDOMP 3DE3
	survey; M = NNRCMP/MCA MBES survey; Px = extended project surveys; P =
	project surveys34
Table 2.2 – Resu	ults from wave statistics and depth of closure
Table 2.3 – Mud	, sand, gravel ratios by weight taken from samples at the instrumented array.
Table 3.1 – Data	collected as part of the National Network of Coastal Monitoring Programmes of
	England NNRCMP used in the analysis of upper beach volumetric analysis.
Table 3.2 – Peve	ensey Bay bar characteristics measured from 2013 MBES data (Channel Coastal
	Observatory, 2013). *For those bars with a Chevron form, the length and angles
	are given for both the upper \mid lower sections of the bar, with the sum or average
	given in brackets69
Table 3.3 – Migra	ation rate vs average daily wave power71
Table 3.4 – Trans	sverse Finger Bar classifications in the context of the wider coastal setting, with
	distinction between transient and persistent intermediate energy finger bars
	(adapted from Pellón et al. (2014); and Levoy et al. (2013)).Classification of
	Pevensey Bay Transverse Finger bars shown in bold. N.B. Transverse Bars and
	Rips are excluded from this table80
Table 4.1 – Storr	m scenarios derived from the Pevensey Wave Buoy record (19-years data).91
Table 4.2 – The r	model runs showing each test bed (hydrodynamics, bed slope and sediment
	composition) and the respective test cases. The cases highlighted in bold are
	the default values for the other test cases, for example, when the 1 in 100 storm
	conditions are tested, a 6.3 tidal range is used, the natural profile, and 30:70
	sand to gravel ratio92
Table 5.1 – Upda	ate to 'Mud, sand, gravel ratios by weight taken from samples at the
	instrumented array' as presented in Paper 1, Table 2.2, following additional
	samples being processed110

Figure 1.1 – Tools	s used to understand coastal sediment processes (lefthand graph adap	ted from
I	Nicholls et al. (2013))	18
Figure 1.2 – Thes	is outline with chapter signposts	20
Figure 1.3 – Study	y site extent and regional location. Figure contains OS data © Crown Co	pyright
;	and database rights 2023. Contains data from OS Zoomstack	21
Figure 1.4 – Wide	er geological setting of Pevensey Bay, showing various chalk, sand, mud	and
:	siltstones of various ages, with elevation of the wider area inset. Geolog	ical
•	data, 625K Bedrock, provided by ©British Geological Survey. Elevation o	lata,
•	Ordnance Survey Terrain 50 open height dataset, © Crown copyright and	d
(database right 2023	22
Figure 1.5 – A) A r	reconstruction drawing showing the Norman fleet of 700 ships landing a	it
1	Pevensey Bay on the morning of 28 September 1066 © Historic England	,
i	illustration by Peter Urmston; B) Pagham Harbour, representing a simila	ır gravel
I	barrier system to that which may have existed at Pevensey Bay in the pa	st.
		23
Figure 1.6 – Beac	ch works carried out by PCDL at Pevensey Bay to maintain beach width a	and
•	volume, including A) recharge (approx. 20,000 cubic m pa); B) bypassing	g of
1	material from Langley Point into Pevensey Bay (approx. 8,000 cubic m p	a); and
•	C) beach recycling (approx. 90,000 cubic m pa)	24
Figure 1.7 – Partio	cle grain size diameter for six samples taken across the beach face in	
1	Beachlands at coastal monitoring beach profile 4c01702 on the 11/09/2	2023.
		25
Figure 2.1 – The p	physical parameters influencing the depth of closure; waves and curren	ts, bed
:	slope, and sediment composition are shown in relation to the influence	s on
•	depth of closure, namely, 'Energy required to mobilise sediment' (yellow	v),
•	'Energy available to mobilise sediment' (blue), and 'Bed slope' (orange)	.28
Figure 2.2 – Peve	nsey Bay study site; green and grey areas showing rural and urban land	use,
1	respectively. Yellow area representing upper beach. Black profile lines s	show
1	the position of bathymetric surveys with names corresponding to the Na	ational
1	Network of Regional Coastal Monitoring Programme (NNRCMP) beach բ	orofiles.
-	The wave rose shows binned data from the Pevensey Wave buoy (position	on

shown by red marker) for the period June 2003 – November 2022. Bathymetric
data composite of 2012 Centre for Environmental Fisheries and Aquaculture
Science (CEFAS), 2013 Channel Coastal Observatory (CCO) data (1 km inshore
and 2015 Maritime and Coastguard Agency (MCA). Inset map showing the
south east of England and the regional setting of Pevensey Bay. Grid projection:
UTM 31 N31

- Figure 2.3 Mean profile and surveyed cross section of Central profile 4c01702 (A) and elevation variation between surveys, 04/09/2003 to 25/01/2022 (B to L). Sections with no data shown in grey, where topographic and bathymetric surveys did not overlap fully. The duration between the two surveys is indicated in parentheses. Time periods approaching 6 months and greater highlighted in bold.......39

rigule 2.0 – Lst	infaced tong and cross-shore sediment transport approximated on the beach
	face at the Westernmost (4c01729), Central (4c01702) and Easternmost
	(4c01677) profiles. Cross-shore transport is estimated using Bailard and
	Inman, (1981) whilst longshore transport is estimated using Damsgaard and
	Soulsby (1996) and Soulsby, (1997) for the coarse (medium pebble, 12 mm) and
	fine (fine sand, 161.5 µm) fractions, respectively
Figure 2.7 – NN	RCMP beach profile locations showing A) Shoreline orientation relative to
	degrees north (°N) where a beach facing South would be 90°N, whilst a beach
	facing North would be 270°N; B) Change in lateral position of MHWN and
	MLWN relative to their position in 2003, with outliers shown as white dots; and
	C) the cross sectional area for the 18 surveyed profiles displayed with error
	bars showing the upper error estimate of ±0.3 m multiplied by the length of the
	profile to give areal error47
Figure 3.1 – Tra	nsverse finger bar locations in relation to the Crumbles and Dungeness cuspate
	foreland formations with regional setting inset. Star shows location of the
	Datawell MkIII directional wave buoy within Pevensey Bay, which is part of the
	NNRCMP network (channelcoast.org). The data from this wave buoy between
	June 2003 and November 2022 is shown binned as a wave rose. Figure contains
	Ordnance Survey Terrain 50 open height dataset © Crown copyright and
	database right 2023. Surficial sediment deposits © British Geological Survey
	202459
Figure 3.2 – A) 2	256 raw radar images (representing about 5 minutes real time); B) long exposure
	image (an average of the 256 images); C) image where each pixel has had the
	square root then spatial derivative taken; D) images are binned into 12 M2 tidal
	phase bins; E) the tidal signal is removed by fitting an M2 sine wave to average
	pixel values per bin (per week) and then subtracting that value; F) the resultant
	sea surface roughness image with extent of; G) Zoom-in of F64
Figure 3.3 – A) E	Bathymetry of 14 transverse finger bars showing gravel outcrops to the east,
	smoothed 1 m contours, with orthorectified aerial photography (both collected
	as part of the NNCMP). Note the presence of two surface water outfalls just
	north of the 13th bar; B) Cross section through the bathymetry data showing
	local elevation of bars68

Figure 3.4 – Sea	surface roughness gradient along a transect approximately 250 m parallel to the
	shoreline indicating the location of the bars and their movement over time.
	70
Figure 3.5 – The	migration distances are shown within the observation period both cumulatively
	(A) and weekly (B) with average values shown by the black marker; followed by
	cumulative and weekly distance plots for each individual bar, (C) & (D)
	respectively. The bottom two plots show the wave power (E) and peak wave
	direction (F) as recorded by the Pevensey wave buoy73
Figure 3.6 – Dist	tribution of wave height (Hs, top left), peak period (Tp, top right), wave direction
	(bottom left) and incoming wave spread (bottom right), over the three study
	periods Winter 2020/2021, Summer 2021, and Winter 2021/202274
Figure 3.7 – Line	ear regression of the weekly mean littoral drift potential (m3/s) and the weekly
	median bar migration (m)75
Figure 3.8 – Yea	r on year contour plot for beach volumetric change across Pevensey Bay 2003- 2022
Figure 4.1 Eve	male of had layer underling in recognize to eregion for two fractions (F1 and F2)
rigule 4. i – Exa	mple of bed layer updating in response to erosion for two fractions (F1 and F2).
	Following 0.02m of erosion from the top layer, the variable layer decreases in
	depth by 0.02m to replace the material lost. The 'feeding' of material from the
	variable layer to the top layer results in an adjusted sediment bed composition (adapted from Rijper, 2019)90
Figure 4.2 – Abs	olute bed elevation change for the hydrodynamic runs alongside the beach
	profile bed elevation. Note the beach toe (which is defined as the change in
	slope between the upper steeper and the lower flatter part of the beach) is
	located at 3 680 m chainage93
Figure 4.3 – Bed	morphology (left) and sediment composition (right) responses to varying
	hydrodynamic forces, namely A) Storminess; B) Increasing period; C)
	Increasing water levels; and D) Spring/Neap/No tides. Mean sea level shown in
	dark blue horizontal line, high mean spring tide, and mean low and high neap
	tide levels shown in light blue96
Figure 4.4 – Cha	ange in bed elevation (A, B) and sediment composition (C, D) over time for a 1 in
	1 storm under spring tide (A, C) and neap tide (B, D) conditions. The dashed red
	line shows the position of the beach toe at the start of the simulation for

	reference, and the black dashed line shows the still water level (ignoring wave
	run-up). Note the offshore boundary is to the left97
Figure 4.5 – Bea	ch profile response to the 1 in 1 storm for the natural beach profile, 1 in 5 and 1
	in 12 graded slopes. N.B. the natural slope is offset by 25 metres for improved
	readability98
Figure 4.6 – Effe	cts of varying bimodality proportions of sand and gravel fractions at the end of
	the model run to A) bed level (mOD); B) bed level change (m); and C) cross-
	shore sorting (surface sediments percentage gravel) 100
Figure 4.7 – A) V	olumetric bed elevation change across the different model runs; B) relative
	percentage change on shore and offshore where the boundary used is the initial
	position of change in bed slope (beach toe). a chainage 3680 m 101
Figure 5.1 – Use	of radar in detecting depth of closure taking a probabilistic approach, showing
	A) a histogram of depth derived profiles, B) Depth saturation parameter.106
Figure 5.2 – Two	examples of rhythmic bedforms found in the study site; A) small scale gravel
	ridges found alongshore (wavelength ~5-10 m); B) larger scale surface
	undulations as shown in difference model between 2018 and 2019 NNRCMP
	data (wavelength ~200 to ~400 m). Data from NNRCMP freely available from
	www.channelcoast.org. Contains OS Data (c) Crown Copyright and database
	right 2023; contains data from OS Zoomstack
Figure 5.3 – Pho	tos taken at low tide before and after a storm event on the 1st of Nov 2022,
	highlighting the change in surficial sediment composition and reduction in
	beach levels. Wave data pictured taken from the Pevensey wave buoy, part of
	the NNRCMP (freely available from www.channelcoast.org)
Figure 5.4 – Find	ding the 'null point,' or Landward Minimum Morphological Change (LMMC) on a
	modelled mixed sediment composite beach (Paper 3)114
Figure 5.5 – Cor	nceptual model outlining key findings of PhD research116
Figure B.1 - Ima	ge showing the 50m polygons used in the analysis of the upper beach
	topographic datasets. 50 m polygons produced by Canterbury City Council as
	part of the project 'Eastbourne to Rye Regional Shingle Beach Management
	Plan' completed in 2015 on behalf of the Environment Agency. Map data ©
	OpenStreetMap contributors, Microsoft, Facebook, Inc. and its affiliates, Esri
	Community Maps contributors, Map layer by Esri

Research Thesis: Declaration of Authorship

Research Thesis: Declaration of Authorship

Print name: Dominique Townsend

Title of thesis: Mixed sand and gravel beach morphodynamics: observations and modelling across the

nearshore

I declare that this thesis and the work presented in it are my own and has been generated by me

as the result of my own original research.

I confirm that:

1. This work was done wholly or mainly while in candidature for a research degree at this

University;

2. Where any part of this thesis has previously been submitted for a degree or any other

qualification at this University or any other institution, this has been clearly stated;

3. Where I have consulted the published work of others, this is always clearly attributed;

4. Where I have quoted from the work of others, the source is always given. With the exception

of such quotations, this thesis is entirely my own work;

5. I have acknowledged all main sources of help;

6. Where the thesis is based on work done by myself jointly with others, I have made clear

exactly what was done by others and what I have contributed myself;

Parts of this work have been published as:-

Townsend, D., Leyland, J., Kassem, H., Thompson, C., and Townend, I.: Exploring nearshore bed

dynamics of a mixed beach using the depth of closure conceptual model, Geomorphology, 454,

109150, https://doi.org/10.1016/j.geomorph.2024.109150, 2024.

Signature	•••••	Date
oignature.		Date

Acknowledgements

First and foremost, my thanks go to my four PhD supervisors: Julian Leyland, Hachem Kassem, Charlie Thompson and Ian Townend. You have been unequivocally generous with your time, (possibly patience) and have helped me to develop into an independent researcher. I never quite got round to 'believing', but if I had, I would have found that you were right!

Secondly, I can't thank enough Ian Thomas and Amber Carr of Pevensey Coastal Defence Ltd; it was always a joy to come and work from the site office and talk about our shared interest in Pevensey Beach! I am indebted to you for the bottomless cups of tea, storm-wave chasing, as well as the support with surveys and sharing your knowledge of the coast. Further thanks go to Peter Aimes and Uwe Dornbusch of the Environment Agency for continued support throughout the project. Additionally, without the help of Duncan and James of the Pevensey Bay Sailing Club, it would not have been possible to carry out our PicoCAT surveying. Thankyou so much for your kindness.

Working with the team at Marlan Maritime Ltd (now CoastSense Ltd), in particular Cai Bird and Alex Sinclair, and Paul Bell of the National Oceanographic Centre, has been a lot of fun and I am very thankful for the time and effort that you have put into both producing the radar outputs and helping me understand them. To Dan Amos, Stuart McVey, Hannah Walker and Claire French of the South East Regional Coastal Monitoring Programmes, thankyou so much for all the time you have spent answering my questions and digging out archive data. Thanks to my former colleague Sean Palmer at Jacobs for providing numerous SANDS licences over the years. An additional thankyou must go to Connor McCarron, Ollie Foss, Kris Ions and Jenny Brown for the assistance with (beloved) XBeach. A last huge thankyou to Gregor Lützenburg and everyone I met in Copenhagen, my placement with you in 2022 was a pivotal time for me which I will never forget!

Finally, my wholehearted gratitude and thanks to my family and friends. To all the tea-makers, tail waggers, rib-ticklers, side splitters, glitterball fanatics, motivational texters, to the person that gave me that very last slice of the too small pizza, this is for you. Sofa sharers, sea-swimmers, internet fixers, ceiling painters, bin runners, fossil hunters, and simply the kindest neighbours, this is for you. This all was possible because of you. Thankyou.

Dedicated to my extraordinary grandmothers.

Acknowledgements

"A walk, not more than a mile
along the barricade of land
between the ocean and the grey lagoon.
Six of us, hand in hand,
connected by blood. Underfoot
a billion stones and pebbles new potatoes, mint imperials,
the eggs of birds each rock more infinitely formed
than anything we own."

Simon Armitage, The Stone Beach

Chapter 1 Introduction

1.1 Overview and motivation

Coasts matter. A transitional zone between land and sea, coasts are economically, socially and environmentally significant at a global scale. By the end of this decade 46 million people are predicted to be living on the immediate coast, less than 5 m above mean sea level and within 5 km of the shoreline (Kummu et al., 2016). Looking below 10 m above mean sea level, in 2015 populations were estimated at 700 million people, creating an approximate wealth of \$13 trillion each year (Kirezci et al., 2023). Coasts are important global resources supporting 1) food production; agriculture and fishing, 2) raw material extraction: aggregate, mineral and petrochemicals and 3) ecosystem services (Martínez et al., 2007). Tourism and recreation also make significant contributions to local economies (Lazarow, 2007; Williams and Shaw, 2009). Coasts are also shown to be some of the most biodiverse places on earth supporting a vast array of intertidal and subtidal habitats: mangroves, coral reefs, kelp forests, seagrass, estuaries, tidal flats, salt marshes, wetlands and coastal wooded habitat (Ray, 1991). Because of their position at the interface of land and sea, coasts are the recipients of the world's wave energy, with shallow zones attenuating and dissipating wave energy (Elgar et al., 1997). This makes them some of the most geomorphologically active regions on earth.

The majority of the world's beaches are thought to be comprised of mixed sediment (Holland and Elmore, 2008). That is to say, the material making up the beach consists of heterogeneous sediments, whereby any two of the size classes defined by Folk (1954), *i.e.* gravel, sand and mud, exceed a 9:1 ratio. Remarkably, despite their global prevalence, mixed sediment beaches are relatively understudied in comparison to sandy and gravel beaches, and their more complex morphodynamic behaviour is still not fully understood (Mason and Coates, 2001; Pontee, Pye and Blott, 2004; Atkinson, 2019; Dornbusch, 2021). Primarily, the sediment composition (*i.e.* the *ratio* of mud: sand: gravel) exerts significant control over the response of a beach to hydrodynamic forcing, and this is known to vary spatially (along, across and through the beach) as well as through time, for example the stripping or deposition of finer sediment from/to the beach face and the reworking of coarser sediment by waves (Mason and Coates, 2001; She, Horn and Canning, 2006; Elsner et al., 2015).

For coarse grained beaches sand content affects the hydraulic conductivity (permeability) of the beach altering infiltration/exfiltration (McCall *et al.*, 2014) as well as beach slope gradient (Woodruff *et al.*, 2021), which are both known to affect sediment entrainment. Furthermore, tracer studies of mixed sediment beaches have shown that sediment size and shape can affect

the transport pathways of individual grains (Ciavola and Castiglione, 2009; Hemmingsen, Eikaas and Marsden, 2019). For example, in Porto Recanati, Italy, Ciavola and Castiglione (2009) found the transport of sand and fine gravel was longshore dominated, whilst gravels and pebbles typically moved in a cross-shore direction. On the surface differently sized grains also influence each other's mobility. Larger grains sit more prominently, and smaller ones less protrusively, than they would amongst sediments of uniform size, which respectively raises or lowers the critical threshold of bed shear stress required to mobilise those sediments (Egiazaroff, 1965). This hide-exposure effect is responsible for reducing the critical shear stress by up to 75% for gravels and increasing it by up to 64% for sand in comparison to the critical shear stress of uniform sediments (McCarron et al., 2019).

Sediment mobilisation is also related to the cohesive sediment content; laboratory tests showed that gravel mixtures containing higher proportions of clay required greater bed shear stress for mobilisation (Singh and Ahmad, 2019). For mud sand mixtures, Mitchener and Torfs (1995) identified significant resistance to erosion after only small increases in mud content, with cohesive behaviour displayed after the mud content reached 3-15%. Small increases in the percentage of mud have also been shown to affect the behaviour of migrating bedforms, with increased migration rate and bedload transport approaching a certain 'mud threshold' and a decreased effect above this threshold (Fernandez *et al.*, 2022). In addition to clay content, Grabowski et al. (2011) recognized the importance of other sediment properties on the erodibility of cohesive sediments, including the packing density, water salinity and factors relating to biotic processes such as sediment disturbance, organic content and biofilm production. Natural cementation, and the formation of 'beach rock' can also reduce the erodibility of sediments (Zarkogiannis *et al.*, 2018).

The body of knowledge for mixed sediment beaches is largely built on sub-aerial field data, and rarely have studies in this area examined the full nearshore zone (Karunarathna *et al.*, 2012; Roberts, Wang and Puleo, 2013). Many definitions exist for the nearshore zone (USACE, 1998), throughout this thesis it is defined as the area between the very upper reach of the swash zone, down to the depth of closure, encompassing the geomorphologically active zone over short to medium timescales (days to decades). This zone is not only known to be highly important in terms of the transfer of sediment (Thieler *et al.*, 2001; Finkl, 2004; French *et al.*, 2016; Anthony and Aagaard, 2020) but also in dissipating and focusing incoming wave energy (Szczyrba *et al.*, 2023), which is linked to the behaviour of the upper beach (Backstrom *et al.*, 2015). Moreover, the behaviour of mixed sediment beaches is strongly affected by the sediment composition (Mason and Coates, 2001) yet the cross-shore and longshore exchange of these sediments within the nearshore has not been thoroughly investigated.

Understanding the nearshore sediment exchange is crucial in comprehending not only the short term, seasonal changes in the beach, but also in interpreting longer-term trends. As coastal development accelerates engineering intervention increases, with an aim to preserve one particular moment in a dynamic system's lifetime, interrupting longshore flows of sediment and constricting any landward transgression. Coastal steepening, whereby beach profiles transition to a steeper gradient (Soulsby, Sutherland and Brampton, 1999; Taylor, Murdock and Pontee, 2004; Burningham and French, 2017), is thought have many causes (Pontee, 2013) yet the impact of steepening is unified. Larger waves reach the shoreline with greater available energy to transport sediment (Sutherland and Wolf, 2002; Burcharth, Lykke Andersen and Lara, 2014). Exacerbated by sea level rise, both hard and soft management approaches will face increased maintenance costs as a result of these changes to the nearshore. As a significant proportion of the world's population lives on coasts, there is the need to understand these trends over a variety of timescales (Figure 1.1).

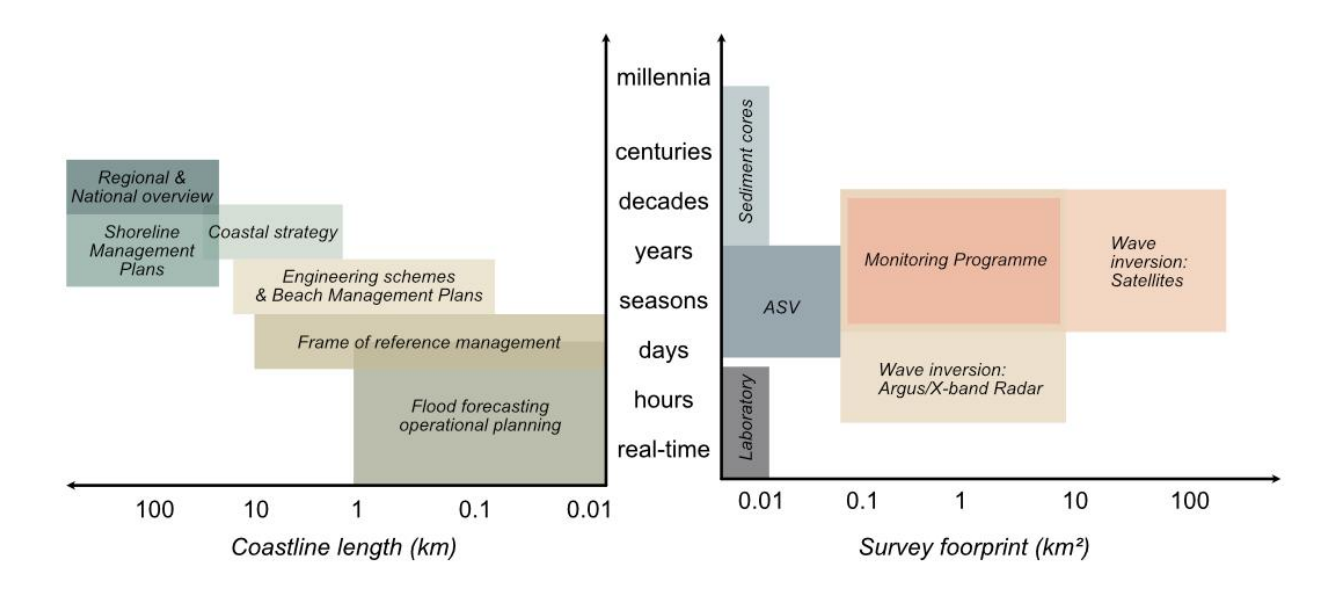


Figure 1.1 – Tools used to understand coastal sediment processes (lefthand graph adapted from Nicholls et al. (2013)).

In the United Kingdom, mixed sediment beaches make up around one third of the coastline and a significant proportion of those beaches are utilised as a primary element of defence against coastal flooding. For instance, along the South East coast alone over 180 km of shingle beaches are actively managed as flood assets (Polidoro, Dornbusch and Pullen, 2013). It is also recognised that the coastal communities that these defences protect are some of the most deprived in the UK; challenged with poorer health, poorer standards of education and poorer economic prospects (House of Lords, 2023). Limited economic buoyancy has resulted from declines in fishing, shipbuilding and tourism industries alongside inadequate transport connectivity (Barton et al., 2022). With ongoing pressure from extreme sea levels and increased risk of flooding and erosion from sea level rise throughout the 21st century (Vitousek et al.,

2017; Wahl *et al.*, 2017) we are running out of time to understand the fundamentals of these mixed sediment beaches, which are so important for those vulnerable communities that live alongside them.

This thesis seeks to address this challenge, investigating the current gap in knowledge surrounding the nearshore zone of mixed sediment beaches, using novel data collections over a range of temporal and spatial scales (Figure 1.1).

1.2 Research questions

The thesis has an overarching aim to develop a conceptual model for sediment exchange and morphological behaviour within the shallow nearshore of a mixed composite beach, which undergoes regular anthropogenic interventions in the upper beach; and is subject to changing hydrodynamics. This will build on the work of Costa *et al.* (2008) who created a conceptual model of the mixed composite beaches of Normandy, France, however lacked suitable information on the shoreface to understand the nearshore zone. This model will be based on real data across the geomorphologically active zone of the beach, using novel methods, at high frequencies and timescales which will provide useful information to those living on the coast and utilising the beach as a flood defence. Modelling will be used to expand the range of scenarios that are examined, using real data to provide a robust physical basis. The research questions (RQs) are designed to expand our knowledge of mixed sediment systems by exploring the shallow nearshore:

- RQ I What is the cross-shore extent of the geomorphologically active zone within a mixed sediment environment?
- RQ II How does sediment move through and within a mixed sediment system contribute to short-term and long-term change?
- RQ III How does cross-shore sediment exchange vary under a variety of hydrodynamic, morphodynamic and sedimentological conditions?

1.3 Thesis outline

The thesis structure is illustrated in Figure 1.2. Data collection informs analysis undertaken to inform the conceptual model and address the three research questions. Each research question broadly maps to one of the three research papers, which each complement each other to form a coherent understanding of the nearshore zone of mixed sediment beaches.

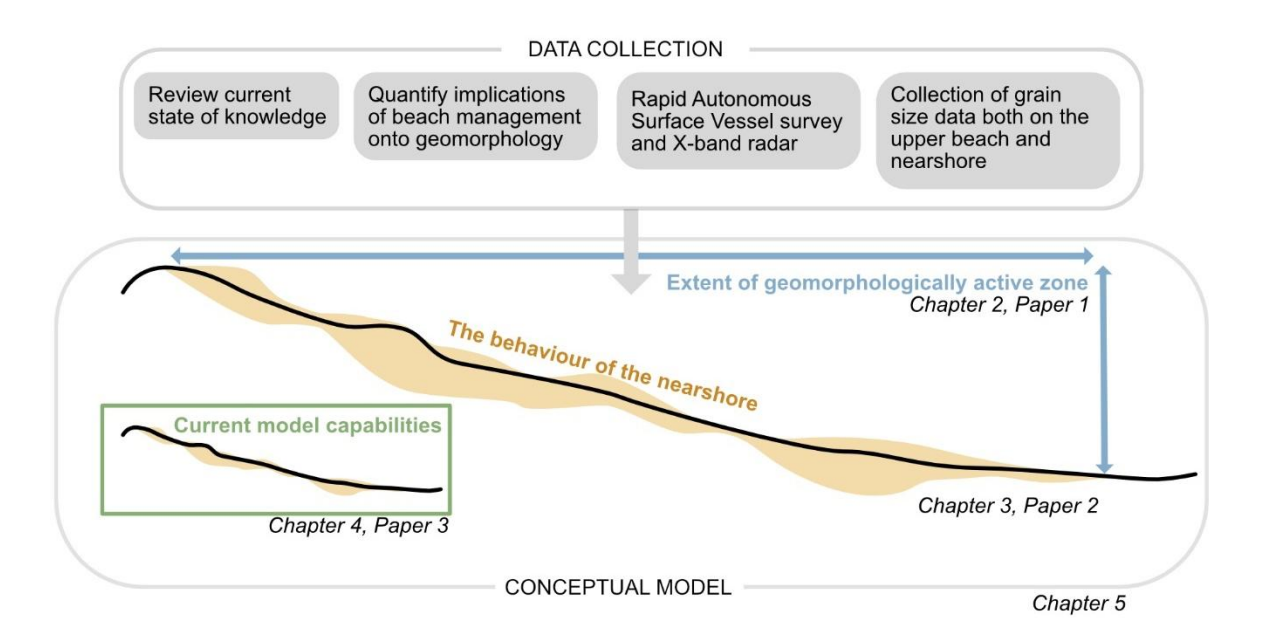


Figure 1.2 – Thesis outline with chapter signposts

Chapter 1 (this chapter) aims to orientate the reader.

Chapter 2 (Paper 1, https://doi.org/10.1016/j.geomorph.2024.109150) addresses RQ1 by examining over 19 years of bathymetric data at a range of different timescales from a mixed sediment site. Measures of geomorphological change were extracted from the data and a conceptual model was developed for the depth of closure, which is then used to understand local variations.

Chapter 3 (Paper 2, Submitted to Geomorphology) directly tackles RQ2 by studying a series of mobile bedforms within the site, both in the sub-tidal and intertidal region and links their migration rate to hydrodynamic drivers.

Chapter 4 (Paper 3, Intention to submit to Ocean Management) engages with RQ3 by using XBeach, a 1-D process-based model to explore sediment sorting and cross-shore sediment exchange under a series of different hydrodynamic, bed slope and sediment composition scenarios.

Chapter 5 provides a synthesis of the describing the conceptual model of a mixed sediment nearshore, addressing each research question in turn. The conclusion summarises the significant original contributions to knowledge and recommendations for further research are outlined.

1.4 Study site

1.4.1 Why Pevensey?

Pevensey Bay is a 9km long mixed gravel-sand barrier beach located on the South East coast of England. The beach is maintained as an important flood defence asset by Pevensey Coastal Defence Ltd (PCDL), on behalf of the Environment Agency, in a Public-Private Initiative (PPI, Figure 1.3). The PPI contract was for a period of 25 years and began in June 2000. Approaching the end of the contract, the PhD studentship, X-Band radar deployment, offshore bed sediment samples and bathymetry surveys were all carried out as part of the project "Delivering Legacy from the Pevensey Bay Coastal Defence Scheme" (PI: Kassem, H.; Contract: 201-09-SD10), which was funded by the Environment Agency.

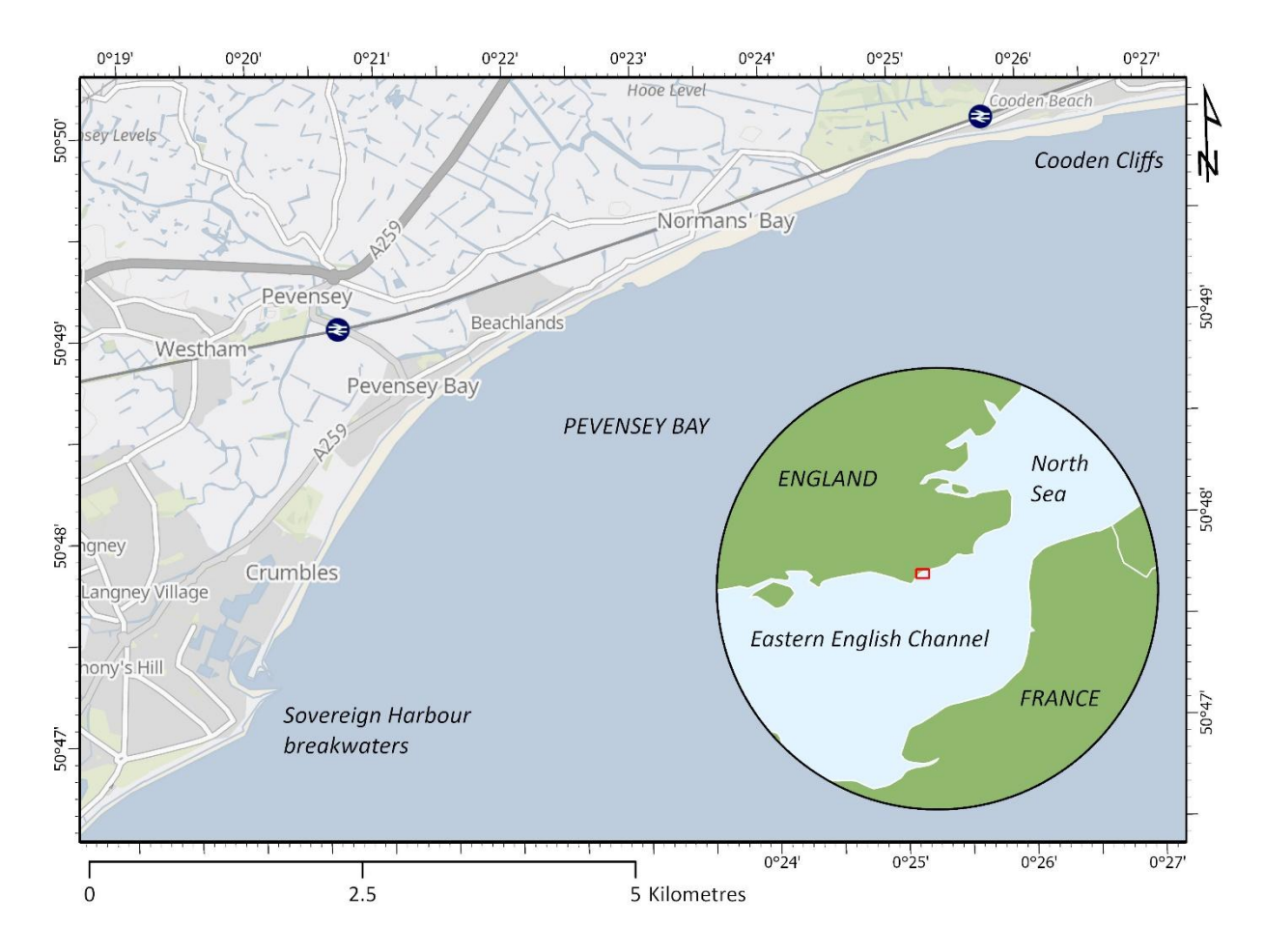


Figure 1.3 – Study site extent and regional location. Figure contains OS data © Crown Copyright and database rights 2023. Contains data from OS Zoomstack.

1.4.2 Geological & sedimentary setting

The site falls within the Weald Basin, a geological formation consisting of an uplifted area (the High Weald) boarded by the (chalk) South and North Downs (Figure 1.4). The uplift is thought to have occurred approximately 30 to 25 mya, as a result of the pressure created by the collision of the African and European continental plates. The uplifted land has eroded over time, with the greatest erosion at the centre of the anticline where the uplift is greatest. Here the earliest underlying sediments are exposed whilst furthest from the anticline, newer deposits, e.g. the chalk which forms the South and North Downs is exposed.

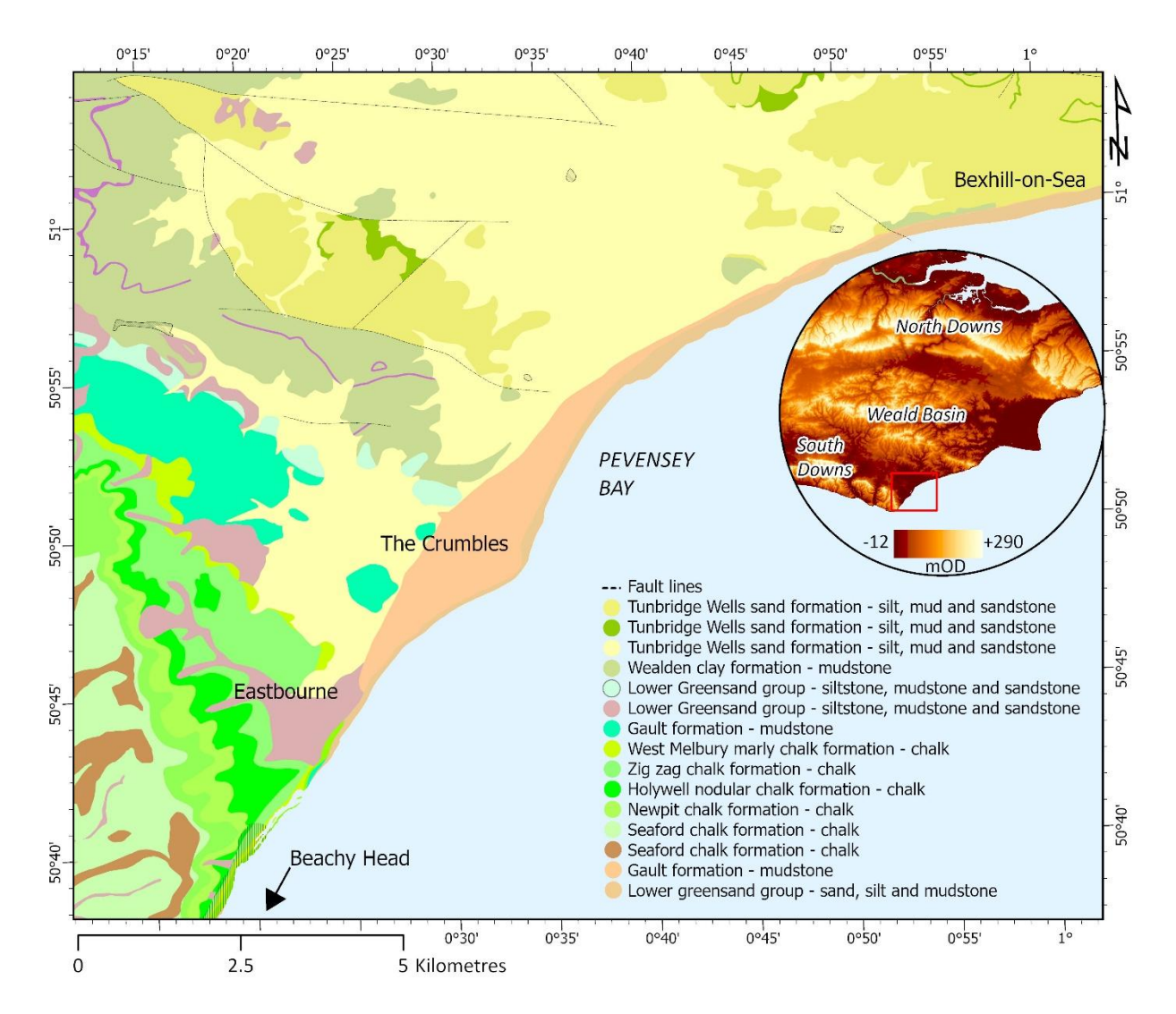


Figure 1.4 – Wider geological setting of Pevensey Bay, showing various chalk, sand, mud and siltstones of various ages, with elevation of the wider area inset. Geological data, 625K Bedrock, provided by ©British Geological Survey. Elevation data, Ordnance Survey Terrain 50 open height dataset, © Crown copyright and database right 2023.

Pevensey Bay lies at the junction between high elevation chalk outcrops forming the South Downs, running from the southeast to northwest, and low-lying underlying clays. The bay is the smaller of two local depocentres (the other is located approximately 30km to the northeast at

Rye Bay). The oldest records of Pevensey Bay suggest a very different coastline to that which it is today, whereby the tidal extent reached much further inland than at present. In 1066 the Norman fleet of 700 ships which invaded Britain landed at Pevensey Bay, at the roman built port of Anderitum, Figure 1.5 A (now a Scheduled Monument). This natural harbour may have born a resemblance to Pagham harbour at present, with a shingle barrier fronting a large intertidal area (Figure 1.5 B). Overtime the intertidal area silted up, which allowed for progressive reclamation to occur in the 14th century (Hartmann, 2017).



Figure 1.5 – A) A reconstruction drawing showing the Norman fleet of 700 ships landing at

Pevensey Bay on the morning of 28 September 1066 © Historic England, illustration
by Peter Urmston; B) Pagham Harbour, representing a similar gravel barrier system
to that which may have existed at Pevensey Bay in the past.

A cuspate foreland, known locally as the 'Crumbles' is thought to have formed between 1100AD and 1600AD (Jennings and Smyth, 1990). There is no agreed consensus on whether the large supply of sediment which caused the cuspate foreland to form was the result of longshore (Nicholls, 1991) or onshore (Jennings and Smyth, 1987) sediment transport. Historic mapping suggests that the Crumbles has been eroding ever since the 1600s, and that the feature now only occupies a fraction of its former extent (Tyhurst, 1972). Since the late 1800s the foreland has been subject to numerous human interventions, namely the construction of groynes in various phases from 1875 onwards and Langley outfall in 1907. Between 1872 and 1950 net erosion of the shoreline occurred in the magnitude of 100-150 metres, which is the equivalent of 1.0 - 1.5 m each year (Halcrow, 2000). In 1992 Sovereign Harbour was built, through the expansion of gravel pit extraction and the construction of two large breakwaters, interrupting the east to west flow of sediment along the coast. Since June 2000, the human interventions have consisted of active beach management, including nourishment, bypassing and recycling (Figure 1.6) and construction of four strategically placed 'terminal' groynes (Sutherland and Thomas, 2011).



Figure 1.6 – Beach works carried out by PCDL at Pevensey Bay to maintain beach width and volume, including A) recharge (approx. 20,000 cubic m pa); B) bypassing of material from Langley Point into Pevensey Bay (approx. 8,000 cubic m pa); and C) beach recycling (approx. 90,000 cubic m pa).

The beach can be described as a mixed composite beach, whereby, the upper beach sediments are a mixture of gravel (~70%) and sand (~30%) which are fronted by a flat sandy low-tide terrace. Nearshore bed sediment mapping by the Channel Coastal Observatory suggests that the nearshore sediments are a complex mosaic of pure sand and gravel, mixed sediments and rocky outcrops which partially constrain the site to the east (Channel Coastal Observatory, 2014). Samples taken from the upper beach show that there is considerable variation in the surface sediment grain size distribution likely due to cross shore processes, which has also been previously reflected in work by Watt et al. (2008) on the same beach. Coarser material with less fines is found at the beach crest and toe, with mixed sediment comprising most of the beach face slope, and a sandy terrace fronting the steeper upper beach (Figure 1.7). Concurrent work, carried out by Dornbusch et al. (2005b) found that surficial sediments at Pevensey Bay

were not representative of grain size distribution at depth, and that sediments >10cm below the surface were consistently finer than those on the surface.

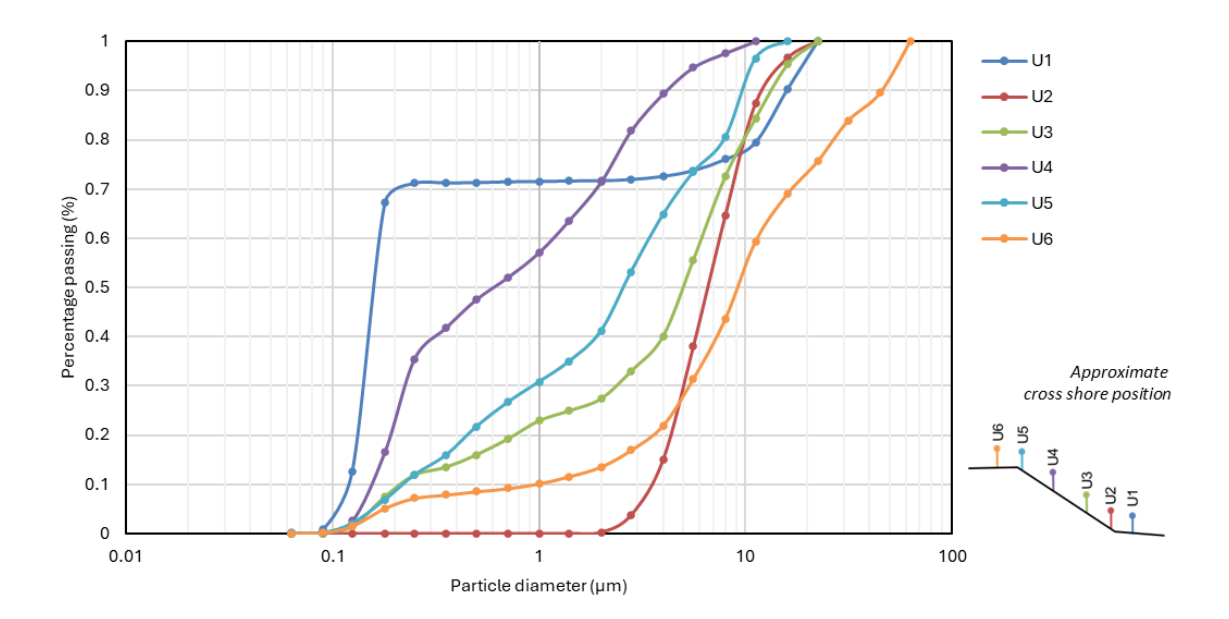


Figure 1.7 – Particle grain size diameter for six samples taken across the beach face in Beachlands at coastal monitoring beach profile 4c01702 on the 11/09/2023.

Chapter 2 Exploring nearshore bed dynamics of a mixed beach using the depth of closure conceptual model

Dominique Townsend₁, Julian Leyland₁, Hachem Kassem₂, Charlie Thompson₂₃, Ian Townend₂

¹ School of Geography and Environmental Science, University Road, Southampton, Hampshire SO17 1BJ

² School of Ocean and Earth Science, University of Southampton, Waterfront Campus, National Oceanography Centre, European Way, Southampton, SO14 3ZH, UK

³ Channel Coastal Observatory, Waterfront Campus, National Oceanography Centre, European Way, Southampton, SO14 3ZH, UK

2.1 Abstract

Mixed sediment beaches are globally commonplace, yet little is understood of the extent and behaviour of their nearshore zones, potentially underestimating total cross-shore change. This paper is the first study to investigate the lateral and vertical extent of the active zone of the gravel-rich mixed beach in Pevensey Bay, a study site on the South East UK coastline.

Morphodynamic change in the nearshore zone was studied at a range of timescales (days, months, years) suggesting that the width of the active nearshore zone correlated with the magnitude of the peak morphological change, whilst the depth of closure was influenced by bed slope, grain size and local variation in wave conditions. A conceptual model detailing the physical parameters responsible for local variations in the depth of closure was used to help understand differences between the observed and predicted depths of closure. Finally, ongoing chronic loss of sediment from below Mean Sea Level (MSL) was examined, which was shown to be independent of the depth of closure, but closely linked to the wider geomorphic setting of the bay.

2.2 Introduction

The nearshore zone (defined here as the area extending from the highest reach of the swash zone to the point at which waves begin to shoal) is a complex and dynamic environment that plays a critical role in coastal processes, ecological systems, and related human activities.

Understanding its dynamics and morphology is important for effective coastal management and

for maintaining the health and resilience of coastal communities and ecosystems. Bedforms and shoreline morphology combine to dissipate or focus wave energy, in turn influencing sediment transport and erosional and depositional dynamics. These process-form interactions are further complicated by the nature of the sediment found in the nearshore zone, specifically in terms of grain size distribution and spatial variability.

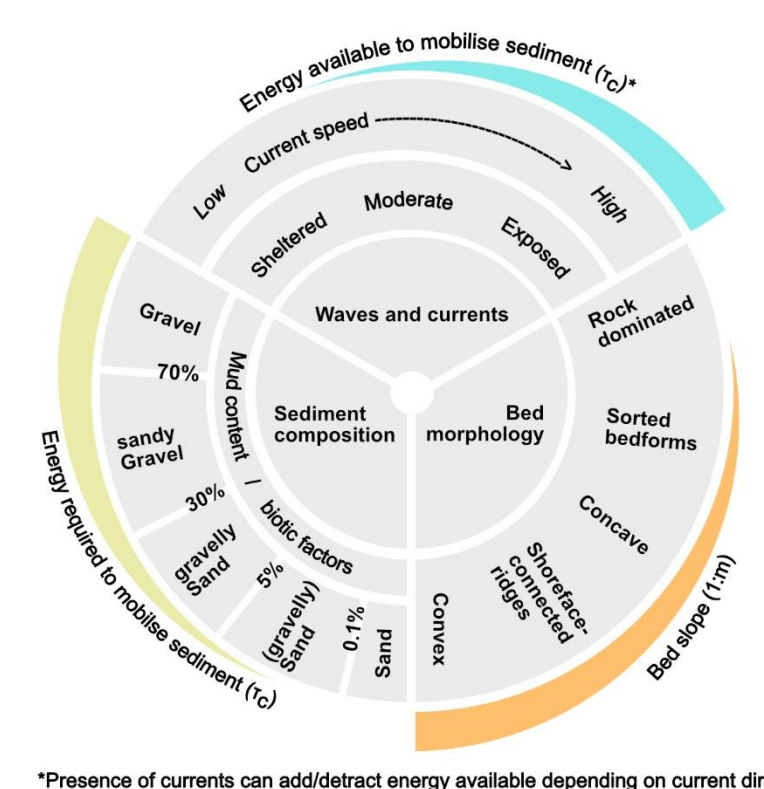
When considering the extent of the nearshore, a useful theoretical concept is that of the depth of closure, which marks the seaward extent of the nearshore zone, as the point at which the seabed becomes morphologically inactive over a specified timescale (Kraus, Larson and Wise, 1998). The concept was originally devised to pinpoint a limit to seasonal bed movements in sandy beaches to assist in beach nourishment design (Hallermeier, 1977, 1978, 1981). However, the depth of closure is now widely applied in engineering design, providing boundaries to both sediment budgets and coastal modelling tools (de Figueiredo, Goulart and Calliari, 2020) for a wide range of open-coast environments (Brutsché, Iii and Pollock, 2015). Broadly, the literature on the depth of closure addresses field methods and predictive models. The former includes methods to identify the point of closure through repeat bathymetric surveys (e.g. Birkemeier, 1985; Hartman and Kennedy, 2016; Nicholls et al., 1998), analysis of sediment facies (e.g. Dumas and Arnott, 2006), or grain size analysis (e.g. Aragonés et al., 2018). On the other hand, predictive methods for estimating the depth of closure include: equations accounting for wave parameters only (e.g. Hallermeier, 1978; Birkemeier, 1985; Nicholls et al., 1998a), utilising equilibrium profile theory (e.g. Nicholls et al., 1998b; Ortiz and Ashton, 2016), as well as including data on sediment size and incident wave angle utilising machine learning approaches (e.g. Aragonés et al., 2015). A number of studies seek to improve understanding of the depth of closure through the comparison between the predicted and the observed closure depth (Hinton and Nicholls, 1998; Robertson et al., 2008; Polska et al., 2015; Hartman and Kennedy, 2016; Valiente et al., 2017; Aragonés et al., 2019; Udo et al., 2020; Barrineau et al., 2021). A conceptual summary of the physical parameters influencing the depth of closure is provided in Figure 2.1 and can be used to help interpret local variations in the depth of closure obtained from repeat bathymetry data. There are three main components which can moderate the depth of closure, namely waves and currents, bed morphology/slope and sediment composition:

Waves and currents: The presence and magnitude of waves directly impact the energy available to entrain sediment in the nearshore and therefore as a coastline becomes more exposed, the energy available to mobilise material increases (Nicholls et al., 1996; Francois et al., 2005). Similarly, as the incident wave angle approaches 45°, the maximum wave radiation stresses are reached and maximum transport occurs (Ashton and Murray, 2006). Currents have also been shown to moderate the depth of closure by

suppressing or enhancing bed level change (Kraus, Larson and Wise, 1998; Valiente et al., 2019).

- Bed morphology: Bed morphology can vary greatly depending on underlying geology and the availability of superficial sediments (Robertson et al., 2008; Hartman and Kennedy, 2016; Anthony and Aagaard, 2020). A key factor on how the morphology affects the depth of closure is the bed slope, as a greater slope allows for greater offshore transport (downslope) (Ortiz and Ashton, 2016; Hamon-Kerivel et al., 2020).
- Sediment composition: The critical threshold for sediment entrainment is related to grain size and therefore this is an important factor in determining the depth of closure (Udo, Ranasinghe and Takeda, 2020). In mixed sediment environments, the presence of gravel and/or mud can increase the amount of energy required to mobilise sand (Panagiotopoulos et al., 1994; Mitchener and Torfs, 1995; McCarron et al., 2019). Sediment properties, the presence of biota (biofilms to macroalgae) and natural cementation also alter the critical bed shear stress needed for entrainment.

This conceptual model can be used to help interpret local and regional variation in the depth of closure, where the observed depth of closure is different to that estimated by established empirical formulae (cf. 2.1 Depth of closure – wave energy approach).



^{*}Presence of currents can add/detract energy available depending on current direction

Figure 2.1 – The physical parameters influencing the depth of closure; waves and currents, bed slope, and sediment composition are shown in relation to the influences on depth of

closure, namely, 'Energy required to mobilise sediment' (yellow), 'Energy available to mobilise sediment' (blue), and 'Bed slope' (orange).

Beach management activities, including beach recharge, recycling and bypassing, have been employed globally to counter erosion along highly-populated coasts (de Schipper et al., 2021; Staudt et al., 2021). With limited effects on downdrift sediment supply, these 'soft' engineering approaches have been adopted widely despite requiring higher levels of intervention than traditional 'hard' engineering. In recent years, the social, ecological and geomorphological sustainability of these schemes have been brought into question (Parkinson and Ogurcak, 2018; Staudt et al., 2021) although much of the focus has been on sandy shores. For decades, soft engineering works have been carried out on mixed sediment beaches on the south eastern English coastline with little consideration of the nearshore zone as the predominantly gravel upper beach is often treated as a fixed coastal defence, independent from its surroundings (Dornbusch and Hardiman, 2020). Our study site, Pevensey Bay, East Sussex, UK, is a key example of this, and concerns have been raised over the long term sustainability of the current management approach, as over a thirteen year period approximately 8,000 m³ of sediment from below the mean sea level mark have been lost from the 9 km long frontage each year (Thomas, 2015). This paper examines the relationship between the shoreline management of the upper beach and the nearshore zone, by measuring width and depth of the nearshore zone in a mixed sediment environment over time, using the depth of closure concept. Bathymetric data covering short (days) to medium (months to years) timescales for the mixed sediment beach of Pevensey Bay are used to address the following objectives:

- 1) compare observed and predicted depths of closure for a mixed sediment environment;
- interpret temporal and spatial differences in the observed depth of closure using the conceptual model set out in Figure 2.1; and
- 3) understand the changes in the nearshore zone in relation to the current shoreline management.

2.2.1 Study site

The study site, Pevensey Bay, is a 9km barrier beach located on the East Sussex coast, southeast England, UK (Figure 2.2). The beach at Pevensey is described as a composite mixed beach, comprising a reflective, mixed sand gravel upper beach and a dissipative sandy foreshore/low-tide terrace (Horn and Walton, 2007; Sutherland and Thomas, 2011). The upper mixed sand gravel beach has a median grain diameter (D_{50}) ranging between 8 and 16 mm across the site (Watt *et al.*, 2006). Six trial pits dug at the high water mark down to 0 mOD revealed an upper predominantly gravel layer (less than 5% sand), approximately 0.1m deep

capping the beach sediments, and a higher sand content below this layer between 10-40% sand, which resulted in a median diameter (D_{50}) ranging between c. 3 mm to just over 30 mm as the percentage of sand varied with depth (Dornbusch et al., 2005). Visual interpretation of multibeam backscatter data, whereby surface roughness can be inferred, suggested a largely sandy bed with outcrops of gravel in the centre of the site, with an area of mixed sediment in the west and exposed rock outcrops to the eastern extent within a kilometre of the coastline (Channel Coastal Observatory, 2014).

The bay is mostly exposed to large south westerly waves (Hs <= 2.5 m) for ~85% of the time, and smaller, less frequent easterly waves (Hs <= 1.5 m) for ~15% of time (Figure 2.2, Sutherland and Thomas, 2011). Wave conditions are typically calm in the summer period between April and August (Hs ~0.6m), and are more energetic in the winter period between September and March, with average monthly Hs peaking at just over 1.0m in December (National Network of Regional Coastal Monitoring Programmes., no date). The spring and neap tidal ranges are 6.7 m and 2.3 m respectively (Horn and Walton, 2007; Elsner et al., 2015). Depth averaged tidal currents vary from an average rate of 0.5 ms⁻¹ at mean spring conditions to 0.3 ms⁻¹ during mean neap conditions, and residual (non-tidal) currents have been shown to flow as quickly as 0.71 ms⁻¹, with average flows generally between 0.11 and 0.04 ms⁻¹ (Fugro Emu Ltd, 2016). The beach is actively managed as a flood asset, protecting approximately 50 km² of low-lying land, c.10,000 properties as well as nationally and internationally important wildlife sites from inundation (Sutherland and Thomas, 2011). To maintain the barrier width and beach volume, each year an average of 80,000 m³ of sediment are recycled within the study site, 10,000 m³ are bypassed into the site from west of the Sovereign Harbour breakwaters and a further 20,000 m³ are recharged from an offshore source, Owers Bank, 9 km offshore of Littlehampton, West Sussex and ~60 km west of the study site (Thomas 2023, pers. comm.).

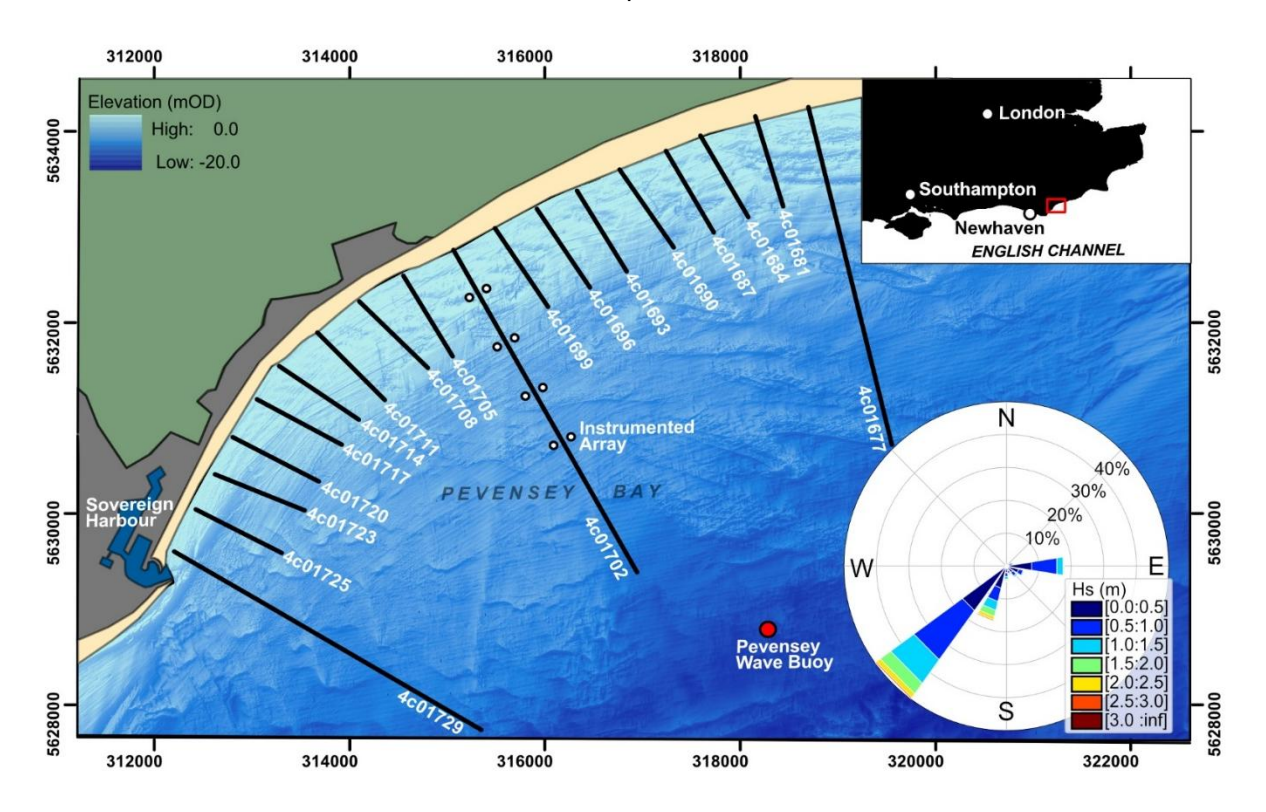


Figure 2.2 – Pevensey Bay study site; green and grey areas showing rural and urban land use, respectively. Yellow area representing upper beach. Black profile lines show the position of bathymetric surveys with names corresponding to the National Network of Regional Coastal Monitoring Programme (NNRCMP) beach profiles. The wave rose shows binned data from the Pevensey Wave buoy (position shown by red marker) for the period June 2003 – November 2022. Bathymetric data composite of 2012 Centre for Environmental Fisheries and Aquaculture Science (CEFAS), 2013 Channel Coastal Observatory (CCO) data (1 km inshore) and 2015 Maritime and Coastguard Agency (MCA). Inset map showing the south east of England and the regional setting of Pevensey Bay. Grid projection: UTM 31 N.

2.3 Methods

The following section details five stages of work. Firstly, the estimation of depth of closure from hydrodynamic input is given (2.1 Depth of closure – wave energy approach), followed by the identification of the observational depth of closure including description on the collection and interpretation of 19 years of bathymetry data with variable temporal resolution within that period (2.2 Depth of closure – observational approach). Long and cross-shore sediment transport are also estimated at three inshore locations (2.3 Nearshore transport estimation). The method for sediment grain size analysis is documented (2.4 Sediment analysis). Finally, a sediment balance exercise is described comprising an analysis of the upper beach slope over time and cross sectional area of the nearshore (2.5 Sediment balance).

2.3.1 Depth of closure – wave energy approach

The seasonal limit to sand movement, also referred to as the inner limit (d_i), was calculated using the Hallermeier (1978, 1977) and Birkemeier (1985) equations (1 – 4) for comparison to depth of closure measurements from observational data. The equation for the inner limit as given by Hallermeier (1978) is:

$$d_{lh} = 2.28 H_e - 68.5 \left(\frac{H_e^2}{g T_e^2}\right)$$
 Equation 1

where g is the acceleration due to gravity, H_e is the non-breaking significant wave height exceeded 12 hours per year, and T_e is the associated wave period. The 12 hourly exceedance was taken from the wave record between 08/07/2003 and 31/10/2019 of the Pevensey Bay Wave Buoy, which is recording in a water depth of approximately 9.8 m below Chart Datum (Figure 2.2) and is available to freely download from the Channel Coastal Observatory website at https://coastalmonitoring.org/.

Hallermeier's (1977) simplified equation for the inner limit is:

$$d_{lhs} = 2\overline{H}_s + 11\sigma_s$$
 Equation 2

where \overline{H}_s is the annual, mean significant wave height and σ_s is the associated standard deviation. Birkemeier (1985) adjusted the equation for the inner depth of closure:

$$d_{lb} = 1.75 \, H_e - 57.9 \bigg(\frac{H_e^2}{g T_e^2} \bigg) \hspace{1cm} \text{Equation 3}$$

and Birkemeier's (1985) simplified the equation:

$$d_{lbs} = 1.57 H_e$$
 Equation 4

Whilst Hallermeier's d_l gives a 'seaward limit to extreme surf-related effects', they recognized that waves begin to interact with the seabed through shoaling, further offshore. To mark the start of the shoaling zone, Hallermeier identified the outer closure limit (d_i) , using both mean annual wave values and the median grain size (D_{50}) . This zone represents a 'buffer area where expected waves have neither strong nor negligible effects on the sand bed during a typical annual cycle of wave action' (Hallermeier, 1981). This is the deepest limit that wave-driven bed level change will occur. This was calculated herein using Hallermeier's (1983) revised equation:

$$d_i = 0.018 H_m T_m \sqrt{\frac{g}{D_{50} (s-1)}}$$
 Equation 5

where H_m is the mean annual significant wave height, T_m is the associated wave period, D_{50} the median sediment size and s is the specific gravity (ratio of sediment density to water density).

The D_{50} used herein was taken as the average grain size for sediments found on the foreshore from samples taken on the 19/11/2019 as detailed in Section 2.3.4.

2.3.2 Depth of closure – observational approach

2.3.2.1 Data collection

A series of bathymetry surveys were undertaken at the study site, namely two 'bay wide' surveys, consisting of 18 shore normal profiles (aligned with existing National Network of Regional Coastal Monitoring Programmes for England (NNRCMP) beach profiles) on the 15/09/2020 and 30/03/2021 with an aim to capture change over the 2020/2021 winter storm season (September to March). The profiles extended 1 km offshore, with the exception of three profiles, 4c01677, 4c01702 and 4c01729 which extended out to the estimated Hallermeier's outer depth of closure, (equation 5), between 3.6 to 3.9 km offshore (Figure 2.2). For simplicity these extended profiles are referred to as the Easternmost (4c01677), Central (4c01702) and Westernmost (4c01729) profiles throughout the text. The extended profiles were also surveyed on the 14/04/2022, and Profile 4c01702 was surveyed (in part) an additional six times between March 2021 and February 2022, Table 2.1. For every bathymetric survey completed, a complimentary upper beach topographic survey was carried out during the preceding/subsequent low water periods to gain a full picture of the beach profile. This was done by the University of Southampton or by Adur-Worthing Councils, as part of the Southeast Regional Coastal Monitoring Programme. All topographic data crossed the highest sub-aerial elevation of the beach, but, beyond this point most data were limited by private property boundaries. Topographic data were collected using real time kinematic Global Navigation Satellite System (GNSS) equipment, whereby points were collected at a maximum of 5 metre spacing across the beach profiles with additional points recorded if a change in slope was observed. This approach is consistent with the NNRCMP.

Table 2.1 – Summary of extended profile survey dates and source. Note: N=NNRCMP SBES survey; M = NNRCMP/MCA MBES survey; Px = extended project surveys; P = project surveys.

Location	04/09/2003	12/03/2006	01/08/2013	15/09/2020	30/03/2021	28/04/2021	27/05/2021	15/11/2021	25/11/2021	16/12/2021	25/01/2022	14/04/2022
4c01729	N	N	М	Px	Px							Px
(Westernmost)												
4c01727 to 4c01705	Ν	Ν	M	Р	Р							
4c01702	Ν	Ν	М	Px	Px	Р	Р	Р	Р	Р	Р	Px
(Central)												
4c01699 to 4c01681	N	Ν	M	Р	Р							
4c01677	N	Ν	М	Px	Px							Px
(Easternmost)												

Bathymetric surveys were carried out by the University of Southampton and external IHO Category A contractors, the details of which are provided in the supplementary information. Single-Beam Echo Sounding (SBES) was used for the bay wide surveys, whilst Multi-Beam Echo Soundings (MBES) were used for all but one of the surveys of the Central profile 4c01702. The horizontal resolution varied between 0.01 and 0.5m; the vertical resolution was sub-centimetre for all systems. The horizontal error ranged between ±0.03 m and ±0.10 m, and the vertical error ranged between ±0.06 m and ±0.3 m (New Forest District Council, 2020; Shoreline Surveys Ltd, 2021; Unmanned Survey Solutions, GeoSight, HydroSurv personal communication 26/04/2023;). The bathymetry data were converted to British National Grid with vertical elevations to the Ordnance Datum Newlyn using the OSGM15 model. Prior to further analysis, all raw multibeam soundings collected by the University of Southampton were checked and filtered for outliers within the post-processing software, BeamworX AutoClean (https://www.beamworx.com/). Here, we used a simple 95% confidence interval filter, meaning that any soundings lying more than two standard deviations from the mean depth within a grid cell (0.5 m) are removed as outliers.

Additional bathymetry profile data were extracted using bilinear interpolation from the NNRCMP/ Maritime Coastguard Agency multibeam echosounder survey, carried out 01/08/2013, and from the NNRCMP SBES surveys, recorded on the 04/09/2003 and 12/03/2006 at a resolution of 0.01 m in the cross-shore and ~50.0 m in the longshore to +/-0.2 m vertical accuracy (Channel Coastal Observatory, 2003, 2006). Raster surfaces for the SBES data were generated through firstly creating a Triangular Irregular Network (TIN) of the SBES points, and

then converting the TIN into a raster grid. The bathymetric data are freely available to download from the NNRCMP website, https://coastalmonitoring.org/.

The bathymetry and topographic profiles were initially processed using Python to generate a chainage for each data point, i.e. the distance between the data point and the NNRCMP start point of each profile line, which is typically the most landward point of the profile. These processed files were then imported into the beach profile analysis software SANDS (Shoreline And Nearshore Data System, @ 2023 Jacobs; see https://www.sandsuser.com/ for more information). The software works as a database for topographic beach profile data and was used to quality check the data visually, through inter-survey profile comparison and checking for spikes or irregular surface features, such as those caused by interference from grains of sediment mobilised near the bed by the tide. If any such spikes were found, these were manually deleted (note that this was only for very small, localised areas of one survey). SANDS was then used to combine the topographic and bathymetric profile data creating complete, backshore to offshore, beach profiles (Bradbury, Mason and Barter, 2005). This was done by linking the topographic profile line with the bathymetric profile line, with the bathymetric profile taking precedence in overlapping areas as this data consistently captured a fuller profile at the toe of the beach. The profiles were then interpolated at 1 m spacing with a univariate interpolation, using the Python SciPy module package.

2.3.2.2 Data analysis

The observational depth of closure method examines variation in elevation between two or more profile surveys, where the depth of closure is found at the point where the absolute difference or standard deviation becomes constant. This represents the survey error and is also known as a non-zero tail (Hinton and Nicholls, 1998). Change above the non-zero tail is considered to be detectable change. Initially, the standard deviation of the elevation was calculated over the range of surveys completed at the three extended profiles. Following this, the absolute difference in elevation was calculated between any two surveys at each chainage point along every profile. From this, the locations of the landward minimum morphological change, peak morphological change and the depth of closure were identified. The landward minimum morphological change was identified as the first point where conditions meet Kraus et al.'s (1998) guidance "the depth of closure is defined as the most landward depth at which no significant change occurs". The depth of closure was identified as the most seaward point at which no detectable change begins to occur, encompassing all areas of closure and 'reopening' as defined by Hinton and Nicholls (1998). The location of peak morphological change was identified at the cross-shore chainage with the greatest value of absolute difference. The secondary peak was identified to show the largest natural change when this was masked by

human interventions to the crest from beach re-profiling. Additionally, the average seabed slope was calculated for profiles between the locations of Mean Sea Level (MSL) and the depth of closure.

2.3.3 Nearshore transport estimation

To understand the variation in the wave driven processes across the frontage, namely long and cross-shore transport, the wave buoy record (08/07/2003-31/10/2019) was propagated to three nearshore points (located along the three extended profiles) using CoastalTools, an open source, MATLAB based GUI (https://www.coastalsea.uk/). The wave record from the Pevensey Bay wave buoy (Figure 2.2) was transformed to give the breaking wave height at the edge of the surf zone using water levels for the same time period from the Newhaven tide gauge (Figure 2.2). This was done using linear wave theory, with plane bed refraction and shoaling, together with Weggel's (1972) empirical work relating beach slope to breaking wave height as given in equations 2-92, 2-93 and 2-94 of the Shoreline Protection Manual (USACE, 1984).

From this inshore transformation of the wave record, both littoral drift potential and cross-shore transport rates were calculated independently for both fine sand (159 – 164 mm) and medium pebbles (12mm), using locally derived shoreline angles for each profile. The chosen grain sizes were based on the average of samples collected by Dornbusch et al. (2005) for the upper beach and using samples of the sandy foreshore as described in Section 2.3.4. Cross shore transport rates were estimated using Bailard and Inman (1981), accounting for both the suspended and bed loads. Longshore transport rates were estimated using Damsgaard and Soulsby (1996) for the medium pebbles, a physics based equation used to predict longshore bedload transport, calibrated against a 3 year field dataset of longshore sediment transport on a shingle beach in the south of the UK. Finally, the simplified version of the CERC equation (which does not take into account bed slope nor grain size), *i.e.* the SANDS formula, was utilised to represent sand transport (Soulsby, 1997). The full equations for the wave transformation and sediment transport are provided within the supplementary information.

2.3.4 Sediment analysis

Eight van Veen grab samples were retrieved at the locations of an instrument array of benthic landers on the 04/07/2022 and the 07/09/2022 (locations shown with white circles in Figure 2.2). As work by Dornbusch et al. (2005) did not provide information on the sandy foreshore, samples were also taken from this zone on the 19/11/2019. Grain size analysis was completed complying to BS EN ISO 17892-4:2016. Using the arithmetic method of Krumbein and Pettijohn (1938), the textural statistics were calculated, namely median grain size, sorting, skewness and kurtosis.

2.3.5 Sediment balance

To better understand the observed chronic loss of sediment at Pevensey Bay (Thomas, 2015) change in upper beach profile slope (Section 2.3.5.1) and cross sectional area of the nearshore over time were analysed (Section 2.3.5.2).

2.3.5.1 Upper beach slope analysis

Change in the lateral position of MSL is not natural at Pevensey Bay as the gravel barrier is maintained to a design width. However, the beach slope is not maintained (despite small amounts of reprofiling after the placement of recycled/recharge material) which means that long-term rotational movement of the cross-shore intertidal profile, i.e. steepening/flattening, can be examined. This was done by analysing the relative positional changes of mean low water and mean high water which were extracted for each NNRCMP beach profile, following Taylor et al.'s (2004) method. The changes were calculated for each spring topographic survey from 2003 to 2022 carried out by the NNRCMP. Specifically, Mean High Water Neap (MHWN) and Mean Low Water Neap (MLWN) elevations were used to allow the widest coverage across the bay as some NNRCMP profiles did not extend down to the Mean Low Water Springs (MLWS).

2.3.5.2 Nearshore cross-sectional area

The cross-sectional area above the datum -12.0mOD for which all bathymetric surveys covered was calculated for each profile (Figure 2.2, Table 2.1). This analysis was carried out in the software SANDS. The results of this analysis provide an indication of the volume of material across the bay over the time periods where data were available (Table 2.1).

2.4 Results

2.4.1 Depth of closure – wave energy approach

The predicted depth of closure ranged between -8.03 and -11.02 m Ordnance Datum (OD) for the inner closure depth representing seasonal change, and -12.94mOD for the outer limit (Table 2.2).

Table 2.2 – Results from wave statistics and depth of closure.

Description	Value	Units				
Wave statistics						
Не	3.68	m				
Те	6.23	S				
Depth of closure results						
Hallermeier	-9.60	mOD				
Hallermeier simplified	-11.02	mOD				
Birkemeier	-8.03	mOD				
Birkemeier simplified	-9.43	mOD				
Hallermeier outer	-12.94	mOD				

2.4.2 Depth of closure – observational approach

Historic and repeat surveys of the Central profile 4c01702 indicate the level and extent of bed elevation change over different timescales (Figure 2.3). Subplot A of Figure 2.3 illustrates the profile surveyed at different time periods and shows the steeper upper beach located within the first 100 m chainage, and the flatter shoreface slope seawards beyond this. The absolute difference in bed elevation between surveys shows change occurring over the full extent of the surveyed area over longer timescales (greater than six months (Figure 2.3, subplot E and H) to years (Figure 2.3, subplots B to D)), whereas analysis of shorter timescales (less than three months, Figure 2.3, subplot F, G, I to L) shows change limited to certain areas at approximately 300 m, 600 m and 950 m offshore. These changes are caused by the apparent progressive onshore movement of bar features over the course of a year. Multibeam bathymetry and X-band radar reflectance imagery have shown that these are transverse finger bars, which lie at ~45 degrees to the coastline and are moving easterly at a rate of approximately 100 m a-1 (Townsend et al., 2023). Over longer timescales (subplots B-D) changes occur up to the survey limit (1km offshore) and therefore the depth of closure may be further offshore. The short spike in the absolute difference at approximately 30 m chainage is caused by the change in crest position, from erosion and cliffing events, as well as ad hoc beach recycling to maintain the width of a haulage route which runs between the barrier crest and a row of beachfront properties.

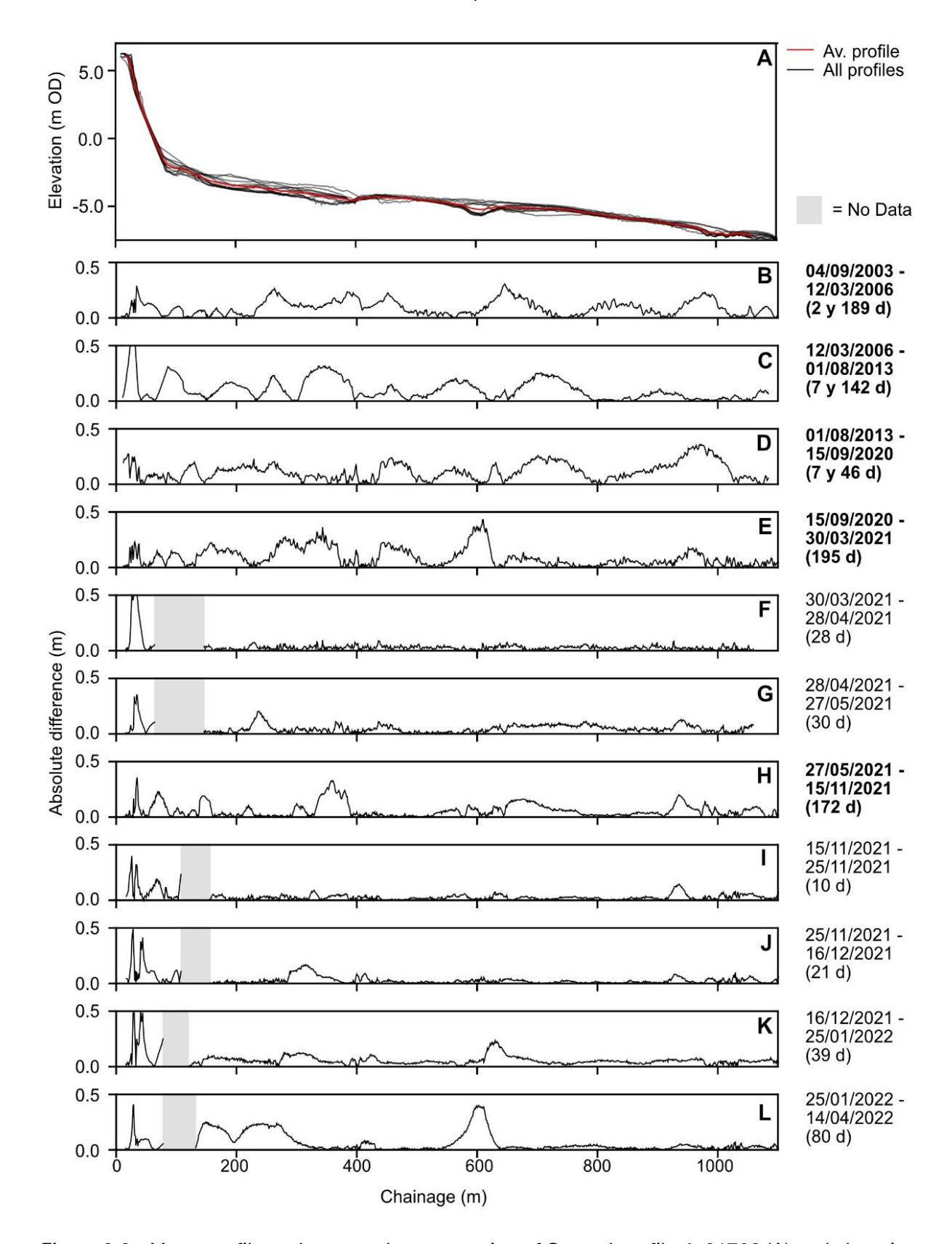


Figure 2.3 – Mean profile and surveyed cross section of Central profile 4c01702 (A) and elevation variation between surveys, 04/09/2003 to 25/01/2022 (B to L). Sections with no data shown in grey, where topographic and bathymetric surveys did not overlap fully. The duration between the two surveys is indicated in parentheses. Time periods approaching 6 months and greater highlighted in bold.

Chapter 2

We used the absolute difference between the bed level change for the 2020 Autumn and 2021 Spring surveys to capture the change caused by winter storms (Figure 2.4). The landward minimum morphological change was found to be shallower than the Lowest Astronomical Tide (LAT) for 11 out of 18 profiles, but for some profiles in the east, this depth was below LAT. The intertidal area is roughly the same width throughout the study site, whilst the deeper contours of -5.0 and -6.0 mOD show that the shoreface is steeper in the west, closest to Sovereign Harbour, but flattens out and becomes shallower, towards the east. The depth of closure follows this pattern, moving further offshore as the bed slope decreases to the east. The location of peak morphological change for nearly all the profiles west of the Central profile 4c1702 is above MSL, around the barrier crest, possibly in response to beach reprofiling works. To the east of the Central profile (4c01702), the peak morphological change is found to be much greater than in the west and further offshore in water depths greater than the -5.0mOD contour.

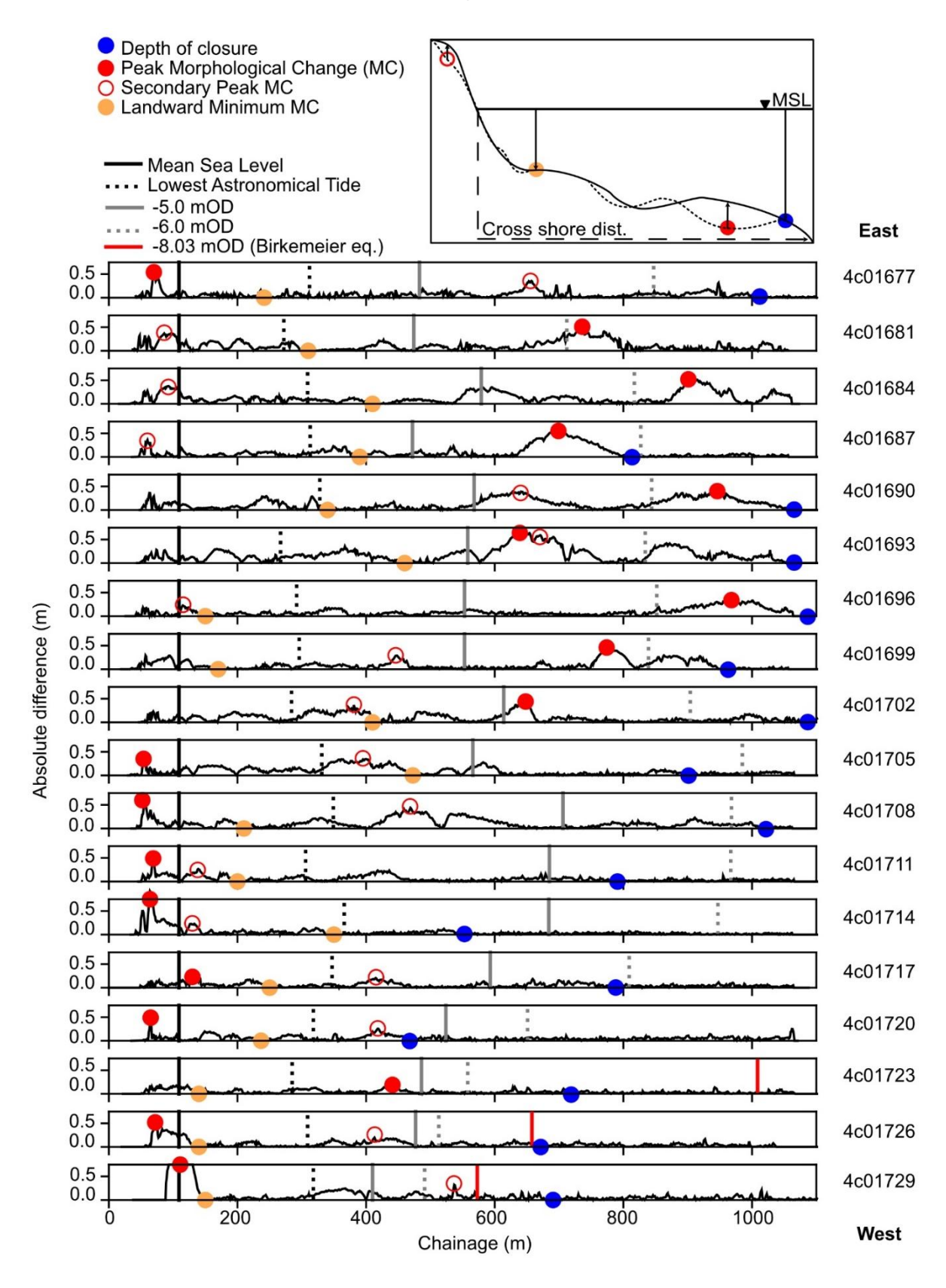


Figure 2.4 – Top right) Depth of closure, alongside peak, secondary peak and landward minimum morphological change with 0 mOD reference point for measuring cross-shore distance. Main figure) Absolute difference between Autumn 2020 and Spring 2021 'bay wide' surveys. All profiles plotted relative to the 0 mOD contour chainage, representing Mean Sea Level (shown as thick black vertical line). Dashed black, solid grey and dashed grey vertical lines show the position of the LAT (–3.65mOD), -

5mOD and -6mOD contours respectively. N.B. large variation at 100 m chainage on Westernmost profile 4c01729 is due to beach management activities.

2.4.3 Depth of closure – wave energy vs observational approach

The observed depth of closure for the study site is shallower than the predicted depths estimated using the Hallermeier and Birkemeier equations (Figure 2.5, equations 1 - 4), but the Birkemeier equation (equation 3) provides the best estimate of closure depth. Over a 9 year timescale, the observed depths of closure were within 0.23 m on average of the Birkemeier equation (equation 3), but ranged on average from 1.63 m, 1.80 m and 3.22 m shallower for the simplified Birkemeier, Hallermeier and simplified Hallermeier equations (equations 4, 1 and 2) respectively (Figure 2.5, Panel A). Over a single winter period the observed depth of closure ranged between 0.37 deeper and -3.33 m shallower than the Birkemeier equation (Figure 2.5, panel B).

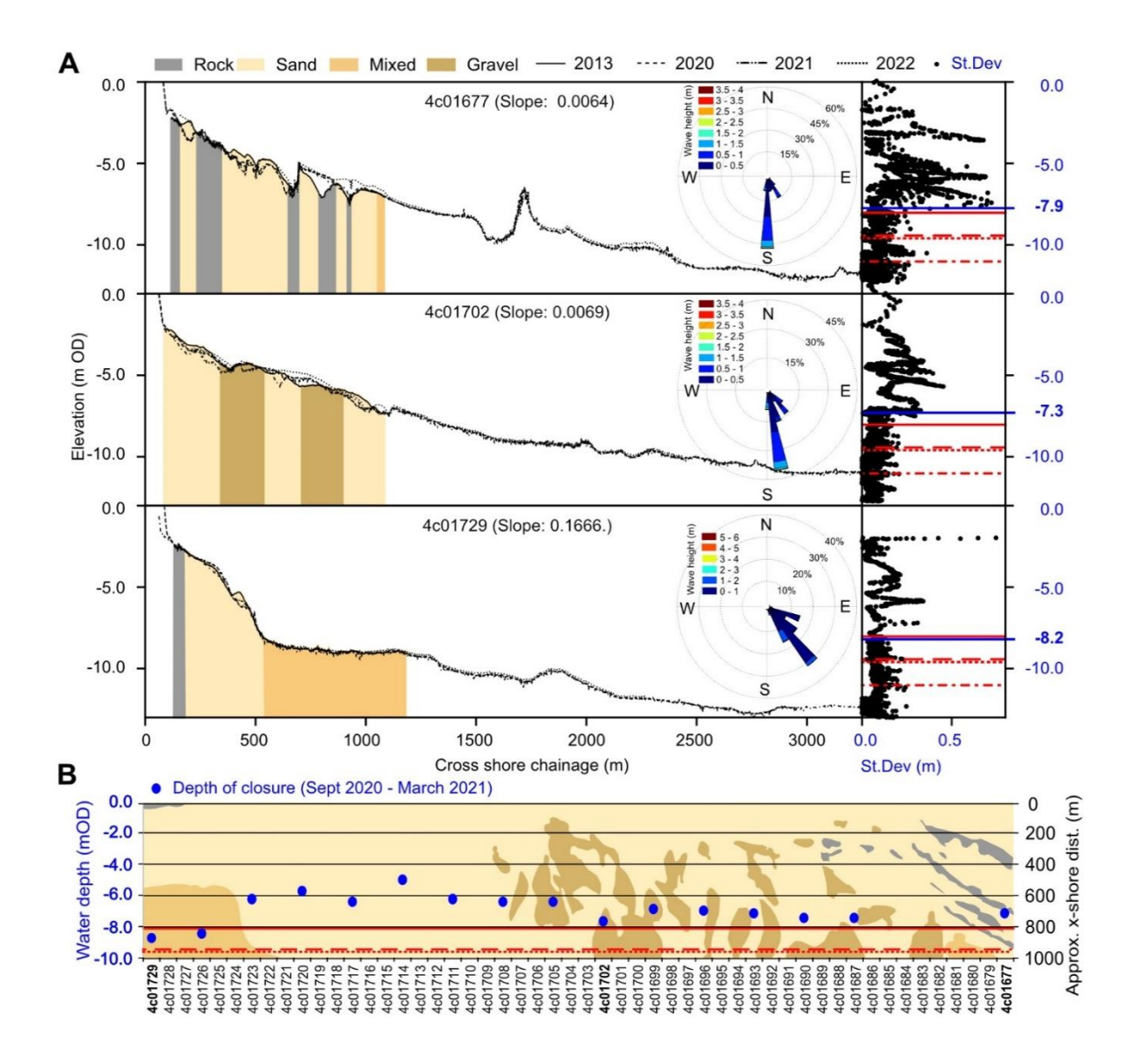


Figure 2.5 – Variation of the three extended cross-shore profiles (Easternmost: 4c01677, Central: 4c01702 & Westernmost: 4c01729) through time. The standard deviation of bed level vs depth is shown, together with the observational depth of closure (blue lines, i.e. when SD reaches a constant non-zero tail, which is around 0.15 m for this dataset) and the predicted depth of closure (red bars, namely Birkemeier (–8.03 mOD, solid red), simplified Birkemeier (–9.43 mOD, dashed red), Hallermeier (–9.60 mOD, dotted red) and simplified Hallermeier (–11.02 mOD, dash-dot red). The slope between MSL and the observed closure depth is also given with the profile name label. Indicative bed composition from the 2013 backscatter interpretation is also shown, as gravel, sand, mixed and rock (N.B. this method cannot detect mud). The inset roses show propagated nearshore wave record for each beach profile derived from CoastalTools. (For interpretation of the references to colour in this figure legend, the reader is referred to the web version of this article.)

The variations in nearshore waves, bed slope and surface roughness across the frontage are presented against the observational depth of closure in panel A of Figure 2.5. The indicative bed type shows that the predominant surficial sediment type across the bay's nearshore is sand, and that nearshore morphology becomes more dynamic eastwards. Westernmost profile 4c01729 is noticeably steeper than the other profiles and fronted by a planar bed of mixed sediment. Changes in bed elevation appear to be limited to a nearshore bar, located at around 450 m offshore. Notably, the annual beach recharge (~20,000m³ material) is deposited here, which is evident in the most shoreward part of the profile, between surveys in 2020 (just after nourishment) and 2021 (after winter storms/erosion). There are extensive areas of gravel along the Central profile, 4c01702, which do not seem to inhibit bed movement overtime. However, there appears to be an area which has experienced very little bed elevation change at approximately 400 m offshore. The elevation of the areas identified as rocky outcrops in the Easternmost profile 4c01677 typically does not change over time, except for two areas which were exposed in 2013 but subsequently buried, around 300 and 800 m offshore.

Panel B shows the depth of closure to be at its shallowest around Profile 4c01714, becoming progressively deeper in both directions away from this minimum. From the Central profile 4c01702 eastwards, the depth of closure is relatively stable with the exception of two profiles, 4c01684 and 4c01681, where closure did not occur within the 1km survey area. The area in which the depth of closure becomes shallower (Westernmost profile 4c01729 to 4c01714) correlates with an increasingly wide nearshore zone shown by the position of the -5.0 mOD contour (Figure 2.4); and a reduction in bed slope from the steepest Westernmost profile 4c01729, which was two orders of magnitude greater than the Central (4c01702) and Easternmost (4c01677) profiles (Figure 2.5, panel A). East of Profile 4c01714, the bed slope is relatively constant (Figure 2.5) and so cannot explain variations in the depth of closure in this area.

2.4.4 Nearshore transport estimation

The estimated volumetric sediment transport rates suggest that easterly longshore transport is dominant, being an order of magnitude greater than westerly transport, and two to three orders of magnitude greater than cross-shore transport (Figure 2.6). As different longshore sediment transport equations are used for the fine and coarse fractions, the results are not directly comparable. However, these indicatively suggest that the transport rate of sand may be up to one order of magnitude greater than for the coarse sediment. The gradient in longshore transport rate shows a west to east transition from a more erosive environment to a depositional environment.

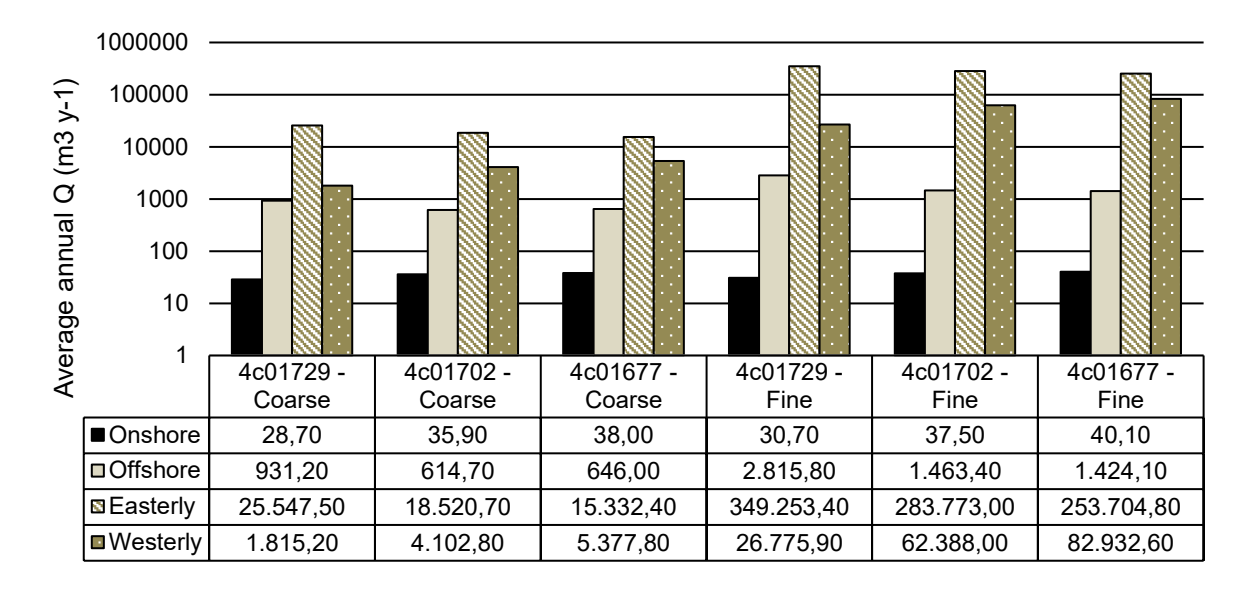


Figure 2.6 – Estimated long and cross-shore sediment transport approximated on the beach face at the Westernmost (4c01729), Central (4c01702) and Easternmost (4c01677) profiles. Cross-shore transport is estimated using Bailard and Inman, (1981) whilst longshore transport is estimated using Damsgaard and Soulsby (1996) and Soulsby, (1997) for the coarse (medium pebble, 12 mm) and fine (fine sand, 161.5 μm) fractions, respectively.

2.4.5 Sediment analysis

The sediment sampling which took place along the central profile (Figure 2.2) showed that mud is abundant within the nearshore sediments of Pevensey Bay (Table 2.3). The sample types varied from unimodal to polymodal and were typically very poorly sorted, but occasionally moderately sorted. The mud content of the total sample weight varied between 5-30% with an average of 12% mud content in July, and 2-73% with an average of 39% in September. Small amounts of gravel were present in the grabs recorded in July, supporting the backscatter substrate mapping shown in Figure 2.5. However further samples taken in the winter months may confirm this as fine material allowed to settle out in the summer months is resuspended.

Table 2.3 – Mud, sand, gravel ratios by weight taken from samples at the instrumented array.

	West array			East array				
Metres	% mud	% sand	% gravel	class	% mud	% sand	% gravel	class
offshore								
July sample								
500	5	95	0	sand	7	92	1	sand
1100	6	94	0	sand	30	70	0	sandy mud
1700	5	65	30	gravelly sand	27	73	0	sandy mud
2300	7	93	0	sand	8	78	14	gravelly sand
September sample								
500	31	69	0	muddy sand	35	65	0	muddy sand
1100	34	66	0	muddy sand	53	47	0	sandy mud
1700	64	36	0	sandy mud	73	27	0	sandy mud
2300	21	79	0	muddy sand	2	98	0	sand

2.4.6 Sediment balance

The majority of the beach profiles have experienced steepening between 2003 and 2022 (Figure 2.7, panel B). East of Profile 4c01719, the steepening was typified by the landward retreat of the MLWN mark (averaging ~15 m with a peak value of nearly 40 m), and a relatively stationary MHWN mark (+/-5 m change), most likely due to the beach management activities work to maintain the position of the crest. West of Profile 4c01719, the changes in MHWN and MLWN were generally of a smaller magnitude and showed retreat, suggesting regression of the shoreline in this area. The bay planform is of a typical embayment, with the beach orientation becoming aligned with oncoming wave crests with increased distance from the fixed 'headland' at Sovereign Harbour. The beach orientation is also shown on Figure 2.7, panel A. The shoreline orientation suggests a switch from beach profile regression to steepening as the beach orientation becomes greater than ~30°N. Overall changes in the cross-sectional area of the nearshore overtime suggest loss of sediment across the bay (Figure 2.7, panel C). Although the error is relatively high, consistent loss over the years across the bay suggest a clear trend.

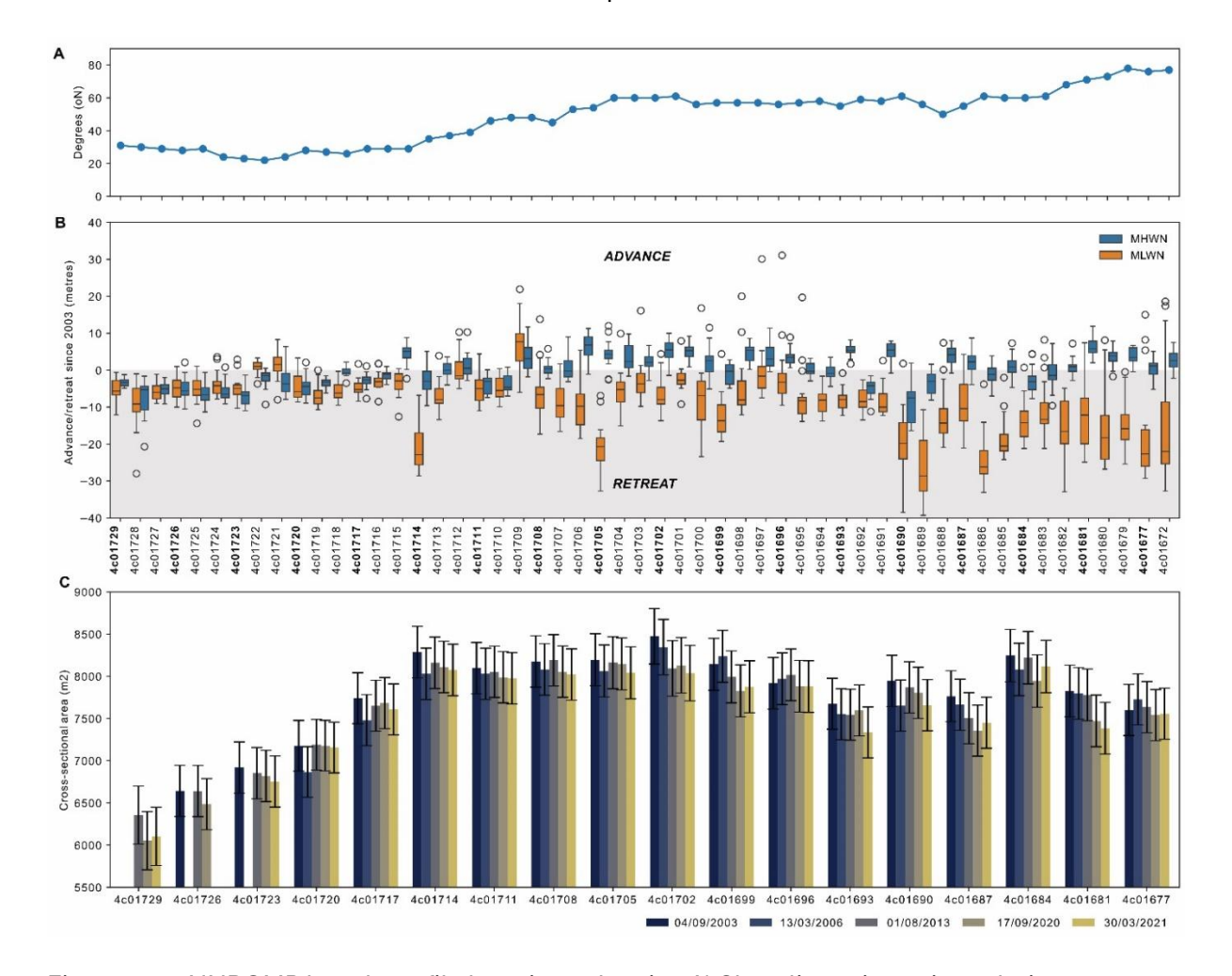


Figure 2.7 – NNRCMP beach profile locations showing A) Shoreline orientation relative to degrees north (°N) where a beach facing South would be 90°N, whilst a beach facing North would be 270°N; B) Change in lateral position of MHWN and MLWN relative to their position in 2003, with outliers shown as white dots; and C) the cross sectional area for the 18 surveyed profiles displayed with error bars showing the upper error estimate of ±0.3 m multiplied by the length of the profile to give areal error.

2.5 Discussion

Heterogenous, mixed sediment environments have a variable depth of closure which varies spatially due to the distribution of sediments and variations in grain size. In a controlled environment, mixed sediments are likely to contribute to a shallower depth of closure, and lower bed elevation change in comparison to an equivalent 'pure sand' setting due to a higher critical threshold for motion, related to increased sediment size, the shielding of finer sediments and/or the cohesive effects of muds and clays. When compared to the predictive equations, the observed depths of closure were consistently shallower, however, results indicating a shallower observed depth of closure are common (Barrineau, Janmaat and Kana, 2021) and explanations include: 1) 'real-world' conditions never reaching an equilibrium state due to non-stationarity; 2)

constraining geology; and 3) bathymetry surveys not capturing the greatest change, as the profile of the seabed recovers after the peak of the storm (Robertson et al., 2008).

The interpretation of the variation in the depth of closure at complex sites such as Pevensey can be assisted through systematic assessment of the physical parameters outlined in Figure 2.1, namely 1) bed slope, 2) bed resistance, and 3) hydrodynamics.

At Pevensey, changes in the depth of closure were likely related to the availability of mobile sediment and bed slope. The gradient of the longshore transport rate (high to low moving west to east) results in a transition from a more erosive to more depositional environment. We postulate that as hydrodynamic conditions become more conducive to deposition, there is greater sediment availability (mainly in the form of bedform features) and that this contributes to a deeper depth of closure in this area. The impacts of this progression explain the increase in bed elevation change from west to east (Figure 2.4) as the increased likelihood of deposition leads to sediment available for mobilisation. Additionally, each year approximately 20,000 m³ of sediment is placed at the Westernmost (4c01729) profile locally increasing the volume of available sediment. These observations go some way to explaining the variations in the depth of closure within the study site, which was shown to decrease in depth from west to east between the Westernmost (4c01729) profile and profile 4c01714, and then gradually deepen from the minimum at 4c01714 towards the Easternmost (4c01677) profile. It is also thought that the very steep nearshore slopes in the very west of the frontage (Westernmost profile 4c01729 to 4c01723) may contribute to a deeper closure depth at this location, due to greater offshore transport. The indicative bed type did not help explain variations in the depth of closure. Notably the shallowest depth of closure was observed in a purely sandy area, whilst the areas with gravel outcrops were up to ~3m deeper over the short term (Figure 2.5, panel B). This may be due to the fact that the gravel beds only make up a small percentage of the total bed material in this area, and we postulate that the observed depth of closure is dependent on the modal or smallest sediment size, rather than the larger grain sizes. The influence of cohesive sediments at Pevensey is not understood, as the sediment sampling showed that the distribution of mud varied widely in both space and time. It is likely that the cohesive sediments are exerting some form of control, as the effects of mud strengthening bed resistance have been observed with thresholds as low as 3-18% in sand mud environments (Mitchener and Torfs, 1995), and they were found to average 12 to 39 % at the study site. However, the cohesiveness of the muds will also be influenced by their mineral composition, water content and whether any biofilms were present (Grabowski, Droppo and Wharton, 2011; Jacobs et al., 2011). These factors could play an important role in the dynamics of mixed sediment nearshore environments, and further work is required to understand both the wider spatial distribution and the effects on bed mobilisation. The exploration of the nearshore zone of this mixed sediment environment using observational data, brought to light three specific findings which may be applicable to sites of a similar nature:

- 1. Low magnitude observed bed elevation change: The site generally experiences very low magnitude bed elevation change across the frontage, which does not increase over the medium term (19 years of data). For instance, between the Autumn 2020 and Spring 2021 surveys bed elevation change across the frontage typically ranged between 0.1 0.6 m, only exceeding this at the Westernmost profile, 4c01729, following a beach recharge (Figure 2.4). At the Central profile 4c01702, the bed levels across the subtidal profile were shown to consistently fluctuate between 0 and 0.3 m over the longer time periods (~6 months and greater), and at the shorter time intervals changes related to the transverse bars could be seen (Figure 2.3), suggesting that the bed elevation change is tied to the amplitude of these bedforms. This is a problem for detecting the depth of closure using a survey error threshold approach, such as that employed by Pagán et al. (2017), as there is a reasonable chance that the maximum survey error threshold (±0.3m) may not be exceeded. Using the absolute survey difference, or standard deviation between more than two surveys to find the depth of closure from the non-zero tail was a suitable alternative to this.
- 2. Wave driven morphodynamic change: Spikes in bed elevation change, found around the 300 m, 600 m and 950 m chainage show that sediments are mobile across this area, which are due to the infilling of troughs as a transverse finger bar system moves alongshore (Figure 2.3; Townsend et al., 2023). Figure 2.3 also shows that there is no bed change in these areas during the summer, which suggests this movement is seasonal and driven by waves, not tidal currents. To successfully capture the lower limit of this active area, it was necessary to ensure all areas of reopening were captured above the depth of closure as the landward minimum morphological change, was found in much shallower water. It is unknown why there is an area of minimum morphological change in this area, between larger magnitude changes on the upper mixed gravel sand beach and further offshore. However, we postulate that the peak changes are related to the different sediment fractions response to waves, with the offshore peak morphological change linked to a more mobile sandy bed, whilst the changes in the upper beach reflect berm movement, either by waves or through beach management activities.

 Between these two peaks sits the landward minimum morphological change, representing an area which is relatively stable in comparison to the changes around it.
- **3. Peak morphological change.** The identification of the location of peak and secondary peak morphological change, show that the largest volumes of bed level changes are primarily found offshore, between the -5.0 and -6.0 mOD depth contours, located approximately 0.4 to 1.0 km offshore. Greater variation in bed elevation across nearshore profiles was found towards the

east (Figure 2.4); suggesting that there is more sediment availability and mobility on a wider nearshore platform. This agrees with the work of Hamon-Kerivel et al. (2020) who classified the shoreface based on sediment availability. The upper, reflective part of the beach was also highlighted as a key area of change. Although without the active recycling works and artificial import of sediment countering erosion, the changes in this area could be far larger.

Long term loss of sediment was observed across the nearshore since 2003, which is concurrent with the findings of Thomas (2015) who found loss of intertidal sediment below MSL between 2003 and 2015. The losses observed across the nearshore equate to small changes in elevation, but over a much larger area, are vast in comparison to the observed changes in the upper beach sediments, something that was also highlighted by the analysis of the location of the peak morphological change. The beach management efforts at Pevensey are effectively locking the shoreline in place, leading to coastal steepening along two thirds of the beach profiles (Figure 2.7). The loss of volume of nearshore sediment is most likely due to the dominant easterly transport (Figure 2.6) with limited supply of sediment from the west. Littoral drift analysis showed shingle volumes that were comparable to those deducted from a regional sediment budget for the upper beach (Environment Agency, 2015) however, the sand volumes, which were an order of magnitude larger, remain unvalidated. Should the changes observed in the nearshore and lower intertidal area continue, increases in wave power reaching the shore may be expected, compounding the effects of sea level rise. Dornbusch (2017) showed that to prevent the drowning of 190km gravel barrier beaches in the South East of the UK (including Pevensey Bay) from sea level rise, increases in barrier crest height, and therefore upper beach volume, and longshore transport control measures would be required, resulting in significant increases to cost. The beach management activities which are undertaken today counteract the ongoing loss of upper beach (mainly coarse) sediment from the study area, but they do not address the long-term loss of nearshore sediments. Unless the upper beach can be allowed to migrate landward and form a more natural profile, the beach could be expected to continue to move towards a maximum steepness, leading to increased wave reflection and ongoing loss of fines from the foreshore and requiring increased engineering intervention to prevent drowning/breach of the shingle barrier.

Further work is needed to understand the nearshore zone and quantify its changing behaviour on the current shoreline policy of hold the line. To aid in this advance, we make the following recommendations. Firstly, it is imperative that greater assurance is gained from bathymetric data to help inform management decisions. Currently, bathymetric data is generally quoted as having +/-0.3m vertical accuracy, which encompasses composite error from both the sonar instrumentation, Inertial Motion Units and positional error (from Global Navigation Satellite System). Secondly, this work has shown the importance of the nearshore to the upper beach

sediments, and therefore strategic coastal monitoring should adapt to take these findings into account. Finally, the interpretation of the backscatter imagery from the 2013 multibeam survey and sediment samples taken from the array area showed a highly variable spatial and temporal distribution of sediments. From the information we have at present we cannot derive an accurate picture of how the bed changes overtime and whether the changes observed are the result of loss of fines, or whether coarser material is also being lost. Therefore, to better understand the resilience of this shoreline, a better understanding of the sediments distribution through space and time should be gleaned.

2.6 Conclusions

This paper examines the relationship between the effects of shoreline management on beach steepening and the nearshore zone; using the bed elevation change and the depth of closure to describe the extent and behaviour of the active nearshore zone. Comparisons were made between observed and predicted depths of closure, finding that the Birkemeier equation was the closest approximation for a lower limit of change, yet, variation was found between the observed and predicted depths across the site at both seasonal (differences between 0.37 m deeper and 3.33 m shallower) and decadal (differences between 0.17 m deeper and 0.73 m shallower) timescales. A conceptual model outlining the physical parameters that influence the depth of closure was used to systematically interpret the variations seen across the site. The need for a greater understanding of sediment grain size, including cohesive sediments was highlighted, as sampling from one location revealed high temporal and spatial variability in mud content which is known to affect the mobilisation of sediments. Three further findings specific to the site but of potential interest to other mixed sediment sites were also made: 1) the seabed elevation change is very low (typically c. 0.3 m, the same magnitude as the upper limit for survey error) and thought to be limited in some locations to the amplitude of the bedforms in the area; 2) the magnitude of changes in seabed elevation varied over short timescales, suggesting, as could be expected, most change occurred during the winter months or post storm activity; and 3) it is thought that there is a relationship between the magnitude of the most seaward peak or secondary peak morphodynamic change (ignoring changes to the upper beach) and the width of the nearshore zone, implying that the wider nearshore zone has more freely available sediment. Finally, the long-term changes to the upper beach profile were considered in relation to the nearshore. It was found that coastal steepening had occurred to over two thirds of the beach profiles and that the cross-sectional area of the nearshore zone had also decreased over time, which could both contribute to increased need for beach management activities in the future, although the effects are currently unquantified.

2.7 Declaration of Competing Interest

The authors declare that they have no known competing financial interests or personal relationships that could have appeared to influence the work reported in this paper.

2.8 Acknowledgements

This work was supported by the Environment Agency through the project: "Delivering Legacy from the Pevensey Bay Coastal Defence Scheme (PI: Kassem, H.; Contract: 201-09-SD10). The lead author undertook this work as part of their PhD studentship, funded by NERC INSPIRE DTP (NE/S007210/1), the Graduate School of the National Oceanography Centre, Southampton, and the Environment Agency. Our thanks also go to Ian Thomas and Amber Carr of Pevensey Coastal Defence Ltd, and Peter Amies and Rebecca Manning of the Environment Agency for their time, on-site support, and site background information. Further thanks go to those involved with the National Network of Regional Coastal Monitoring Programme for England, in particular Dan Amos of Adur-Worthing Councils and Stuart McVey of New Forest District Council.

Chapter 3 Seasonal mobility of transverse finger bars within a mixed sand-gravel bay measured using X-band Radar.

Dominique Townsend₁, Julian Leyland₁, Hachem Kassem₂, Charlie Thompson₂₃, Ian Townend₂, Paul Bell₄, Cai Bird₅

- ¹School of Geography and Environmental Science, University Road, Southampton, Hampshire SO17 1BJ
- ² School of Ocean and Earth Science, University of Southampton, Waterfront Campus, National Oceanography Centre, European Way, Southampton, SO14 3ZH, UK
- ³ Channel Coastal Observatory, Waterfront Campus, National Oceanography Centre, European Way, Southampton, SO14 3ZH, UK
- ⁴ National Oceanography Centre, Joseph Proudman Building, 6 Brownlow Street, Liverpool L3 5DA, UK
- ⁵CoastSense Ltd, 320 Mariners House, Liverpool, L1 0BG

3.1 Abstract

Transverse finger bars have largely been associated with sandy coasts. Here we show that these features persist within a wider mixed sediment environment, adjacent to a shingle cuspate foreland, which has not been previously reported. Details of the bar's characteristics were gleaned from analysis of bathymetry data, whilst weekly migration rates were inferred from remote sensing of the sea surface roughness as a proxy of undulating bedforms, using X-band radar reflectance data. The bars were on average ~381 m long, had wavelengths of ~156 m, amplitudes of approximately 0.2 to 0.6 m and were orientated 150 degrees to shore normal. The bars migrated by approximately 150 m over the first 'winter' observation period (15/11/2020 – 02/04/2021) and 70 m in the following winter period (Sept 2021 – Feb 2022) but showed virtually no signs of movement during the intervening summer months. Analysis of hydrodynamic conditions suggested the bar

mobility was related to the dominant longshore currents resulting from high angle, south westerly waves. Low amplitude rhythmic bedforms were also found in the upper beach, migrating at a similar rate to the nearshore bars, which are thought to be driven by the same high-angle wave instability.

3.2 Introduction

Shallow seas occupy around 7.5% of the ocean's surface, comprising the area above 200m depth which marks the transition between the continental shelf and deep ocean. Across the world this area is made up of an incredibly diverse range of sediments, geological and geomorphological features. Amongst the most striking are rhythmic bedforms, with wavelengths ranging in scale from centimetres to 100's of metres: they are found in both deep and shallow water (Swift et al., 1978; Amos and King, 1984; Boczar-Karakiewicz and Bona, 1986). Of these, ripples, dunes, and bars are known to form as near bed flow reaches a critical velocity, which is dependent on grain size. In the right conditions, these features migrate, usually in the dominant direction of flow, transporting sediment in the process. Whilst the conditions for small scale bedform formation can be easily recreated in the lab, there is less confidence in the formation of larger scale features, especially those found within the nearshore zone, i.e. the zone affected by waves and tides, where behaviour is complex and subject to a number of non-linear interactions between waves, currents and the underlying topography itself (Holman, 1995; Chen, Madsen and Basco, 1999; Touboul, Morales-Marquez and Belibassakis, 2024). Observational data from the nearshore zone is typically scarce and hard to come by as it is both expensive and can be challenging to collect. This study uses a unique high temporal resolution dataset collected using X-band radar to study the movement of a series of transverse finger bars in an environment in which they have not previously been observed and links their mobility to driving forces and theory.

Transverse bars, *i.e.* bar like features which lie approximately normal to the shoreline orientation (Shepard, 1952), are reported globally, in various forms on open coast, tidal inlets and sheltered backwaters (Konicki and Holman, 2000; Ribas and Kroon, 2007; Pellón, Garnier and Medina, 2014; Falqués *et al.*, 2021). Their cross-shore extent has been found to range in scale from 10s to 1000s of m (Carter, 1978; Gelfenbaum and Brooks, 2003); they have been found in both microtidal and

macrotidal coasts (Konicki and Holman, 2000; Levoy et al., 2013); and there is no universal agreed formation mechanism (Falqués et al., 2021). Niedoroda and Tanner (1968) described the bars as equilibrium features, forming (permanently or ephemerally) when sediment transport, waves and currents were balanced. Pellón et al., (2014) grouped transverse bars into four groups: transverse bars and rips, large-scale finger bars, finger bars of intermediate beaches and low energy finger bars. Note that the term 'finger' is used to describe bars where the cross-shore length of the bars exceeds the alongshore width, giving a finger like appearance (Niedoroda and Tanner, 1970). 'Transverse bars and rips' are not discussed further here as their formation is due to the onshore welding of crescentic bars, enhanced with rip flow which is different from the other types of transverse bar explored below, and unlike those found within the study site. Instead, we focus on finger bars, collectively comprising three of Pellón et al.'s (2014) transverse bar groups:

- Large-scale finger bars are distinguished from other finger bars by their magnitude, with cross-shore extents typically exceeding 1000 m (Pellón, Garnier and Medina, 2014). They are found on very shallow, low wave energy coasts, and observations of annual migration rates are low, not exceeding 10-20 m per year (Niedoroda and Tanner, 1970; Goud and Aubrey, 1985; Gelfenbaum and Brooks, 2003). These features have been observed over long time periods (in excess of 40 years) and are also typically orientated normal to the shoreline. Additionally, large scale finger bars have been reported on macrotidal coasts, in the vicinity of ebb tidal deltas and inlet systems (Levoy et al., 2013; Brakenhoff, Ruessink and van der Vegt, 2019).
- Intermediate energy finger bars are ephemeral features which can form under certain constant wave conditions, consisting of oblique intermediate energy waves (Ribas, Falque and Montoto, 2003). They are of a smaller magnitude than the large-scale finger bars, (~100's m), can be associated with nearshore bars, and are up-drift orientated (Konicki and Holman, 2000; Ribas and Kroon, 2007).
- Small scale finger bars are found in fetch-limited areas (<10km), and are persistent, downdrift orientated features. They have been shown to migrate during stormy periods, with limited movement during summer periods, although measurements of migration rates are limited (Pellón, Garnier and Medina, 2014).

There are two key theories on the formation of transverse finger bars: the forcing template theory and the self-organisation theory. The first theory, forcing template theory assumes a fixed flow, caused by low-frequency standing edge waves, or progressive infragravity waves, which can moderate shoreline morphology (Guza and Inman, 1975). Edge waves are formed by infragravity waves becoming 'trapped' at the shoreline, due to refraction and reflection effects. Studying the Atlantic shelf of North America Boczar-Karakiewicz and Bona (1986) reasoned, that linear sandy ridge bedforms with wavelengths in the order of km, must have been formed by infra-gravity waves with periods between 0.5 and 5 minutes as only they would be large enough to drive the formation of these bedforms. However, forcing template theory has since been questioned in the context of transverse bars, as it ignores any interaction between the bedforms and the hydrodynamics (Coco and Murray, 2007; Ribas et al., 2015). Furthermore, infragravity waves are known to be progressive and move much faster than the bedform migration (Ribas et al., 2015). The second theory of selforganisation was initially developed by Sonu (1968) suggesting that the formation of transverse bars is caused through positive feedbacks, between longshore hydrodynamic processes (longshore currents) interacting with uneven bathymetry. Falqués et al., (2021) also recognized the potential for cross-shore processes to create positive feedback between wave refraction and bars for shore-normal wave incidence in case of very shallow terraces, i.e. sandy deltas. On the basis of self-organisation theory, several linear and non-linear stability analyses have successfully predicted the number, spacing and amplitude of bars on straight coasts, although they have been found to overestimate migration rates (Ribas and Kroon, 2007; Falqués et al., 2008; Ribas et al., 2011). Further developments show that cross-shore variations in the depth-averaged sediment concentration play a highly important role in determining whether bar features are orientated up or down-drift relative to the predominant current (Ribas et al., 2015).

In heterogenous bed sediments, complex sorted bedforms can form (Murray and Thieler, 2004; Coco et al., 2007; Coco, Murray and Green, 2007). Although typically irregularly spaced, these features can be rhythmic forming every 5 to 400 m and can be found in water ranging from 0 to 90 m depth (Coco et al., 2007). Some, but not all, sorted bedforms have been observed to migrate, however, all are considered to demonstrate sorting of sediments based on size. It is thought that the variations in grain size across the sorted bedforms are caused by variations in near bed turbulence, which is greater in areas of coarser sediments, which in turn enhances entrainment

and reduces the likelihood of fine material settling out. Ergo, finer material favours deposition in areas with a finer grain size bed, and a feedback mechanism is produced, leading to ongoing sorting and more distinct patterns. Similar feedback mechanisms may be important in areas where rhythmic features occur alongside gravel outcrops (McNinch, 2004; Schupp, McNinch and List, 2006).

Although some progress has been made in studying these bars in the last 30 years, the available measurements of their characteristics, migration rate and sedimentological properties are sparse (Pellón, Garnier and Medina, 2014; Ribas et al., 2015). Studies thus far have almost solely explored features found on sandy, microtidal and straight coastlines (Schupp, McNinch and List, 2006; Levoy et al., 2013; Brakenhoff, Ruessink and van der Vegt, 2019). This study aims to expand the current knowledge of these systems by reporting these bar characteristics for the first time on the lee side of a cuspate foreland within a macro-tidal, mixed sediment environment. A thorough investigation of the bars' morphology and behaviour was undertaken through the quantification of bar characteristics, surficial sedimentology, seasonal migration rates and efforts to understand the wider geomorphological setting of the study site.

3.2.1 Study site

The study site, Pevensey Bay, is a composite, mixed sand and gravel barrier beach located on the South East coast of the UK. The steep reflective upper beach is comprised of mixed sandy gravel, with a median grain size (D_{50}) ranging between 8 to 12mm across samples (Dornbusch, Williams and Moses, 2005), and the shallow sandy terrace fronting the upper beach is formed of fine sand with a median grain diameter of $159 - 164 \,\mu m$ (Townsend *et al.*, 2024). The barrier beach fronts approximately $50 \, \mathrm{km^2}$ of freshwater low-lying alluvial deposits, which are bordered to the west by the chalk ridge and headland the South Downs, terminating at Beachy Head, and the Wealden uplift formation to the east (Figure 3.1, Sutherland and Thomas, 2011; Jennings and Smyth, 1990). The beach is fronted by a gently sloping sea bed and is partially constrained in the nearshore by rock outcrops at the western extent of the site (Figure 3.1; Townsend et al., 2024). Subtidal bed sediments are complex mixtures of muds, sands and gravels (Townsend *et al.*, 2024), with evidence for drowned barrier beaches further offshore (Mellett *et al.*, 2012). There is no evidence for present day onshore migration of these large gravel deposits (Nicholls, 1991). The gravel barrier

Chapter 3

which makes up approximately three quarters of the length of the site conjoins with a cuspate foreland, known locally as the 'Crumbles' (Figure 3.1). Pevensey Bay is a local depocentre, *i.e.* the area of greatest sedimentation over the medium- to long-term (Halcrow, 2010), and gravel deposits at the site have been reported to be approximately 33m deep (Jennings and Smyth, 1990). The cuspate foreland was formed between 800 – 300 years before present following the vast supply of gravel rich sediment from the west (Nicholls, 1991), and has since been in decline for 300 years (Jennings and Smyth, 1990). In 1993 the Crumbles cuspate foreland was excavated and transformed into a large commercial harbour, with two rubble mound breakwaters constructed at the entrance (Sutherland and Thomas, 2011). This interrupted the natural flow of sediment and to counter this loss, approximately 110,000 m³ of sediment is recycled, renourished and bypassed into the Pevensey Bay frontage each year, to maintain the volume of the beach which serves as an important flood defence. Approximately 40 km down drift (east) of the Crumbles site, is the much older and larger cuspate foreland system of Dungeness (Plater et al., 2009, Figure 3.1). Transverse finger bar formations are visibly present to the east of both cuspate forelands.

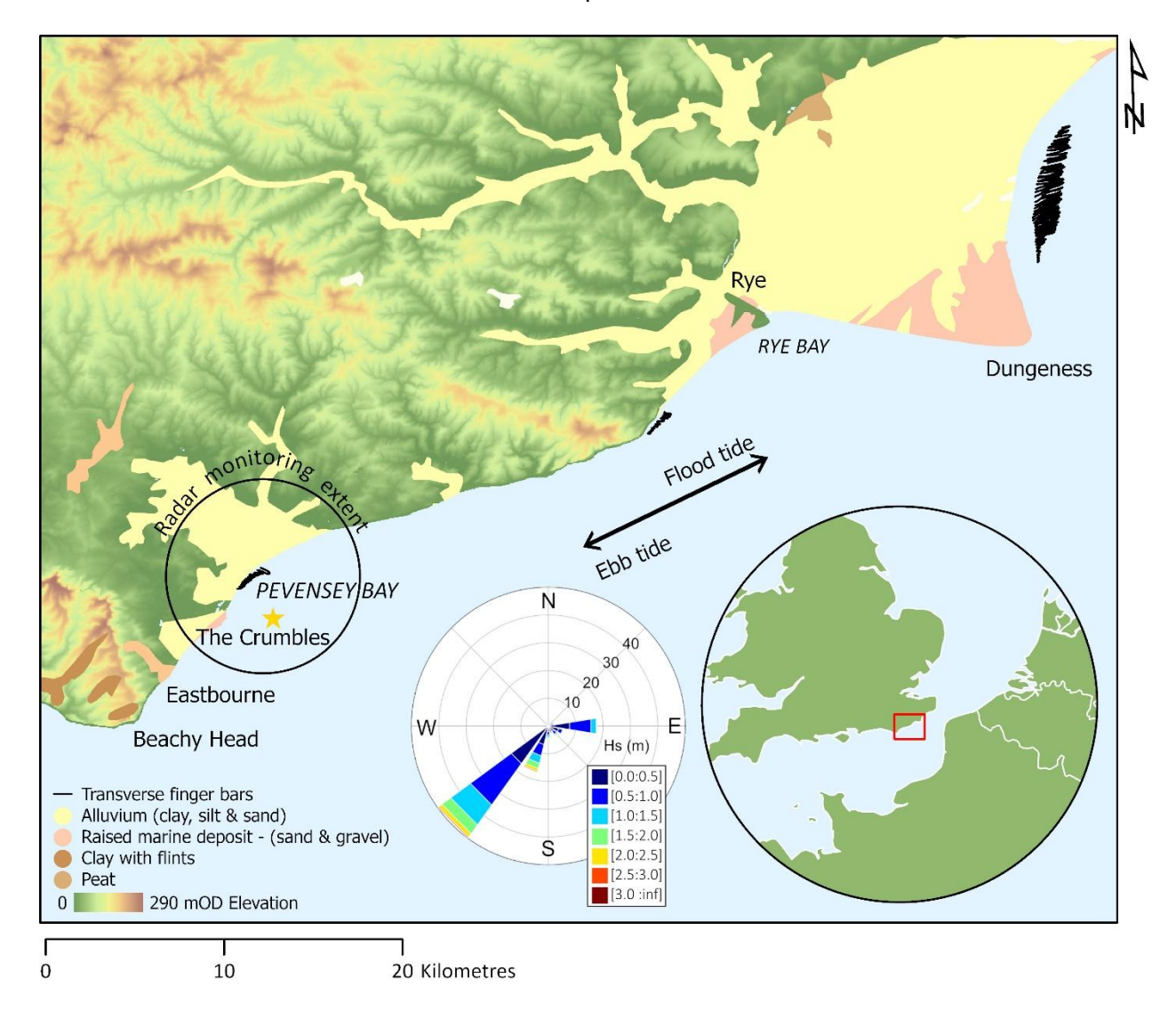


Figure 3.1 – Transverse finger bar locations in relation to the Crumbles and Dungeness cuspate foreland formations with regional setting inset. Star shows location of the Datawell MkIII directional wave buoy within Pevensey Bay, which is part of the NNRCMP network (channelcoast.org). The data from this wave buoy between June 2003 and November 2022 is shown binned as a wave rose. Figure contains Ordnance Survey Terrain 50 open height dataset © Crown copyright and database right 2023. Surficial sediment deposits © British Geological Survey 2024.

3.3 Methods

Geospatial analysis of bar characteristics from Multi Beam Echo-Sounding (MBES) digital elevation models is described in Section 3.3.1. Following this, the collection and analysis of samples to determine grain size statistics are described in Section 3.3.2. Section 3.3.3 gives the procedure used to examine bar movement using surface roughness images created from raw X-band Radar data. Finally, an exploration of rhythmic features in the upper beach at Pevensey Bay are also examined, using 19 years of topographic data.

3.3.1 Bar characteristics measured using MBES

The physical characteristics of the transverse finger bars at Pevensey Bay were measured from MBES data, recorded on the 01/08/2013. The MBES bathymetry survey was commissioned by the National Network of Regional Coastal Monitoring Programmes (NNRCMP) and carried out by EGS International Ltd. The survey extended from Mean Low Water to approximately 1km offshore with 100% seafloor coverage to IHO Order 1a standard, and meeting the Maritime & Coastguard Agency (MCA) Civil Hydrography Programme Survey Specification 2013 (Channel Coastal Observatory, 2014). A Kongsberg EM3002D MBES was used to capture the data, which were processed in IVS Fledermaus version 7.3, by QPS Ltd. Quality-control of the data was undertaken by the UKHO. The data analysed here were downloaded from the Channel Coastal Observatory website (channelcoast.org) and comprised 1 m resolution data, projected to OSGB/Ordnance Datum (OD). For each bar: the length, wavelength (i.e. crest to crest distance), the most landward and seaward depth along the bar crest, form (chevron/linear) and angle (both to °TN and relative to shore normal) were recorded. Contours were generated at every 0.1 m relative to Mean Sea Level (MSL) which were used as a guide to measure the features within GIS software, ESRI's ArcGIS Pro version 3.0.2. The crestlines of the features were digitized from the point at which the first contour deformation was identified, to the deepest deformed contour, marking the base of the feature. In some instances, the orientation of the bar crestline changed direction, forming what we term a 'chevron' morphology. For these features a vertex was recorded at the junction of the change in crestline, and measurements were given for both the 'upper' and 'lower' section of the bar, as well as the combined measurements. The landward and seaward depths were measured from the start and end of these digitized lines, respectively, and the angle was calculated from the landward 'start' and seaward 'end' of each bar, relative to both true north and shore normal.

3.3.2 Sedimentology

Fifteen van Veen grab samples were retrieved along a shore-parallel transect within the transverse finger bar area on the 25/09/2022. The transect was approximately 250 m from the shore and the samples were taken between 10 and 50 m apart, spanning a length of ~500 m. Grain size analysis was completed complying to BS EN ISO 17892-4:2016. Samples were washed to remove salts over a $63\mu m$ sieve, retaining the water and visually checking the water colour for any indication of fine sediments, none were found. The samples were then dried in an oven and sieved with an Octagon200 sieve shaker, with ¼ phi mesh size grading, before weighing. Median grain size, sorting, skewness and kurtosis were calculated using the arithmetic method of Krumbein and Pettijohn (1938) using the Gradistat software (Blott and Pye, 2001).

3.3.3 Bar movement

X-band Radar reflectance imagery was used to detect the presence and migration of bedform features; Section 2.3.1 describes the theory behind the method, and Section 2.3.2 outlines the workflow used in this paper. The raw processing of the radar data and sea surface roughness images were carried out by Marlan Maritime Technologies Ltd (now CoastSense Ltd).

3.3.3.1 X-Band Radar & sea surface roughness

Radar (Radio Detection And Ranging), is the concept of accurately identifying a target and measuring its distance from the radio antenna signal's origin point (*i.e.* a Radar transmitter), using the basic relationship between speed and time. X-band Radar waves have a wavelength of 2.5 cm to 3.8 cm, with a frequency ranging between 8 to 12 gigahertz, which allows them to measure gravity waves on the sea surface in the presence of Bragg scattering (Nieto-Borge *et al.*, 2006). Bragg scattering is caused by the presence of capillary waves (mm scale wavelengths) superimposed on gravity waves (cm to m scale), creates a texturally rough sea surface. This sea surface can be modulated further when fast flowing tidal currents flow over uneven bedform

topography resulting in divergent flow, as turbulent vortices (kolks) are generated in the lee of the bedforms and 'boil' to the surface (Alpers and Hennings, 1984). Following this 'rougher' patch of water, convergent flow 'smooths' the sea surface. Whilst it is not possible to identify these 'smooth' and 'rough' patches of sea from individual snapshots in time, composite Radar images can provide information on surface roughness (Bell *et al.*, 2015).

3.3.3.2 Sea surface roughness to detect bedforms

A GEM Elettronica SuperNET with a 2.2 m radar antenna and a 12kW peak output power mounted was fitted to a lighting column mounting (Bird et al., 2019) and deployed at Pevensey Bay (50°48′51.5″N 0°21′30.3″E) between 11/11/2020 and 28/02/2023, with the antenna located at approximately 17 mOD, during which time it operated continuously until 25/09/2021. After this period, to avoid disturbing local residents the Radar operated on an event-based protocol, when wave conditions were forecast to exceed 1.5 m at the nearest wave buoy (50°46′54.6″N 0°25′06.0″E). During operation, Radar reflectance images were captured every 0.86 seconds covering a radial area of 6 km (4096 by 4096 pixels, 50° 52′ 4.062″N 0° 16′ 7.9176″E to 50° 45′ 38.6712″N 0° 26′ 54.0024″E), and approximately 12 km of coastline (2 km of which was shadowed by the cuspate foreland).

Raw (analogue) radar data were translated to digital signals in real-time by a 50MHz digitiser and computer located within the column of the Radar tower, where they were also stored. Most analogue ship's radars have an intermediate frequency (IF) bandwidth cutoff at around 18MHz, limiting the amount of 'information' capable of being carried by the signal, so the output video signals that are digitised are inherently limited in horizontal resolution to around 10m-20m. The 50MHz digitisation rate is tailored to capture the maximum possible information from such signals.

Once retrieved, the raw data were transformed from polar to cartesian co-ordinates with a x resolution of 4.38 m and a y resolution of 2.61 m to the WGS 1984 geographic co-ordinate system (Figure 2, A). A near real-time telemetry system then transferred these data to a server housed in the Marlan office in Liverpool, UK, where the sea surface roughness analysis was carried out.

The principle of the radar roughness analysis is to detect subtle tidally modulated sea surface roughness variations that can be an indication of the interaction of tides, waves and currents with

relatively small-scale subsurface sea bed features. Such roughness features may not be detectable in individual radar records, but a time series analysis over a number of tides can average out more ephemeral phenomena, revealing the sea surface signatures of more persistent features. While the analysis could be run on a single tide of data records in optimal conditions where sufficient sea surface signatures are present, 1-2 weeks of data are more optimal to reduce the noise and variability introduced from individual weather events and overcome periods of calm seas from which radar backscatter can be insufficient for detection of any sea surface signatures at all. Features of the scale of the finger bars discussed here are unlikely to migrate significantly within such a short time window, although smaller, more ephemeral sea bed sediment features may come and go at that timescale.

Data were averaged over weekly periods, *i.e.* starting at 00:00 Monday morning and finishing at 23:59 Sunday evening, producing 47 long exposure images of the sea surface over the total period of operation. In some instances, especially during the intermittent operation period, the number of images recorded was less than during normal operation; for instance, if the Radar were switched on from Monday to Wednesday, of one week, significantly fewer images would be included within that average. This is not thought to impact the overall results as the strongest signals are captured during the wave events, while during calmer conditions, all of the radar backscatter values are lower and contribute less to the overall imaging of the features.

The analysis procedure follows the flow diagram of Figure 3.2. Data bursts of 256 images were averaged to a single summary image to remove wave signatures and other ephemeral signals (Figure 3.2, A-B). The gradient of the averaged image is then calculated to highlight small scale structures in the signals (Figure 3.2, C). These gradient images were then binned into one of 12 tidal phase bins, associated with the M2 tidal period divided by 12 (Figure 3.2, D). After a week of data have been phase-binned in this way, an M2 tidal signal is fitted to each pixel (Figure 3.2, E). The fitted M2 signal provides an indication of subsurface sea bed features that influence sea surface roughness at a local scale (Bell *et al.*, 2015). The files were stored in Geo tiff file format with an arbitrary measurement unit, ranging between 0 and ~65 000 (Figure 3.2, F-G). The sea surface roughness gradient images were then imported into GIS Software, and the values were extracted every meter along a shore parallel transect, approximately 250 m offshore, which coincided with the mid-point of the crest for the majority of the transverse finger bars.

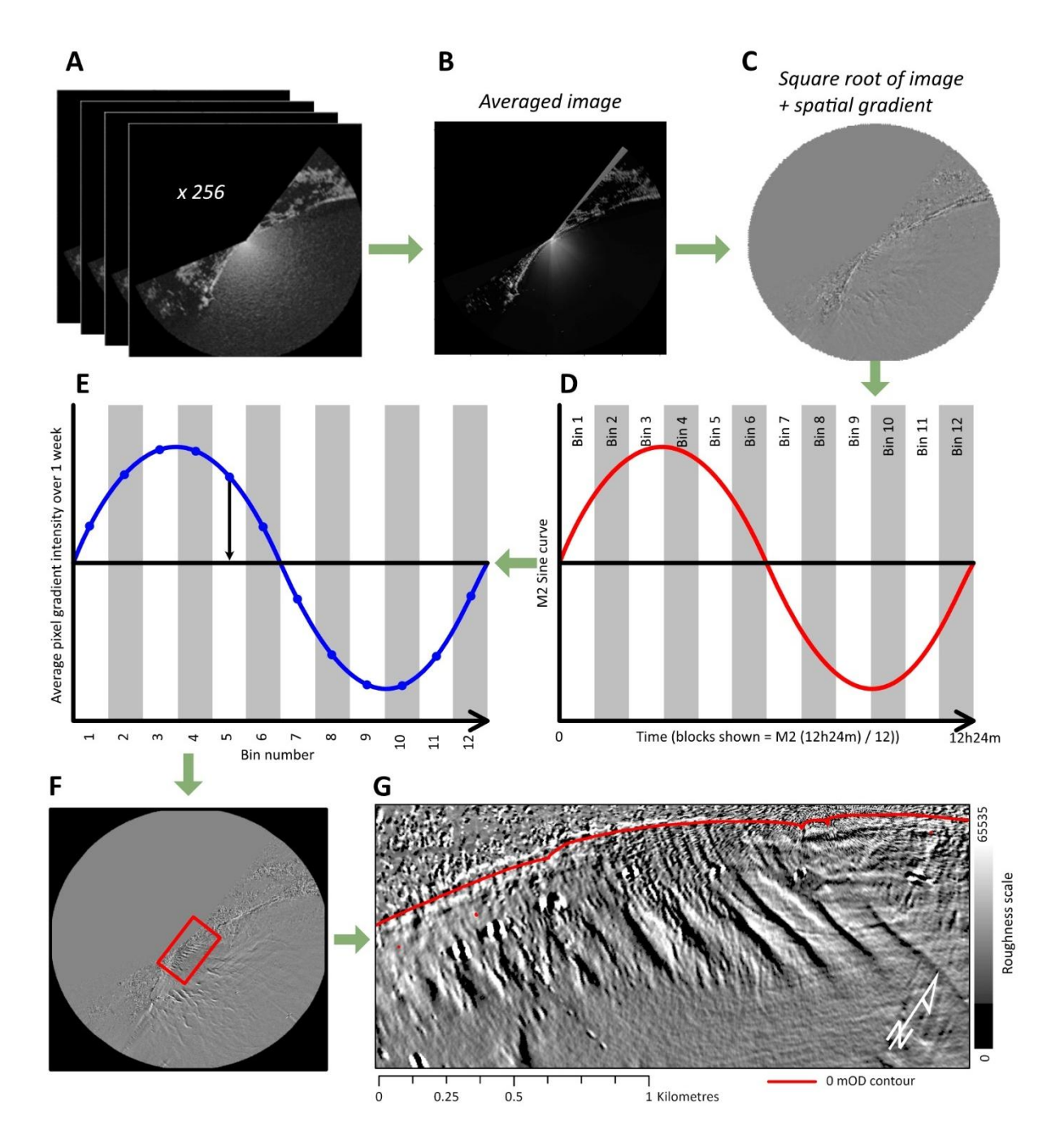


Figure 3.2 – A) 256 raw radar images (representing about 5 minutes real time); B) long exposure image (an average of the 256 images); C) image where each pixel has had the square root then spatial derivative taken; D) images are binned into 12 M2 tidal phase bins; E) the tidal signal is removed by fitting an M2 sine wave to average pixel values per bin (per

week) and then subtracting that value; F) the resultant sea surface roughness image with extent of; G) Zoom-in of F.

3.3.4 Hydrodynamic analysis

To understand the drivers behind bar mobility (between November 2020 and Feb 2022), wave records were analysed from the Datawell MkIII directional wave buoy, located within Pevensey Bay in approximately -9.8 m water depth (50° 46.91' N 000° 25.10' E). The wave buoy is part of the NNRCMP network of wave buoys; the data are freely available to download from https://coastalmonitoring.org/. Firstly, daily, and monthly mean values were calculated for the peak wave direction and wave power, which was calculated by the NNCMP as part of a QC process, for comparison to the Radar observation periods.

Secondly, littoral drift potential was estimated for the area of transverse finger bars. This was done using Soulsby's simplified version of the CERC transport equation (Soulsby, 1997):

$$Q = \frac{0.023g^{\frac{1}{2}}H_{sb}^{\frac{5}{2}}\sin(2\alpha_b)}{(s-1)}$$
 Equation 1

where g is acceleration due to gravity, H_{sb} is the significant wave height at the breaker line, α_b is the angle between wave crest of the breaking wave and the shoreline, and s is the density of the sediment. The significant wave height and wave crest angle was attained by transforming the wave record from the Pevensey Bay wave buoy (Figure 3.1) to a nearshore point at the edge of the surf zone using linear wave theory. Water depths were estimated with records from the Newhaven tide gauge, which lies approximately 20 km west of Pevensey Bay (50° 46.907'N, 0° 3.422'E). The transformation of the nearshore waves and littoral drift potential were calculated in CoastalTools, a freely available MatLab GUI (https://www.coastalsea.uk). A detailed description of the nearshore wave transformation is available in the supplementary material of Townsend et al. (2024) .

3.3.5 Upper beach volumetric analysis

A geospatial analysis calculating volumetric change between topographic surveys over time for the length of the study area within 50m bins has been performed over a 19-year period. The analysis

Chapter 3

used topographic data collected by Adur &Worthing Councils, as part of the NNRCMP (Table 3.1). The topographic surveys covered the entire upper beach, seawards of the beach toe, *i.e.* the point at which the steep mixed sand-gravel upper slope transitions to a flatter, sandier slope, down to the low water mark at the time of the survey. Before 2012, surveys involved backpack/quadbike mounted RTK GPS surveys, whilst from 2012 onwards, the survey is conducted using a quadbike mounted laser scanner. After quality checking the data, Triangular Irregular Network (TIN) surfaces are generated from individual points, and then converted into Digital Terrain Models (Table 3.1). Additionally, the laser scan data undergo a filtering process, removing any points above a set height which is determined per survey site, clipping the data (based on survey extents which helps exclude seawalls for example) and a further bare-earth classification, which ensures only the ground points are used to create the DTM (Dan Amos, *pers. comm*). This removes any unwanted points, e.g. sunspots, people, birds etc. The data are freely available to download from the NNRCMP website; www.channelcoast.org.

Table 3.1 – Data collected as part of the National Network of Coastal Monitoring Programmes of England NNRCMP used in the analysis of upper beach volumetric analysis.

Available DTMs	Survey type	DTM Resolution	Difference models	Analysis carried out by
2003 – 2005	GPS	1 m	2003 – 2004	Canterbury
2007	walked/quad		2004 – 2005	City Council
2009 - 2011	survey		2005 – 2007	(on behalf of
			2007 – 2009	Environment Agency)
			2009 – 2010	Agency
			2010 – 2011	
2012 – 2015	Terrestrial laser	1 m	2011 – 2012	
	scan		2012 – 2013	
			2013 – 2014	
			2014 – 2015	
2015 – 2022	_	Various: 0.5, 1	2015 – 2016	University of
		& 2 m	2016 – 2017	Southampton
			2017 – 2018	
			2018 – 2019	
			2019 – 2020	
			2020 – 2021	
			2021 – 2022	

Difference models, i.e. a surface model showing change in elevation between two time periods, were calculated between annual topographic surveys (Table 3.1), the majority of which were carried out in the winter period (October – April) with an aim to consistently represent the beach at its lowest, following any winter offshore movement of sediment. The difference models were calculated in GIS Software ArcGIS Pro, whereby the 'Raster Calculator' function was used to subtract the older grid data from the newer grid data to give the difference in elevation. The site was dissected by a series of polygon features; 50 m wide in the longshore direction by 500 to 1000 m in length. To accommodate changes in the orientation of the coastline, the orientation of the polygons change from 120°TN to 155°TN at approximately 3000 m chainage, resulting in 4 polygons with a reduced areal extent. To understand the total volume change of each 50 m polygon, the sum of the pixels from the difference model that fell within each polygon was calculated. If the resolution of the pixels was greater or less than 1 m, the result of the sum was adjusted accordingly (Table 3.1). For example, a 2 m resolution raster would be multiplied by four, whilst a 0.5m resolution grid would be divided by four, to convert the volumetric change from 0.5/2 m squared to 1 m squared respectively. The sum was calculated in ArcGIS using the 'Zonal Statistics as Table' tool. This work was an extension of analysis performed by Canterbury City Council on behalf of the Environment Agency as part of a Regional Shingle Beach Management Plan, which originally only covered the time period from 2003 – 2015 (Environment Agency, 2017). The transect area GIS shapefile is available as supplementary information.

3.4 Results

3.4.1 Bar characteristics

Fourteen transverse finger bars were observed in the MBES bathymetry data from 2013 (Figure 3.3). The bars ran parallel to each other, adjusting to changes in shoreline orientation. A cross section through the bars showed a slightly shallower slope on the western flank of the bars, and a steeper slope on the eastern flank, indicating eastward migration of the bars (Figure 3.3, subplot B). Amplitudes of the bars were shown to vary, and at the location of the cross section had local heights varying from 0.2 to 0.6 m (Figure 3.3, subplot B). Four of the bars had, what we term, a 'chevron' form, whereby closer to the coast the bars ran parallel with surrounding bars (downdrift

Chapter 3

aligned) but at some distance offshore had a change in crest orientation, or 'dog-leg' where the lower part of the bars became updrift aligned. The crestline of the bars were linear unlike barchan dunes which have a crescentic form (Hersen, 2004). The amplitudes of the bedforms varied between approximately 0.2 and 0.6 m (Figure 3.3, subplot B).

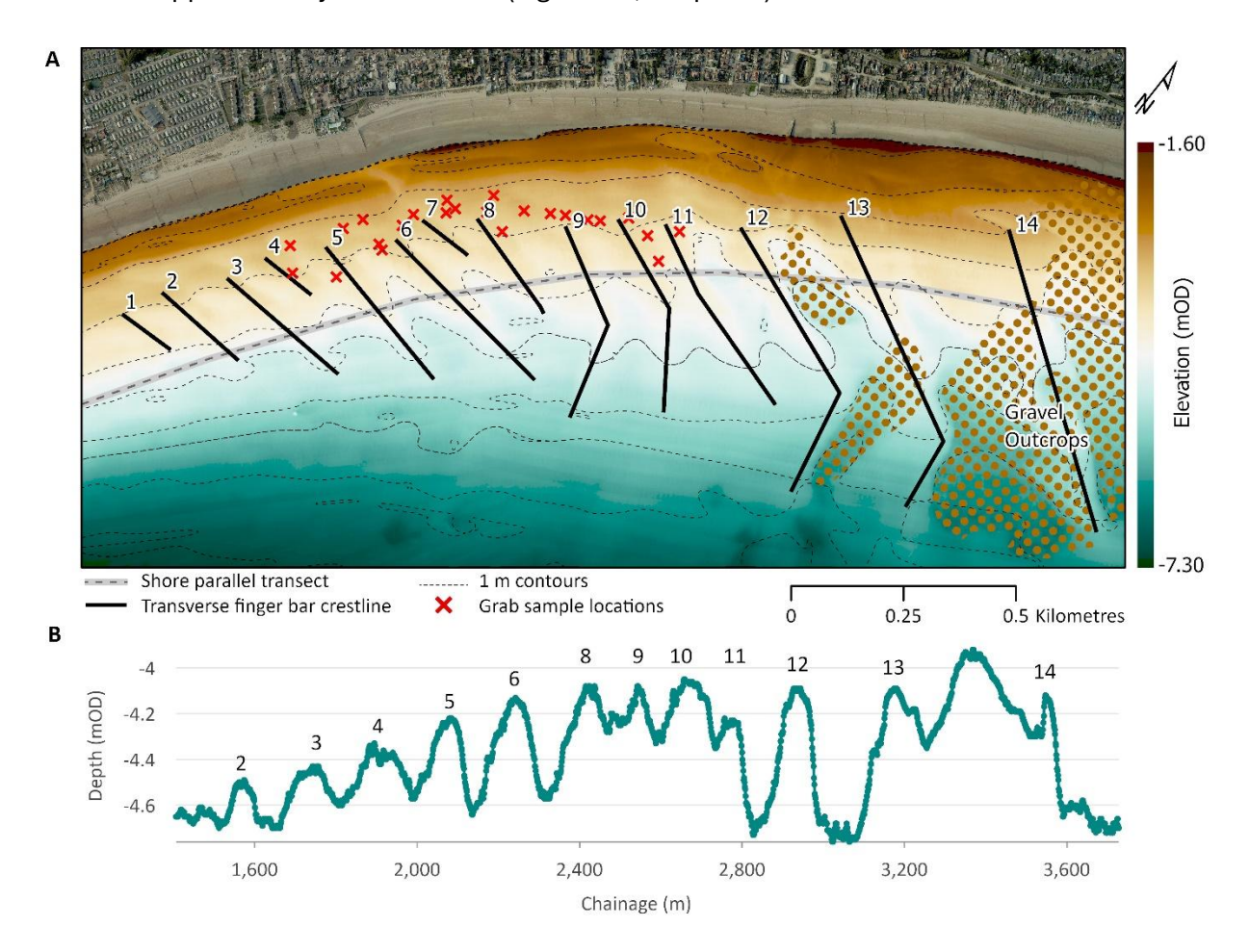


Figure 3.3 – A) Bathymetry of 14 transverse finger bars showing gravel outcrops to the east, smoothed 1 m contours, with orthorectified aerial photography (both collected as part of the NNCMP). Note the presence of two surface water outfalls just north of the 13th bar; B) Cross section through the bathymetry data showing local elevation of bars.

The bars' lengths ranged between 128 and 700 m long (381 m on average, with a standard deviation of 184 m), typically increasing from west to east (Table 3.2). The distance between one crest to the next (i.e., wavelengths) ranged from 74 and 375 m, with an average value of 156 m (Figure 3.3, Table 3.2). The orientation of the bars (the upper section of the chevron bars) was on average of ~93 °TN

Chapter 3

for bars 1-8 progressing to ~114 °TN on average for bars 9-14 as the shoreline orientation; the orientation relative to shore normal remained fairly constant at approximately ~150 degrees.

Table 3.2 – Pevensey Bay bar characteristics measured from 2013 MBES data (Channel Coastal Observatory, 2013). *For those bars with a Chevron form, the length and angles are given for both the upper | lower sections of the bar, with the sum or average given in brackets.

NUMBER	LENGTH*(m)	DISTANCE TO NEXT CREST (m)	LANDWARD DEPTH (mOD)	SEAWARD DEPTH (mOD)	FORM	ANGLE (DEGREES TN) *	ANGLE FROM SHORE NORMAL (DEGREES)*
1	135	101	-3.5	-4.3	Linear	86	147
2	228	148	-3.6	-4.2	Linear	92	150
3	327	96	-3.6	-4.9	Linear	91	151
4	132	137	-3.5	-4	Linear	88	145
5	380	157	-3.5	-4.9	Linear	101	151
6	439	74	-3.6	-5	Linear	95	154
7	128	122	-3.5	-3.9	Linear	88	159
8	259	197	-3.6	-4.6	Linear	105	152
9	239 222 (425)	118	-3.8	-5.3	Chevron	117 163 (139)	156 202 (178)
10	228 231 (441)	106	-3.7	-5.2	Chevron	110 143 (127)	149 180 (131)
11	472	167	-3.8	-5.1	Linear	109	146
12	429 245 (598)	224	-3.7	-5.7	Chevron	109 166 (124)	137 207 (157)
13	551 168 (663)	375	-3.3	-5.8	Chevron	116 170 (127)	166 204 (178)
14	700	0	-3.3	-5.6	Linear	124	152
AVERAGE	332 217 (381)	156	-3.6	-4.9	-	102 161 (107)	151 198 (154)
ST. DEV	165 29 (184)	82.69	0.15	0.60	-	12 10 (17)	7 11 (12)

3.4.2 Sedimentology

Sediment grab samples taken between ~150 and 300 m from the shore spaced at approximately 25 to 100 m from each other (see locations on Figure 3.3) showed that the surface sediments were well sorted, all with a median grain size of 125 μm (very fine sand). The frequency of the samples along the transect was adequate to sample on both stoss and lee sides of the transverse finger bars. No bathymetry data were recorded during the survey, due to equipment failure, so it was not possible to directly relate the positions of the grab samples to morphology of the bars.

3.4.3 Bar movement

A clear distinction between winter (mobile) and summer (immobile) bar movement was found (Figure 3.4). The bars are observed to migrate east by approximately 120 m between the 15/11/2020 and 28/03/2021, and again by ~50 m between 06/09/2021 and 15/02/2022. In contrast, over the interluding summer period (28/03/2021 to 06/09/2021), there is minimal apparent mobilisation.

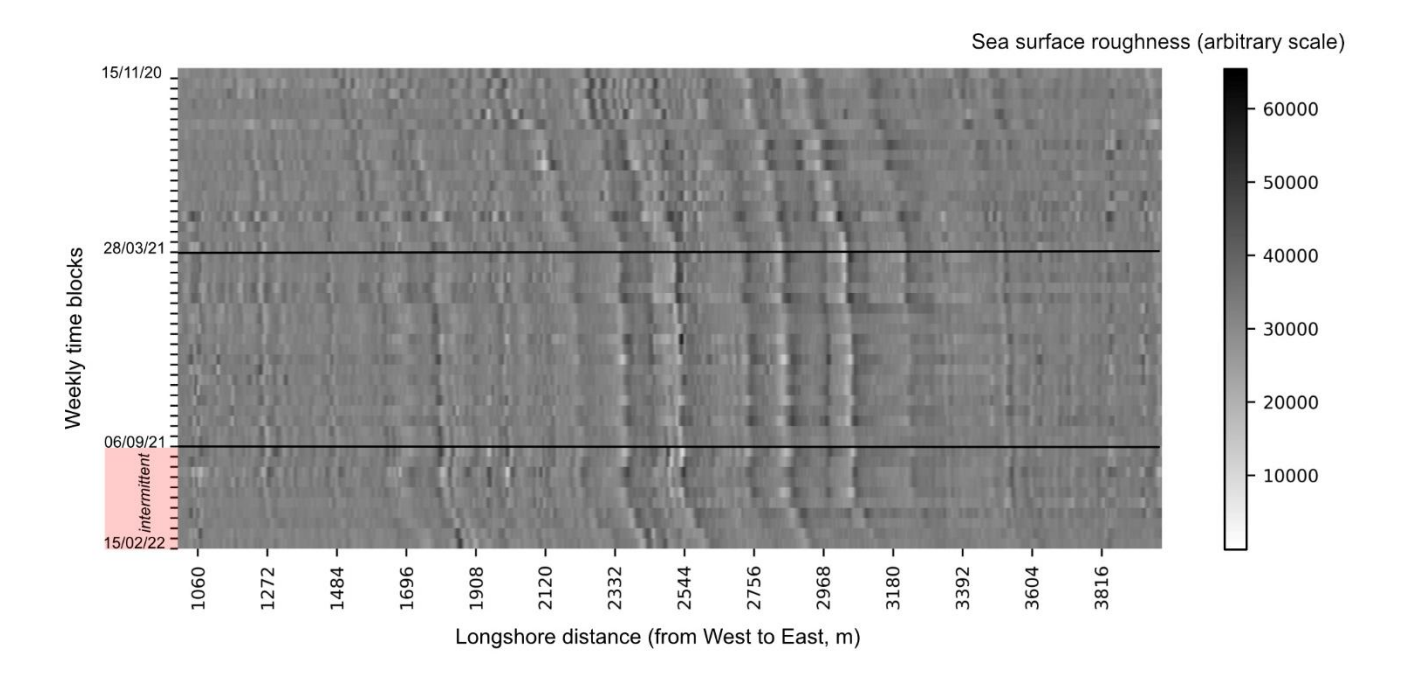


Figure 3.4 – Sea surface roughness gradient along a transect approximately 250 m parallel to the shoreline indicating the location of the bars and their movement over time.

3.4.4 Hydrodynamic analysis

The summer and winter migration rates are presented alongside wave power in Table 3.3. The table shows a clear seasonal distinction both in the distance migrated by the bars (daily rate), but also through the wave power (daily average). Despite this distinction, there was a lower rate of transport during the second winter period, despite nearly identical values for daily-averaged wave power. This could be due to an underestimation of wave power during the Winter 2020/2021 as the wave buoy was out of action for 18 days between the 08/01/2021 and the 26/01/2021.

Table 3.3 – Migration rate vs average daily wave power

Time period	Dates	Duration (days)	Migration distance (m)	Migration rate (m day ⁻¹)
Winter 20/21	15/11/2020 to 28/03/2021	132	122.33	0.93
Summer 21	28/03/2021 to 06/09/2021	161	9.27	0.06
Winter 21/22	06/09/2021 to 15/02/2022	162	50.67	0.31

The seasonal mobilisation trend is presented in a slightly different format in Figure 3.5, subplot A. Whilst the trend is clear within subplot A, the absolute migration rate shows the inherent high variance (subplot B) within the data, and per transverse finger bar (Figure 3.5, subplots C and D). On the whole, movement of the bars is greater in the winter periods in comparison to the summer, and the net migration is towards the east. During the summer, movement to the west counters movement to the east, and the net change becomes small.

Daily averages and peaks of wave power are shown to be elevated over the winter period in comparison to the summer period, although a large storm event can be observed at the end of May (Figure 3.5, subplot E). The wave approach angle shows that waves are typically from the South West, and less frequently arrive from the East. Two periods of sustained easterly waves are observed during the summer, which has a higher incidence of easterly waves than the winter periods (Figure 3.5, subplot F).

Chapter 3

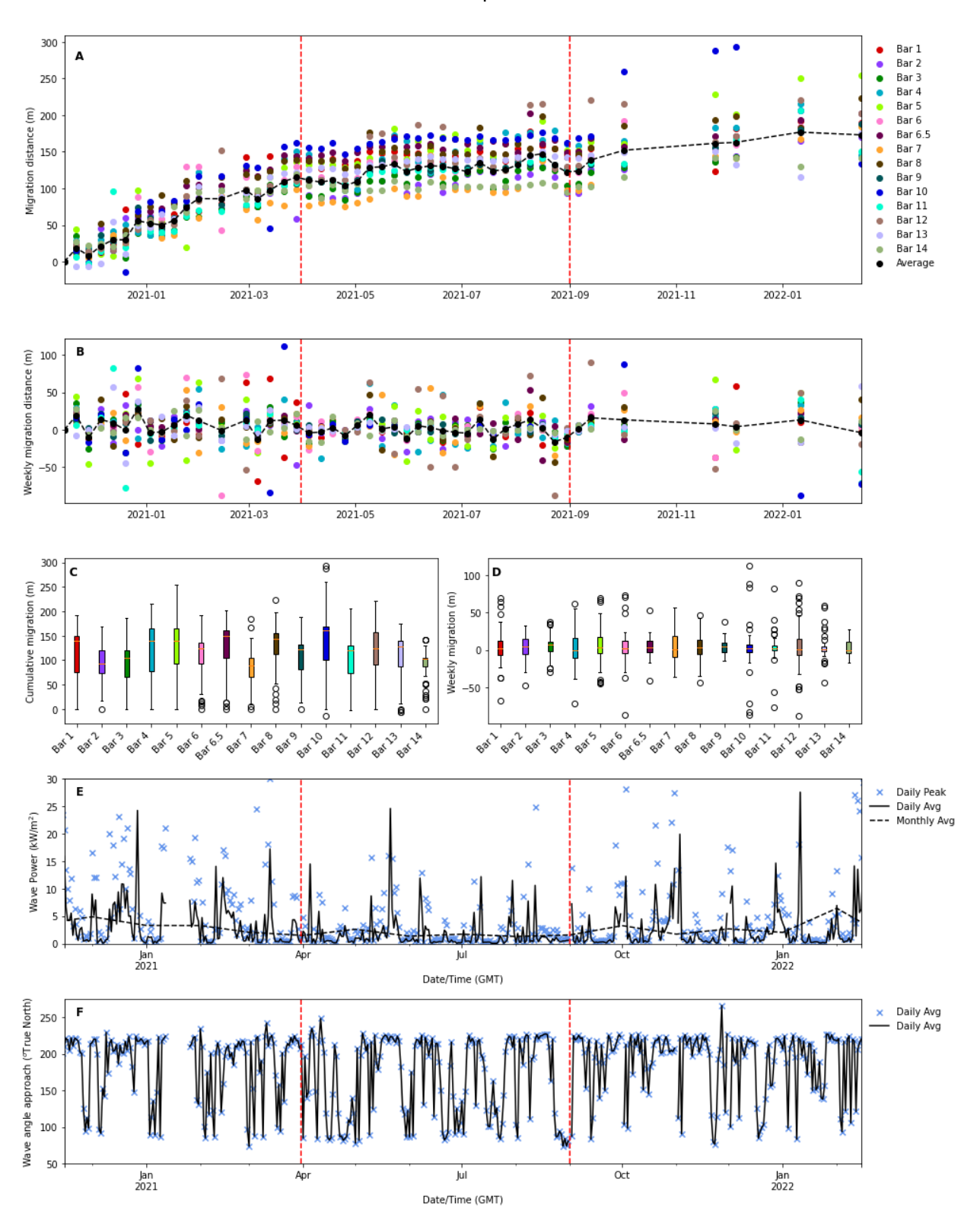


Figure 3.5 – The migration distances are shown within the observation period both cumulatively (A) and weekly (B) with average values shown by the black marker; followed by cumulative and weekly distance plots for each individual bar, (C) & (D) respectively. The bottom two plots show the wave power (E) and peak wave direction (F) as recorded by the Pevensey wave buoy.

The frequency distribution of wave parameters, significant wave height, peak wave period and wave direction were shown to vary between the three time periods considered (Figure 3.6). The modal wave height was 0.5m for all periods, however wave heights exceeding 1 m were much more frequent in the winter (Figure 3.6, top left). The modal peak period for the winter periods was greater than the summer period (3 s and 7 s respectively) and swell waves were indicated by the presence of secondary peaks around 10 s, suggesting more energetic conditions during the winter periods (Figure 3.6, top right). The joint probability showed that the largest wave heights had periods of 5 – 10 s, whilst the higher energy peak period were associated with small wave heights (> 1.0 m), and rarely occurred during the summer, whilst wave heights of up to 3m had been observed in the summer (Figure 3.6, bottom left). Easterly waves were more common in Summer 2020 than the winter periods, and the first winter period (2020/2021) experienced proportionately more easterlies than Winter 2021/2022 (Figure 3.6, bottom right).

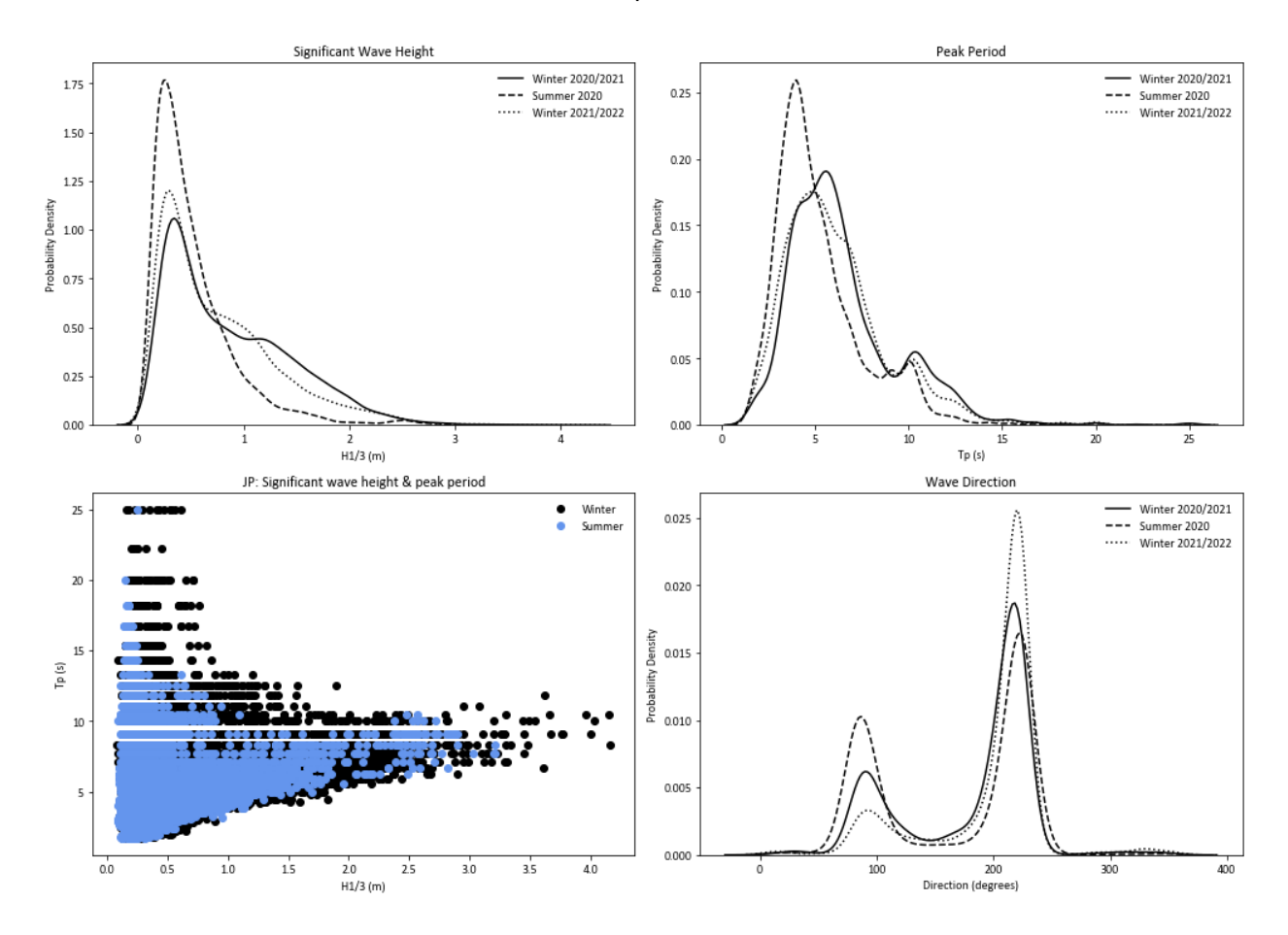


Figure 3.6 – Distribution of wave height (Hs, top left), peak period (Tp, top right), wave direction (bottom left) and incoming wave spread (bottom right), over the three study periods Winter 2020/2021, Summer 2021, and Winter 2021/2022.

The weekly mean migration rate and the median bar migration was found to have a low positive linear relationship (R^2 value of 0.38), with migration rate increasing with littoral drift potential (Figure 3.7). The relationship was found to be highly statistically significant with P < 0.001.

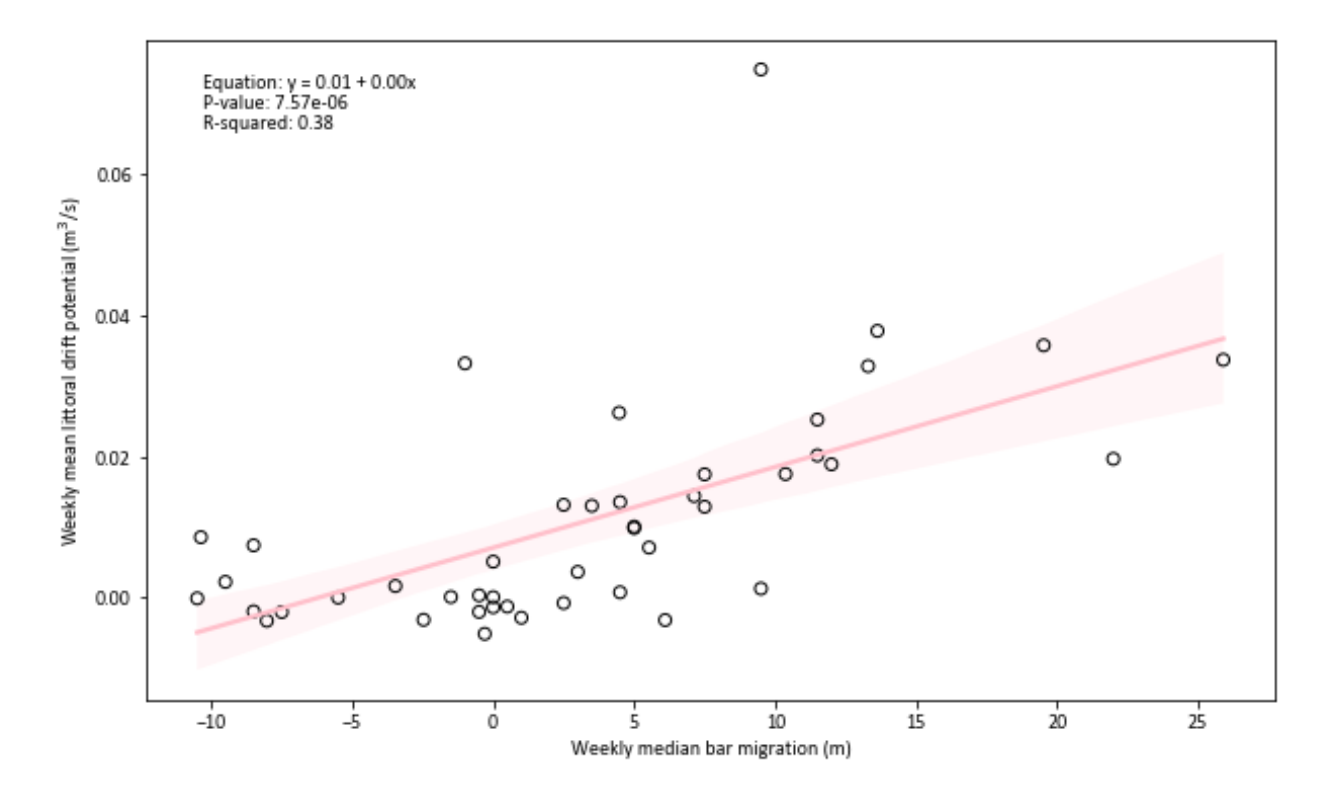


Figure 3.7 – Linear regression of the weekly mean littoral drift potential (m3/s) and the weekly median bar migration (m).

3.4.5 Upper beach volumetric analysis

Rhythmic, largescale, low-level elevation bedforms can be inferred from the binned difference models of the upper beach from the from the easterly migration of areas of erosion and accretion over the 19-year observation period (Figure 3.8). Although there is a large degree of spatial variation, wavelengths of each feature are approximately 750 m long. The bars are migrating by approximately one wavelength every five years, which is equivalent to approximately 150 m per year (measured between ~110 to ~170 m).

The x-axis stars at 500 m chainage to avoid large peaks in the data caused by an annual beach nourishment in this location in the order of $20,000 \, \mathrm{m}^3$ since 2007. At approximately ~ 3000 to 3250 m longshore location, the graph becomes slightly distorted which is caused by smaller area polygons at the junction of a change in coastline orientation.

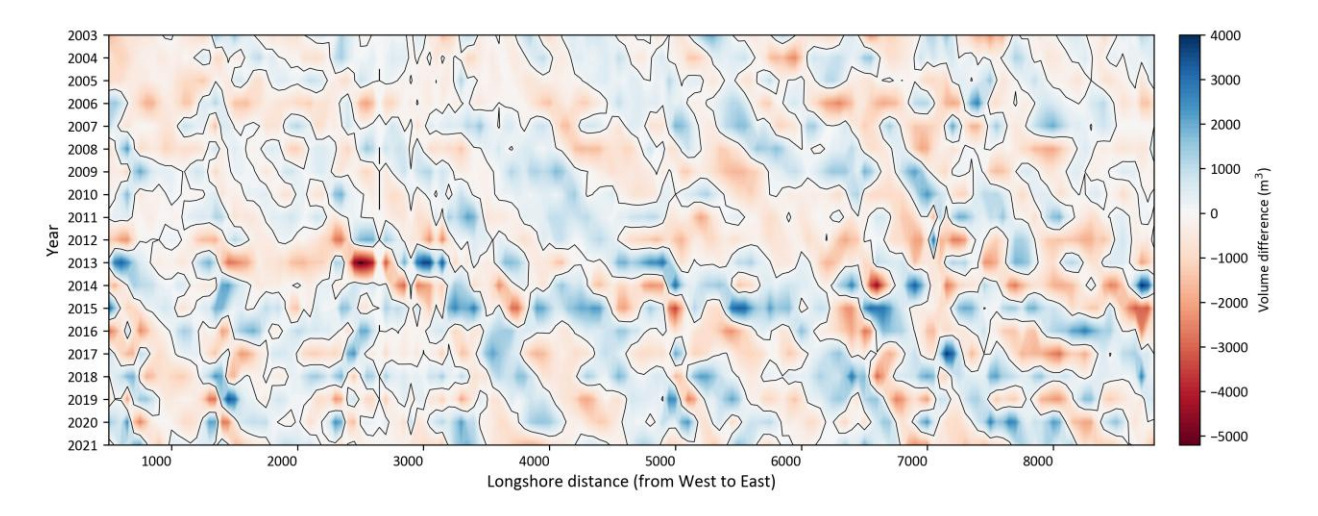


Figure 3.8 – Year on year contour plot for beach volumetric change across Pevensey Bay 2003-2022.

3.5 Discussion

There are both similarities and dissimilarities between the morphology, sediment composition and behaviour of the transverse finger bars identified in Pevensey and other sites reported in the literature (Table 3.4). We find a useful distinction grouping the transverse finger bar classification by Pellón et al., (2014) alongside the coastal configuration (obtuse sheltered, obtuse exposed, straight, and reflex), with a new sub-type, 'persistent intermediate energy finger bars', to describe the bars found at Pevensey and those on the Waddenzee coast as reported by Brakenhoff et al. (2019) (Table 3.4). This accommodates the existing classification giving greater context to the wider coastal environment, whilst field observations remain relatively scarce (Table 3.4). We use the terms 'transient' and 'persistent' following Levoy et al. (2013), and consider the transverse finger bars at Pevensey to be persistent, as the 2013 MBES bathymetry and radar imagery extending between November 2020 and February 2022 suggest that the bars have been present within the region for at least ten years.

The bars increased in length from approximately 130 to 700 m long from west to east, indicating a greater sediment availability to form bedforms, supporting the notion that the site becomes more depositional towards the east (Townsend et al., 2024). The chevron bar morphology identified in

the 2013 MBES data is unique and has not been reported elsewhere, however, as they were not observed within the observed sea roughness images we do not know A) if they were extensions to the transverse finger bar features or irregular underlying bathymetry; nor B) still present. As these features are located in deeper water they may not modulate the sea surface in the same way that the undulating bedforms in shallower water do. Additionally, the change in orientation might suggest a return current, with a reversed near bed flow, or alternatively, in the same way that each bar migrates at a different rate, the migration rate also varies across each bar, e.g. the lower part of the bars migrate much slower than the upper part of the bars, and that the chevrons are the beginnings of 'relict' features. As the bars approach the gravel outcrops, they dissipate and do not continue in a regular rhythmic pattern (Figure 3.3).

The wider geomorphological and sedimentary setting is unique to the transverse finger bars reported within this study. The grab samples indicated that the surface sediments were comprised of very fine sand at the landward limit of the bars, and the 2013 backscatter image interpretation supports this, however, this sandy area is located within a gravel rich environment, both onshore and offshore (Dornbusch, Williams and Moses, 2005; Mellett *et al.*, 2012). This is visible in the area in which they terminate, as gravel outcrops emerge as part of a complex mosaic in and around the 12th to 14th bar (Figure 3.3). It is unknown how mobile the gravel beds are or how much they interact with the mobile features, however it is likely that they are a permanent feature considering their location at the junction of a decreasing longshore transport gradient, as the coastline changes orientation, and being partially constrained by rock outcrops to the east (not shown). Shore-oblique bars were strongly correlated with the occurrence of gravel outcrops along the coasts of Virginia and South Carolina, and it was suggested that their presence played a key role in the formation of the features (McNinch, 2004; Schupp, McNinch and List, 2006). In contrast, at Pevensey, the rhythmic features are not seen beyond (to the east) of the gravel outcrops area, suggesting that the outcrops may play a role in the breakdown of the bedform features.

The movement of the transverse finger bars was shown to be highly seasonal, with greater movement in the winter/stormy season. The weekly migration rate of the bars was found to correlate with the littoral drift potential, explaining about 40% of the bar's movement. Large south westerly waves were highlighted as a key driving condition, however, both the bars and the sea surface roughness data are dependent on multivariate conditions. In terms of bar mobility, the

tidal curents at the site may contribute to sediment stirring, encouraging entrainment, and the dominant flood tide (which travels towards the north east (Fugro Emu, 2016)) may also contribute to the net bar movement. Additionally, the tidal currents are a key component of the imaging process, whereby the moderation of the sea surface roughness will be affected by how fast the currents are flowing, which can vary during different stages of the tide. Moreover, the effects of barometric pressure, negetive or positive surges would affect the water depth and therefore the ability of waves to mobilise sediment. In terms of the imaging process, any effect which may disrupt the flow of water at the surface may affect the position of the peak roughness values which are used to identify the position of the bar. In addition to the wave generated longshore current and tidal currents, this could be locally generated wind-driven currents or even the flow of water from the two outfalls located between bars 12 – 14 which alter the surface flow. The individual morphology of the bars add another layer of complexity, as each bar has a unique depth, slope and wavelength, and so the associated surface flows will be different for each bar (Figure 3.3, Table 3.2).

Rhythmic bedforms in the upper beach are found to control the location of accretion and erosion to some degree, despite regular engineering intervention. This is an important finding for beach managers, working with beach sediments to maintain flood protection, as they do at Pevensey. The winter of 2013/2014 was an especially stormy year for the southern coast of England (Dhoop and Mason, 2018) and as a result greater volumes of erosion are recorded that year within the bay (Figure 3.8). The relationship between the bedforms is not fully understood, but the similar longshore migration rates suggest the bedforms are driven by the same processes. Moreover, as with the transverse finger bars, the upper beach bedforms are not widespread regionally; the analysis presented in Section 3.5 was originally carried out as part of a study extending between Eastbourne to Rye and were only reported in the vicinity of Pevensey Bay management unit, extending only a few hundred metres into the next management unit in Bexhill, not shown in Figure 3.8 (Environment Agency, 2017). However, the transverse finger bars do not extend into the intertidal zone, and a morphologically stable area identified in the shallow nearshore of this site suggests that they are independent of each other (Townsend et al., 2024). Additionally, the upper beach rhythmic features cover a much wider area and have wavelengths roughly 5 times greater than the transverse finger bars. Other instances of independent upper/lower shore rhythmic

bedforms, are those at Dungeness (Figure 3.1, Arriaga et al., 2017) and at El Trubador, Spain as reported by Mujal-Colilles et al. (2019). Mujal-Colilles et al.'s work pointed the formation of rhythmic features to shoreline instability driven by high-angle waves, however, ignores any cross-shore interaction during low-angle conditions. Investigating the role of the bathymetry in moderating the shoreline planform would be a valuable future undertaking to iron out any cross-shore dependencies.

Table 3.4 – Transverse Finger Bar classifications in the context of the wider coastal setting, with distinction between transient and persistent intermediate energy finger bars (adapted from Pellón et al. (2014); and Levoy et al. (2013)). Classification of Pevensey Bay Transverse Finger bars shown in bold. N.B. Transverse Bars and Rips are excluded from this table.

Coastal configuration	Type as per Pellón et al. (2014)	Beach description	Mean wave height (m)	Tidal range	Bar waveleng th (m)	Cross- shore span (m)	Bar orientation	Average (min, max) migration rate (m day ⁻¹)	Observation reference
Obtuse (sheltered)	(Persistent) Small-scale low-energy finger bars	Very fetch limited (< 10km)	<0.1	Micro	<50	<100	Oblique down-current	Lack of data	(Bruner and Smosna, 1989; Falqués, 1989; Nordstrom and Jackson, 2012; Pellón, Garnier and Medina, 2014; Mujal- Colilles, Grifoll and Falqués, 2019)
Obtuse (exposed)	Persistent Intermediate energy finger bars	Intermediate wave dominated beaches	>0.5	Macro	670 150	800 – 2200 100 – 700	Oblique down-current	0.08 (0.005, 0.3); 0.4 (0.06 to 0.93).	(Brakenhoff, Ruessink and van der Vegt, 2019) This study
Straight	Transient Intermediate energy finger bars	Intermediate wave- dominated beaches	>0.5	Micro	50-100	<100	Oblique up- current	40; 3.2 (-9, 22).	(Konicki and Holman, 2000; Khabidov, 2001; Ribas, Falque and Montoto, 2003; Ribas and Kroon, 2007; Ribas et al., 2014)
Reflex	(Persistent) Large scale finger bars	Low-energy beaches, wide (~1km) with gentle slope (0.002)	<0.5	Micro/Ma cro	~100	~1000	Normal or slightly oblique	0.05; 0.03 - 0.06; 0.06 (0.5, 1).	(Niedoroda and Tanner, 1970; Goud and Aubrey, 1985; Gelfenbaum and Brooks, 2003; Levoy et al., 2013)

3.6 Conclusions

This study documents the characteristics, movement, and sedimentology of a series of transverse finger bars located within a unique mixed sand-gravel environment, unlike those settings previously reported. Several comparisons to the existing literature are made, and an existing classification is grouped using the wider coastal setting, allowing for a further subtype to accommodate the bars observed at Pevensey which do not currently easily fit into the existing classification. The bars at Pevensey had wavelengths 75 to 375m, crest lengths between 100 – 700 m, amplitudes were estimated at ~0.2 to ~0.6 m, they were orientated approximately 150 degrees relative to shore normal and were down-current orientated. Grab samples taken from the landward limit of the bars showed that the surficial sediments comprised fine sand, but gravel outcrops occur within the area of the bars, which are situated in a wider mixed sediment environment. X-band radar was used to create a proxy of the bar's location, showing migration rates varying between approximately – 10 to 25 m per week, which was significantly related to the potential longshore transport (0.38 R^2 ; P < 0.001). The bars at Pevensey were shown to display highly seasonal behaviour, migrating in the winter 'stormy' periods when wave heights were highest and largely immobile during the summer months, when wave conditions were largely calm.

3.7 Acknowledgements

This work was supported by the Environment Agency through the project: "Delivering Legacy from the Pevensey Bay Coastal Defence Scheme (PI: Kassem, H.; Contract: 201-09-SD10). The lead author undertook this work as part of their PhD studentship, funded by NERC INSPIRE DTP (NE/S007210/1), the Graduate School of the National Oceanography Centre, Southampton, and the Environment Agency. Our thanks go to Alex Sinclair and Avnir Soni of Marlan Maritime Ltd, for their assistance with supply of the data and operation of the radar tower. Paul Bell was funded under the NERC R3D2 project, (NE/W007347/1). Thanks also go to Ian Thomas and Amber Carr of Pevensey Coastal Defence Ltd., and Peter Amies and Rebecca Manning of the Environment Agency for their time, on-site support, and site background information. Further thanks go to those involved with the National Network of Regional Coastal Monitoring

Programme for England, in particular Dan Amos of Adur-Worthing Councils, Claire Milburn and Hannah Walker of Canterbury City Council for sharing and reprocessing archived data.

Chapter 4 Morphology and sediment sorting of a mixed sediment beach in response to storm conditions

Dominique Townsend₁, Julian Leyland₁, Hachem Kassem₂, Charlie Thompson₂₃, Ian Townend₂

¹ School of Geography and Environmental Science, University Road, Southampton, Hampshire SO17 1BJ

² School of Ocean and Earth Science, University of Southampton, Waterfront Campus, National Oceanography Centre, European Way, Southampton, SO14 3ZH, UK

³ Channel Coastal Observatory, Waterfront Campus, National Oceanography Centre, European Way, Southampton, SO14 3ZH, UK

4.1 Abstract

Mixed sand gravel beaches are globally commonplace, yet a systematic understanding of their behaviour is limited from the relatively scarce field data, their sensitivity to sand content and highly variable sediment composition. Here we examine the behaviour of mixed sediment beaches to storm waves through a process based numerical mode, XBeach-X. The model inputs have a robust physical basis, using conditions found at the mixed composite beach in Pevensey Bay, UK, which is used as a test bed to explore the morphodynamics resulting from changing hydrodynamic, bed slope and sediment compositions. We found a typical draw down response across the beach profile, with the majority of bed elevation changes in the swash zone, and limited subtidal change. Approximately 74% of all bed elevation change happened within the steeper upper beach. A fining:coarsening:fining pattern was observed due to sediment sorting, which closely resembled existing findings in the field. Further model developments are required, mainly the inclusion of groundwater flows for multiple fraction modelling.

4.2 Introduction

The majority of the world's beaches are thought to be comprised of heterogenous sediments, whereby any two of the size classes defined by Folk (1954), i.e. gravel, sand and mud, exceed a 9:1 ratio (Holland and Elmore, 2008). Mixed Sand Gravel (MSG) beaches have been reported in ex-glacial and periglacial shores of New Zealand (Ivamy and Kench, 2006; Dickson, Kench and Kantor, 2011; Hemmingsen, Eikaas and Marsden, 2019), Northern Europe, including the English Channel (Mason and Coates, 2001; Costa et al., 2008; Watt et al., 2008; Curoy et al., 2009), the North Sea (Atkinson et al., 2017; Dolphin et al., 2020), the Baltic Sea (Martewicz, Kalińska and Weckwerth, 2022; Chlachula and Mychko, 2023); the Mediterranean coast (Aragonés et al., 2015; Bergillos, Masselink, et al., 2016; Ortega-Sánchez et al., 2017), the USA East coast and Nova Scotia, Canada (Fitzgerald and Van Heteren, 1999; Roberts, Wang and Puleo, 2013; Hay, Zedel and Stark, 2014; Woodruff et al., 2021), and beaches in Argentina (Lamarchina, Maenza and Isla, 2021). These beaches are of significant interest and importance due to their roles in coastal protection (Polidoro, Dornbusch and Pullen, 2013), their intrinsic ecological value(Walmsley and Davy, 1997; Gauci, Deidun and Schembri, 2005; Gardner and Burningham, 2013), and recreational value (Martínez et al., 2007). Despite their prevalence and economic, environmental and social importance of MSG beaches, there has been relatively little research into their unique morphology and behaviour in contrast to their pure gravel and sand counterparts (Mason and Coates, 2001; Pontee, 2011; Roberts, Wang and Puleo, 2013).

There has been a large body of work on process level understanding of coarse grained beaches in the last 20 years, as the distinction between these beaches and sandy beaches became apparent (Austin and Masselink, 2006; Buscombe and Masselink, 2006; Masselink et al., 2010; Poate et al., 2013; McCall et al., 2014; Almeida et al., 2015; Poate, McCall and Masselink, 2016). MSG sediment beaches, which exist on a spectrum between these two states, have unique morphology and behaviour relative to pure sand and gravel equivalents as well as to MSG on other coasts, and even along the same coastline due to the high spatial variability of sediment distribution and structure (Pontee, Pye and Blott, 2004; Horn and Walton, 2007; Dolphin et al., 2020). This paper is primarily concerned with gravel rich MSG beaches, which we define as beaches containing 50% or more gravel, due to their important role in coastal defence, although many of the topics will be equally applicable to sand rich MSG beaches, e.g. Orford and Carter (1982), Roberts et al., (2013). Gravel rich MSG beaches tend to have a steep, reflective upper beach (Mason and Coates, 2001; Pontee, Pye and Blott, 2004; Ortega-Sánchez

et al., 2017), and can be fronted by a dissipative predominantly sandy foreshore, where they are referred to as mixed composite beaches (Horn and Walton, 2007). During high energy conditions, sand can be stripped from MSG beaches, giving them the appearance of a pure gravel beach, however the core of the beach remains sandy (Mason and Coates, 2001; Pontee, Pye and Blott, 2004; Dornbusch, Williams and Moses, 2005), in contrast to the apparently superficial seasonal transition of pure gravel beaches to composite following low-energy waves (Casamayor et al., 2022; Soloy et al., 2024).

Grain size distributions of MSG beaches are bi- or poly-modal, typically with a grain size 'gap' between 0.5 and 4mm, most likely due to differing sources of sediment (Pontee, Pye and Blott, 2004; Horn and Walton, 2007; Bergillos, Ortega-Sánchez, et al., 2016; Atkinson and Esteves, 2018; Woodruff et al., 2021). For non-cohesive grains, the energy required to initiate sediment motion is a function of the grain size, with more energy required to move larger grains. Due to the relatively small size of sand relative to the energy available; sand is easily mobilised by both currents and waves and can be transported both onshore and offshore. Gravel, on the other hand, requires a greater level of energy to be mobilised and is predominantly driven by wave action (van Rijn and Sutherland, 2011). On pure gravel beaches, the backwash of retreating waves is significantly weaker than the uprush/bore of the incoming wave, as infiltration through the large interstitial spaces between grains dissipates the wave energy (Jamal, Simmonds and Magar, 2014; Poate, McCall and Masselink, 2016). Additionally, exfiltration effects from groundwater flows have been shown to be an important factor in mobilising gravels as the flow reduces the effective weight of the grains and lowering their local threshold for motion (Austin and Masselink, 2006; Buscombe and Masselink, 2006; McCall et al., 2014). As a combination of these effects, berm building is a classic response of gravel beaches to energetic conditions, however this behaviour switches to erosion as the hydraulic conductivity, a measure of porosity and grain size, is reduced (Soloy et al., 2024). However, for mixed sediment beaches it is not so simple. For MSG beaches, the porosity of the beach face is reduced as sand grains fill the pore space between gravel sized grains. Reduced porosity, and therefore reduced infiltration effects, lead to increased wave run-up and wave reflection (Mason, 1997; She, Horn and Canning, 2006). Under energetic conditions the primary response becomes drawdown of beach sediments, and so the behaviour more closely resembles that of a sandy beach rather than a coarse-grained one (Mason, 1997). This is not true for all MSG beaches all of the time, as berm building has been observed in response to energetic conditions both in the field (Bergillos,

Masselink, et al., 2016) and laboratory (López De San and Blanco, 2003), most likely due to increased porosity in the surficial sediments. Pontee et al. (2004) who observed both flattening and steepening of MSG beaches in response to storm waves attributed the behaviour to the sediment supply. Further complexity arises from interaction between sediment fractions from the hide-exposure effect, i.e. where larger grains are more prominently positioned, sheltering smaller grains (Egiazaroff, 1965), raising/lowering the critical threshold of bed shear stress of individual sand/gravel grains (McCarron et al., 2019). This effect on the critical bed shear stress can be as large as a 75% decrease for the gravel fraction and a 64% increase for sand fractions, in comparison to uniform sediments of the same size. Based on modelling bedload transport alone, the net effect seems to be a dampening one, with reduced morphodynamic changes, although changes around some bedforms were amplified (McCarron, 2020). A stabilising effect can also occur within mixed sediments as a result of a reduction in the friction angle which must be overcome for sediment entrainment to occur (Buffington, Dietrich and Kirchner, 1992). Mason and Coates (2001) also further identified clast shape, tidal range, specific gravity, armouring and chemical processes to be secondary order factors affecting sediment transport on MSG beaches.

The numerous, dynamic and inter-related factors which affect the morphodynamic response of MSG beaches result in highly variable and complex behaviour. As these beaches are often utilised as the form of primary coastal defence (Polidoro, Dornbusch and Pullen, 2013; Bergillos, Masselink, et al., 2016; Dornbusch, 2017); it is especially pertinent to try and understand the storm response of mixed sediment beaches better (She et al., 2007). Additionally, there is growing interest in introducing coarser-than-native material as a nature based solution towards erosion, such as dynamic cobble berm revetments (Foss et al., 2023), which would benefit from improved knowledge of MSG beaches. With such limited available datasets, and variable responses, a modelling study into the behaviour of mixed sediment beaches offers an excellent opportunity to examine these complex systems under a range of test conditions. The overall aim of this paper is to improve our understanding of how MSG beach sediment sorting and morphology respond to storm waves under various hydrodynamic conditions, initial bed slope gradients and sediment composition. To do this, the process based XBeach-X model will be used to track changes in bed elevation and distribution of sediment composition across a beach profile, in relation to changing hydrodynamics, bed slope and

initial sediment mixtures. Real beach profile and wave buoy data from a mixed composite beach study site are used to provide a robust physical basis for the model set-up.

4.3 Methods

The open-source, process-based model Xbeach-X was used to generate a series of test cases for a mixed sediment beach, based on an analogue of Pevensey Bay, a composite mixed beach on the South East coast of the United Kingdom (Townsend *et al.*, 2024). The model is introduced in Section 2.1 with details on the model set-up in Section 2.2.

4.3.1 Model description

4.3.1.1 Overview

A 1-D non-hydrostatic simulation was used to model the effects of various hydrodynamic drivers (waves and water levels) and changes to the bed (sediment composition and morphology) through computation of sediment transport (Roelvink *et al.*, 2009; Roelvink, 2015). The non-hydrostatic mode applies a pressure correction term which enables wave run-up on steep faced beaches (such as the test case) to be modelled successfully. The bed is permeable, although the effects of ground water flow are not included. The non-linear shallow water equations (NLSWE) utilised are:

$$\frac{\delta \eta}{\delta t} + \frac{\delta h u}{\delta x} = 0$$
 Equation 1

$$\frac{\delta u}{\delta t} + u \frac{\delta u}{\delta x} - \frac{\delta}{\delta x} \left(u_h \frac{\delta u}{\delta x} \right) = -\frac{1}{\rho} \left[\frac{\delta (\rho p_{nh} + \rho g \eta)}{\delta x} - \frac{\tau_b}{h} \right]$$
 Equation 2

where η is the instantaneous water surface, h is the total water depth, u is the depth averaged cross-shore velocity, x and t are the temporal and spatial co-ordinates, ρ is the density of seawater, ρ_{nh} is the depth averaged pressure (normalized by density), g is acceleration due to gravity and τ_b is the bed shear stress, which is determined from a quadratic stress law:

$$au_b =
ho c_f u |u|$$
 Equation 3

where c_f is the dimensionless friction coefficient. Bed load transportation of sediment (q_b) is estimated using the van Rijn (1993) equation:

$$q_b = 0.006 \rho \omega_s D_{50} M^{0.5} M_e^{0.7}$$
 Equation 4

where ω_s is the particle fall velocity, D_{50} is the median grain size, M is the sediment mobility number (a function of the effective velocity, i.e. the depth averaged velocity magnitude and wave asymmetry) and M_e is the excess sediment mobility number which is a function of the difference between the effective velocity and the critical velocity. The suspended load is calculated using van Rijn (1984):

$$q_s = F \overline{u} dc_a$$
 Equation 5

where F is the F-factor, a function of the concentration reference level, the flow depth and the suspension number; \bar{u} is the mean flow velocity, d is the flow depth; and c_a is the reference concentration. Note in multi-fraction modelling, the sediment transport equations are calculated for each sediment fraction and assume no interaction between the fractions (see Section 2.1.2 for further details on multiple sediment fractions). The bed elevation is updated using the Exner equation:

$$\frac{\delta z_b}{\delta t} + \frac{1}{1 - n_p} \frac{\delta q_b}{\delta x} = 0$$
 Equation 6

A detailed account of the governing equations of the Xbeach-X model is available in the online manual (https://xbeach.readthedocs.io/en/latest/). It should be noted that, whilst the Xbeach-X model is not specifically designed with coarse grained beaches in mind, there is currently no

preferred alternative for process based modelling mixed sediments. There are very few studies within this area: Bergillos et al. (2016a) found that XBeach-G successfully replicated the behaviour of a mixed sediment beach, however as only a single grain size was modelled at any one time cannot provide detail on sediment sorting. Rijper (2018) modified the source code of XBeach-X to apply different sediment transport equations depending on the fraction size (>/< 2mm) however attempts to recreate this work as part of this study were unfortunately not successful. Elsewhere in the literature, modelling grain size sorting has been achieved for sand sized sediment (Reniers et al., 2013; Herrling and Winter, 2014) and aeolian transport (Hoonhout and Vries, 2016).

4.3.1.2 Multiple sediment fraction modelling

Xbeach-X has the capacity to model non-cohesive, mixed sediment environments by defining 2 to 20 sediment fractions, specifying the (15th if desired), 50th and 90th percentiles of the grain size distribution (Roelvink, 2015). The model manages the vertical exchange of sediments through the use of multiple layers, with a minimum of three: comprising a top, variable and bottom layer (Figure 4.1). This allows variation in sediment composition in the horizontal (per grid cell) and vertical (per layer), which can enable processes such as armouring and sorting to be modelled, where the sediment transport equations are calculated for each fraction independently. Sediments are exchanged between the top layer and the water column depending on the sediment balance (Equation 6). The top layer maintains its thickness, in response to bed elevation erosion or deposition, whilst the variable layer underneath adapts its thickness, adjusting its sediment composition to account for the losses/gains made above (Figure 4.1). To avoid numerical mixing, i.e. where the model diffuses sediment across layers that are too deep, the maximum layer depth of the middle layer should be the depth of expected erosion (Roelvink *et al.*, 2010).

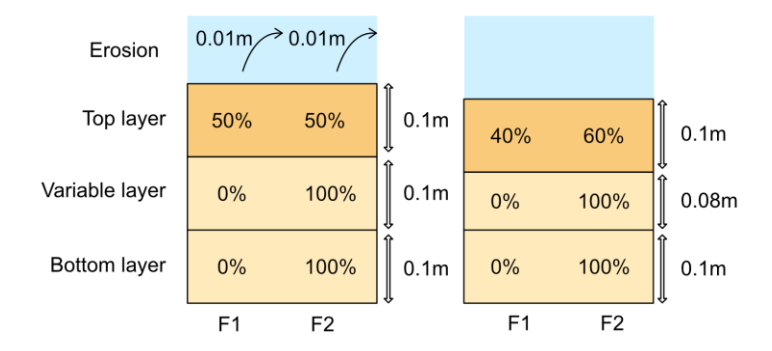


Figure 4.1 – Example of bed layer updating in response to erosion for two fractions (F1 and F2).

Following 0.02m of erosion from the top layer, the variable layer decreases in depth by 0.02m to replace the material lost. The 'feeding' of material from the variable layer to the top layer results in an adjusted sediment bed composition (adapted from Rijper, 2019)

4.3.2 Model set-up

4.3.2.1 Model Grid

A test profile of a generic MSG beach was created using profile data from the analogue site at Pevensey Bay, East Sussex. The location of the shore normal beach profile was positioned to cross the central area of the bay to provide a representative profile. The profile spanned approximately 3.8km from the backshore (50°49'15"N, 000°22'24"E) out to 9.8 mOD water depth along a bearing of 152 degrees to true north. The surface elevations were extracted from the Channel Coastal Observatory's 1 m resolution LiDAR data, collected on the 15/10/2020 and a composite of 2 m gridded Multi Beam Echo Sounding bathymetric data, captured in 2012, 2013 and 2015 by the Channel Coastal Observatory and the Maritime and Coastguard Agency. All elevations are to Ordnance Datum. To avoid instabilities in the offshore boundary conditions, the grid was extended linearly to a water depth of -20 mOD. The combined profile was then transformed into a non-equidistant grid using the Deltares Open Earth Tools (OET) MatLab Toolbox, to create a more computationally efficient grid. Within Xbeach-X, the grid was orientated due North, with oncoming wave parameters set to normal (incoming at 180 degrees).

4.3.2.2 Boundary conditions

The input wave boundary conditions are given in Table 4.1. The significant wave heights and periods of extreme events were derived from a statistical extreme value analysis of the nearshore wave buoy in Pevensey Bay (50° 46.'1' N 000° 25.'0' E). The wave record comprises half hourly readings of wave parameters over a 19-year period. The extreme value analysis, including Peaks-Over-Threshold (POT) and Generalised Pareto Distribution (GPD) analysis, were completed using the Python pyextremes package (Bocharov, 2021). The Peaks-Over-Threshold (POT) analysis was used to extract the peak significant wave heights (Hs) from events exceeding a 2.0 m threshold, and 3 hours apart from any other events. The 2.0m threshold was selected from a parameter stability plot; taken as the largest possible wave height from 100 test cases (thresholds interpolated linearly between the 10th and 90th percentile of the dataset) that fit to a Generalized Pareto Distribution (GPD), which was shown through plotting the modified shape and scale of the GPDs. The resultant statistical model of the extremes value distribution was used to provide an estimation of significant wave heights for low probability events, as shown in Table 4.1. The associated peak wave period (Tp) was calculated from a log trend line, fitted between the filtered (above 2.0 m) Hs and associated Tp records.

Table 4.1 – Storm scenarios derived from the Pevensey Wave Buoy record (19-years data).

Storm return period	Storm Hs (m)	Storm Tm (s)
1 in 1	3.8	7.0
1 in 10	4.6	7.2
1 in 100	5.1	7.3

4.3.2.3 Model run configurations

A series of model runs, designed to test the impact of changing hydrodynamics, bed slope and sediment composition onto beach profile and sediment sorting response under storm waves is given in Table 4.2. The D_{50} and D_{90} of the two fractions were well-sorted coarse sand ($400\mu m$ and $500\mu m$) and fine gravel (4.2mm and 5.4mm) respectively. The upper and lower bed levels thicknesses were set to 0.1m, whilst the middle layer was set to 1m, representing an estimate of expected upper level of erosion based on preliminary runs to minimize numerical mixing (see Section 2.1.2). The full input parameters are available in the supplementary information.

Table 4.2 – The model runs showing each test bed (hydrodynamics, bed slope and sediment composition) and the respective test cases. The cases highlighted in bold are the default values for the other test cases, for example, when the 1 in 100 storm conditions are tested, a 6.3 tidal range is used, the natural profile, and 30:70 sand to gravel ratio.

Test bed	Scenario	# of	Case description	Time duration	
		case			
		S			
Hydrodynamics	Wave height	3	1 in 1, 1 in 10, 1 in 100	14 hours	
			(see Table 4.1)		
	Period	3	7.2 seconds, 10 seconds,	14 hours	
			14 seconds		
	Surge	3	0m, +1m, +2m	14 hours	
	Spring/Neap	2	6.3m (spring) tidal range,	14 hours	
	/No tide		3.1m (neap) tidal range		
			0 m (no) tidal range		
Bed slope	Slope	2	1 in 5, natural slope (1 in 8) ,	14 hours	
			1 in 12		
Sediment	Unimodal	2	100% sand	14 hours	
composition			100% gravel		
	Bimodal	3	Sand-gravel ratios of 10:90,	14 hours	
			20:80, 30:70, 40:60, (50:50),		
			60:40, 70:30, 80:20, 90:10		

4.4 Results

4.4.1 Hydrodynamics

Location of overall change

The most prominent morphodynamic response occurred in the swash zone/upper beach, with negligible bed level changes occurring across the foreshore area (Figure 4.2, Figure 4.3). Within the swash zone, all the storm scenarios triggered draw down/flattening of the beach, leading to the development of a concave-convex profile (whereby seaward movement of sediment has resulted in the upper section of the beach becoming more concave, while the lower section of the beach becomes more convex; as described by Masselink and Puleo (2006)) at the end of each model run (Figure 4.3). The level and magnitude of the drawdown varied under different conditions. The 1 in 10 and 1 in 100 storm conditions (Hs 4.6 m, Tp 7.2 s, and Hs 5.1 m, Tp 7.3 s,

respectively) gave a very similar beach profile response, in terms of the geomorphologically active area, to the 1 in 1 event (Hs 3.8 m, Tp 7.0 s) (Figure 4.3, subplot A1). In contrast, increasing the wave power (by increasing the period of the waves) solicited a response which was an order of magnitude larger (approximately ~20 and ~60 m² net change in contrast to the <4m² net change under the 1 in 1 waves) over the whole beach profile, although the probability of these events occurring at the Pevensey Bay wave buoy have not been calculated, rather represent the highest values recorded, and therefore assumed to be physically possible at the site. Similarly, crest mobilisation only occurred under the longer wave period (10 and 14 second) and the 2 m surge scenarios. Conditions did not reach the trigger levels for crest overwash or overflow, and so the barrier beach largely retained its height and width. Variation in the tidal range controlled the area over which the waves acted, and therefore the development of the beach profile. The beach profile at the end of the neap tide simulation showed drawdown had occurred within a smaller elevation range (largely within the 3.1m neap range) than during the spring tidal range run (Figure 4.3, D1).

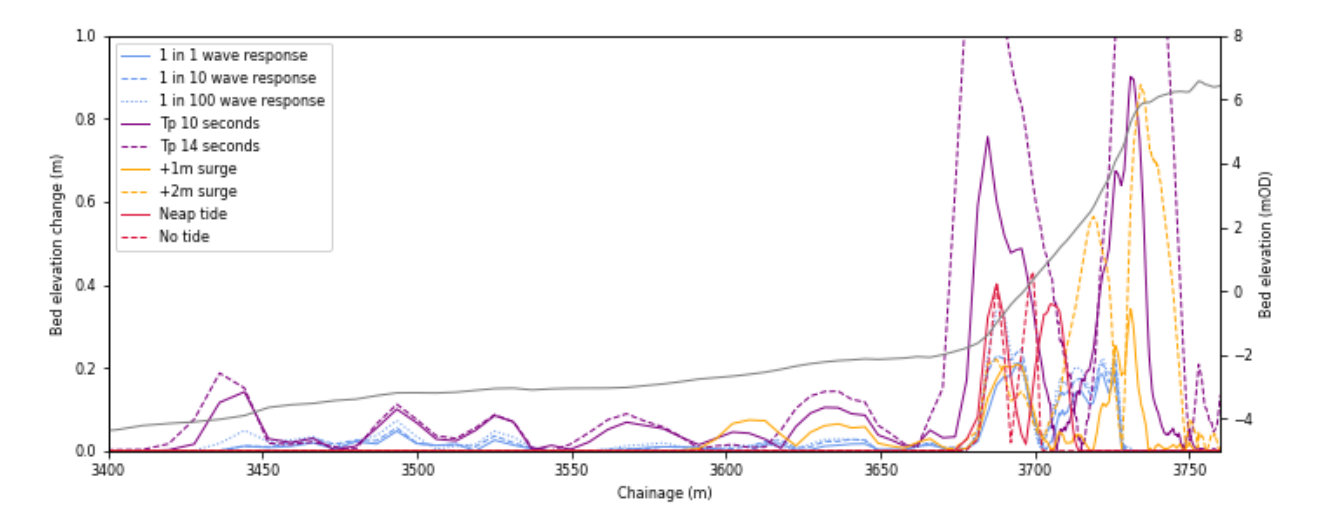


Figure 4.2 – Absolute bed elevation change for the hydrodynamic runs alongside the beach profile bed elevation. Note the beach toe (which is defined as the change in slope between the upper steeper and the lower flatter part of the beach) is located at 3 680 m chainage.

Magnitude of the change

The magnitude of the drawdown also varied in response to the different hydrodynamic driving conditions. The greatest changes were associated with destabilization of the crest, notably during the greatest energy events (Figure 4.3, subplot B1) and the storm surge events (Figure

4.3, subplot C1). Relatively little change in magnitude was observed between the different storm conditions, although the relationship between storminess and volume of bed change appeared to be positive. Larger elevation changes were observed over the neap tidal conditions than the spring tide conditions (Figure 4.3, subplot D1) as the wave energy was focused on a smaller length of the beach profile.

Shape of the change

Largely the patterns of change were similar, with material being extracted from the top of the beach and drawn down to form a berm at approximately MSL, building on the foreshore. The height of the berm decreased slightly with the magnitude of bed level change, for instance, the berm crest formed at just above MSL (0.0mOD) for the 1 in 1 and 1 in 10 event but was closer to -0.4 mOD for the 1 in 100 and 1 in 500 events respectively. The shape of the berm was consistent between all runs but extended seawards in the cases where greater drawn down of material had occurred, for example under the higher wave period runs, and during the neap tide run. This resulted in a wider berm formation. Additionally, the higher the crest of the newly formed berm was, the lower the slope gradient fronting the berm down to the foreshore. The beach slope generally became steeper around the high tide mark, due to the beach draw down, except in instances where the erosion of the crest led to a shallower slope forming.

Sand was more readily mobilised than gravel, which lead to sediment sorting across the swash zone of the beach profiles in response to all hydrodynamic conditions (Figure 4.3, subplots A2 – D2). The sorting was only observed in areas where bed level change had also been observed. The typical pattern of sorting seawards from the upper beach crest was fining, followed by coarsening across the majority of the upper beach slope, followed by fining. Additionally, for under both spring and neap tide runs, there was a finer central section at approximately 3 895 to 3 700 m chainage (Figure 4.3, D2). The lack of fining at the very top of the beach under the no tide scenario indicates the importance of the stronger uprush during the rising tide on the transport and deposition of finer sediments to the top of the beach (Figure 4.3, D2).

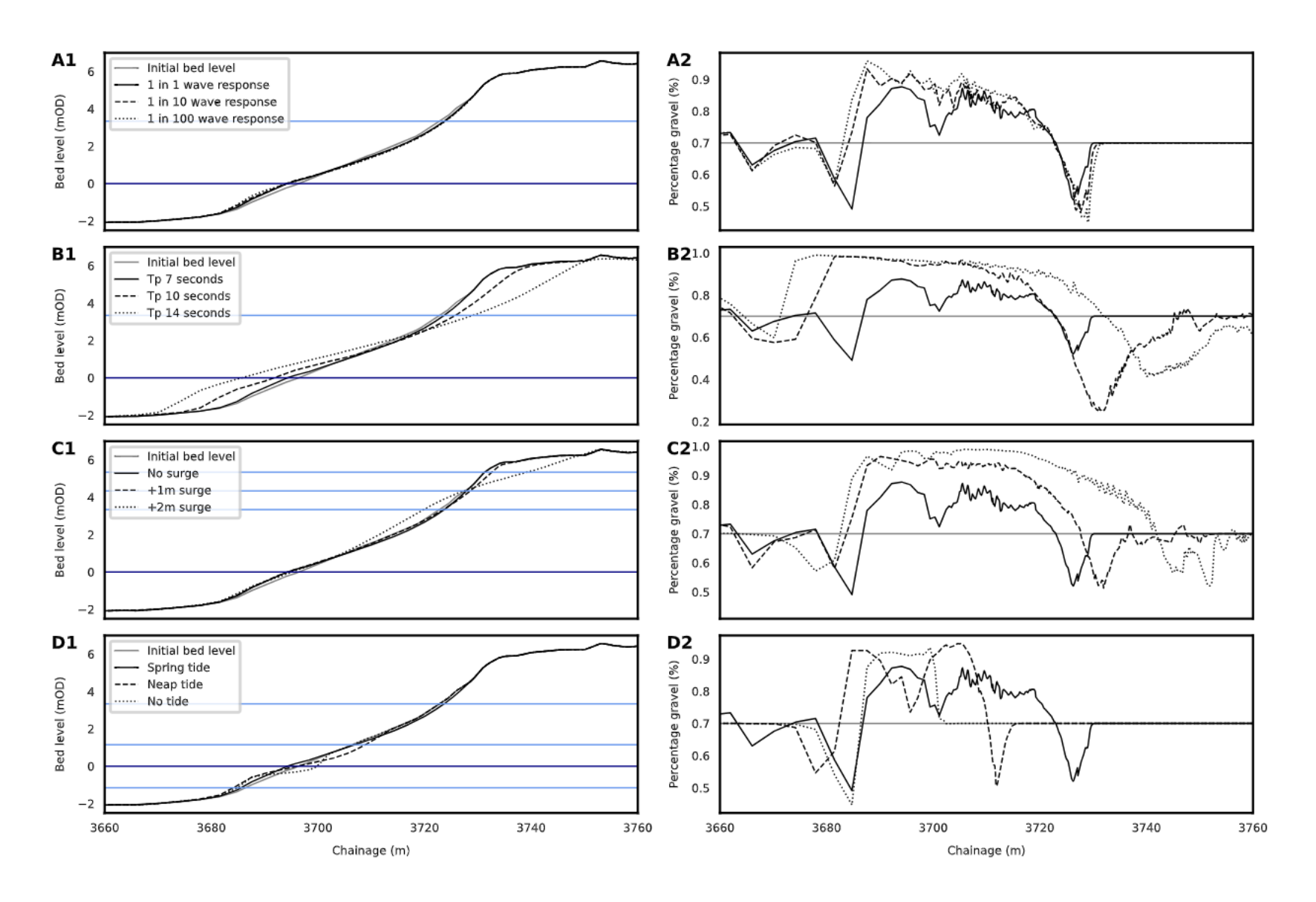


Figure 4.3 – Bed morphology (left) and sediment composition (right) responses to varying hydrodynamic forces, namely A) Storminess; B)

Increasing period; C) Increasing water levels; and D) Spring/Neap/No tides. Mean sea level shown in dark blue horizontal line, high mean spring tide, and mean low and high neap tide levels shown in light blue.

Tidally dependent onshore-offshore movement of sediments is shown in Figure 4.4. Between 10 000 and 15 000 seconds, the distinctive trace of a waterline shows coarsening at the waterline. Below the waterline, small berms are formed, with finer material at the crest and coarser material in between them. This is associated with onshore movement and sorting of sediments. After 15 000 s and up until 23 000 s, fine material is pushed above the waterline, and the area of coarsening becomes greater as the tidal level increases. As the tide recedes and the water level decreases (23 000 s to ~40 000 s) the material in the water column is deposited. Fine material is deposited below the waterline, with coarsening above it, leaving a large expanse of coarser material from around 35 000 s onwards. This is likely caused by the change in slope at around 3680 m chainage, which acts as a base for the drawn down material to build upon. Beyond ~40 000 s there is no more change to the upper beach.

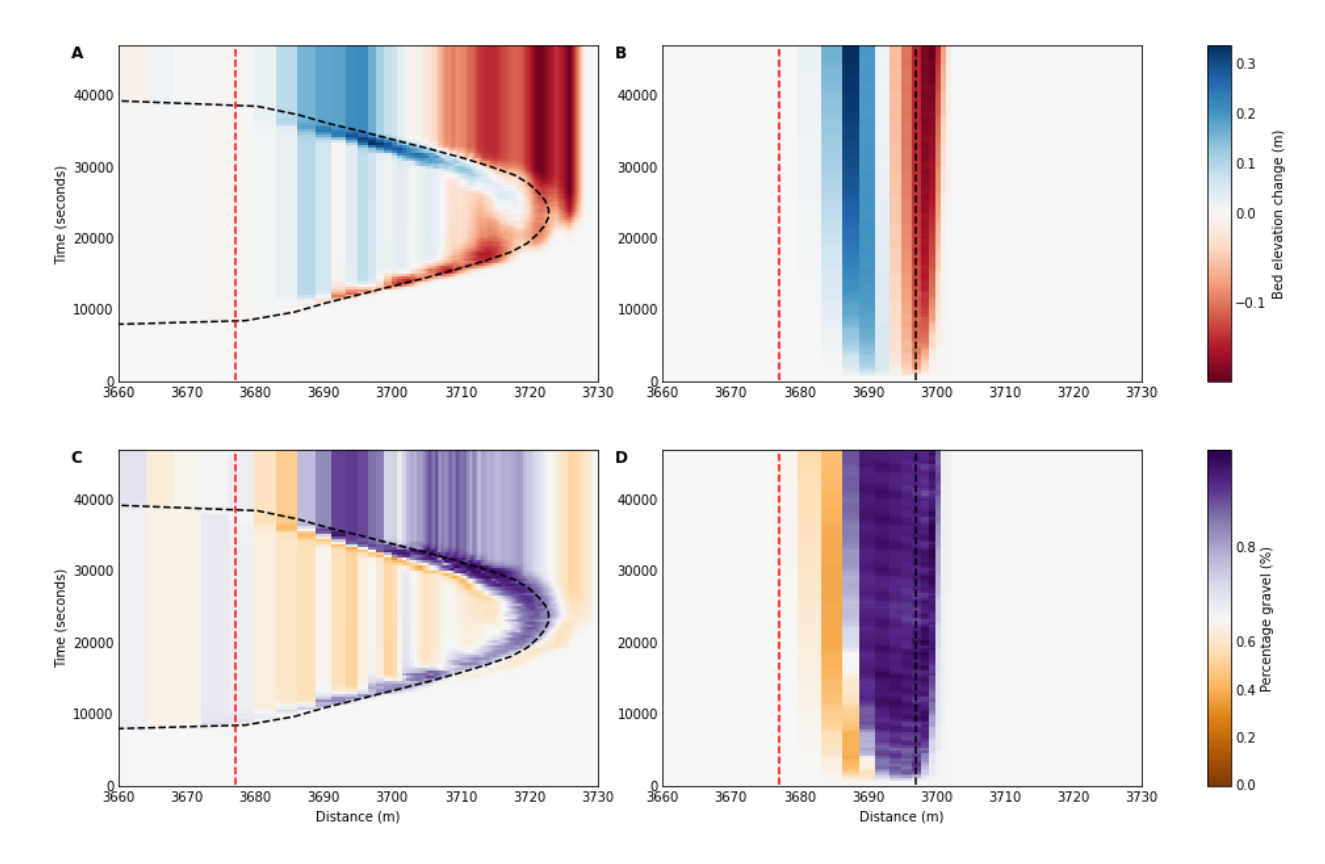


Figure 4.4 – Change in bed elevation (A, B) and sediment composition (C, D) over time for a 1 in 1 storm under spring tide (A, C) and neap tide (B, D) conditions. The dashed red line shows the position of the beach toe at the start of the simulation for reference, and the black dashed line shows the still water level (ignoring wave run-up). Note the offshore boundary is to the left.

4.4.2 Bed slope

The two modelled alternative slope runs, i.e. the 1 in 5 grade and 1 in 12 grade slope, represented the normal upper and lower bounds of mixed sediment beaches as found in nature (Jennings and Shulmeister, 2002). The beach profile response again shows draw down in response to the 1 in 1 year storm conditions, with a developing concave-convex morphology (Figure 4.5). The volume of change is greatest for the steeper slope, as there is greater potential for material to move downslope. Interestingly, both the 1 in 5 and 1 in 12 slope changes extend higher up the beach profile (by ~1.0 m in vertical elevation) and are much larger in volume than the natural slope scenario, which suggests that the Pevensey analogue slope, or 'natural' slope has reached an equilibrium profile. The newly formed berm crest developed around MSL on the natural slope, just below this for the 1 in 12 slope and much higher, at around 2 mOD for the 1 in 5 slope. The position of the newly formed berm crest is likely linked to the volume of material drawn down, which was greatest for the 1 in 5 slope, followed by the 1 in 12 slope. For all slopes, the sediment composition becomes coarser across the active area of sediment transport and becomes finer at the beach toe, where bed elevation change terminates (Figure 4.5, subplot B). For the natural slope, the sediment composition also becomes finer at the very top of the slope, which is not seen in the artificial slopes.

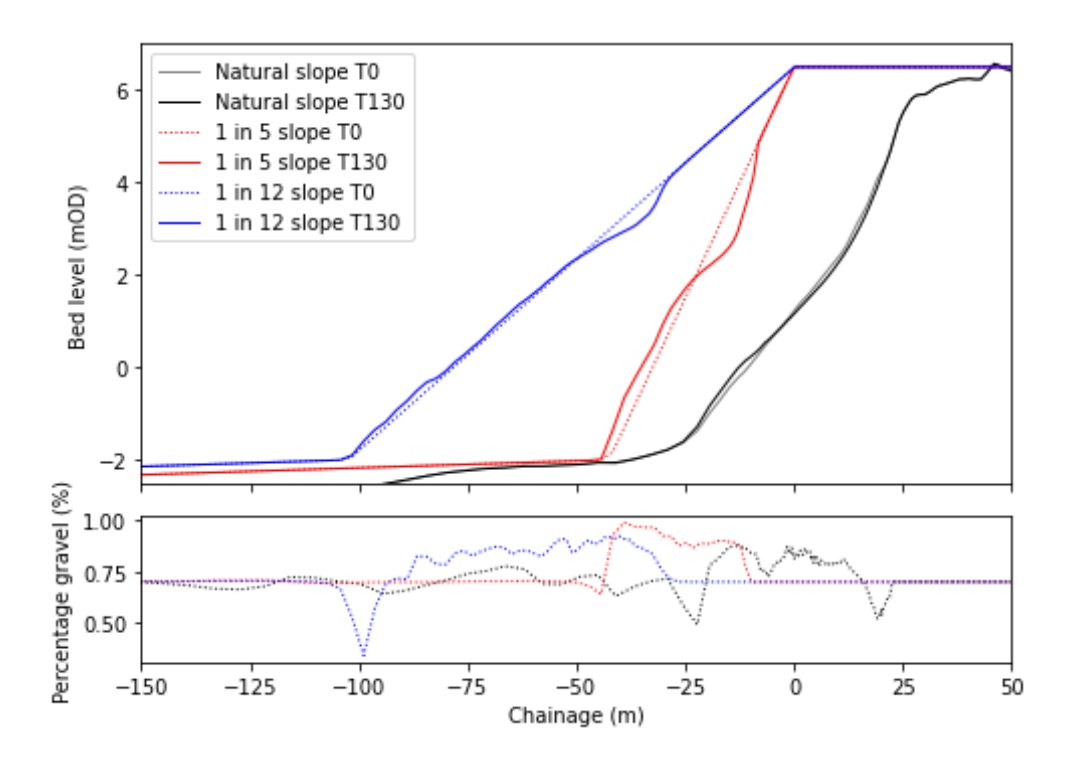


Figure 4.5 – Beach profile response to the 1 in 1 storm for the natural beach profile, 1 in 5 and 1 in 12 graded slopes. N.B. the natural slope is offset by 25 metres for improved readability.

4.4.3 Sediment composition

The same morphological response of beach drawn down within the swash zone is observed across all model runs with varying sediment composition, with some slight differences (Figure 5.6, subplot A). The size of the berm which forms from the drawn down material appears to be proportional to the sand percentage, i.e. a higher sand percentage results in larger berm formation. Conversely, around the upper limit of change, larger vertical changes were associated with a higher gravel composition, although bed displacement was greater for the higher sand percentage beds lower down the beach face (Figure 5.6, subplot B). This is likely due to the greater angle of repose of the larger grain sizes (Beakawi Al-Hashemi and Baghabra Al-Amoudi, 2018) allowing more material to be mobilized at the top of the slope without destabilizing the slope. When gravel percentage was equal to or greater than 60% the beach profile response was very similar, with a steep incision at the top of the beach, and the formation of a berm lower down the beach, with the crest located at approximately 3695 m chainage. In contrast, as sand percentage becomes higher than 40% the beach profile response becomes more dynamic, with more larger changes above and below the crestline of the newly formed berm. This is most pronounced by the shape of the 100% sand scenario, which demonstrates the largest losses of sand across the upper beach profile and the formation of a large sand berm approximately 0.6 m above the original bed, with a distinct crest.

The difference in behaviour in the crest formation between the more sandy/gravelly beds is also marked in the changes in sediment composition (Figure 5.6, subplot C). For the beds with a higher percentage of gravel (>=60% gravel) where the berm formation is similar across the different runs, the berm is formed of coarser material than its surroundings. For the sandier (>=60% sand) the opposite is true, with material being finer than its surroundings.

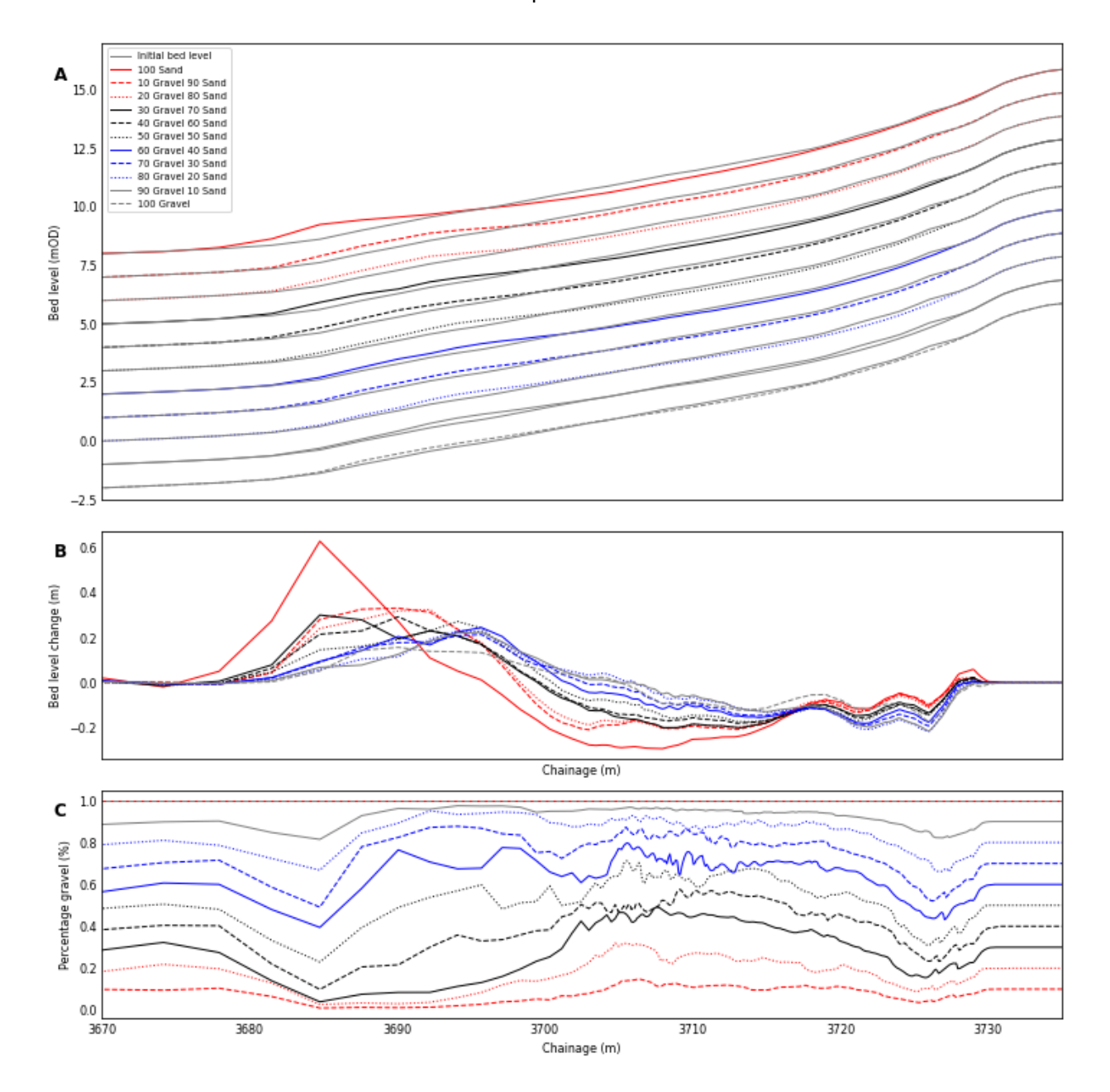


Figure 4.6 – Effects of varying bimodality proportions of sand and gravel fractions at the end of the model run to A) bed level (mOD); B) bed level change (m); and C) cross-shore sorting (surface sediments percentage gravel).

4.4.4 Bed level change overview

The relative level of bed elevation change was quantified through calculating the difference in bed levels between the first and last timestep for each run, and then summing the negative and positive change (Figure 4.7). The results showed that the largest change by far was the two runs where changing peak period was examined, i.e. to 10 and 14 seconds respectively. The change experienced during these two runs was approximately just under 2 to 15 times larger than the other runs. The magnitude of change was seen to increase with the increase in wave power

(runs 1 in 1, 1 in 10, 1 in 100, 10 s, 14 s), and also as water levels increased (1 and 2 m surge). Tidal range was also shown to increase the total bed elevation change, from $2.5m^2$ in the no tide scenario, to 4.0 and 4.2 m² in the neap and spring tide scenarios respectively. Interestingly, bed elevation change increased proportionately (R² 0.98) for sand gravel mixtures with less than 40% gravel, however, the bed elevation change for the 80:20 and 90:10 sand and gravel runs were significantly lower than could be expected (R² of 0.56). It is unknown why this reduction may have occurred.

The majority of beach profile change occurred on the upper beach slope (average 74.2%, with a standard deviation of 12.1%). The exceptions to this were the 2 m surge, the neap tide and the 100% gravel scenario. Due to the model set-up, the minimum water levels for the 2 m surge, and neap tide were -1.30 mOD and -1.13 mOD respectively, meaning that the sandy foreshore was not exposed. In the case of the 100% gravel bed it is expected that there was not enough energy to mobilise these sediments, especially on the flatter bed where the offshore gradient is lower.

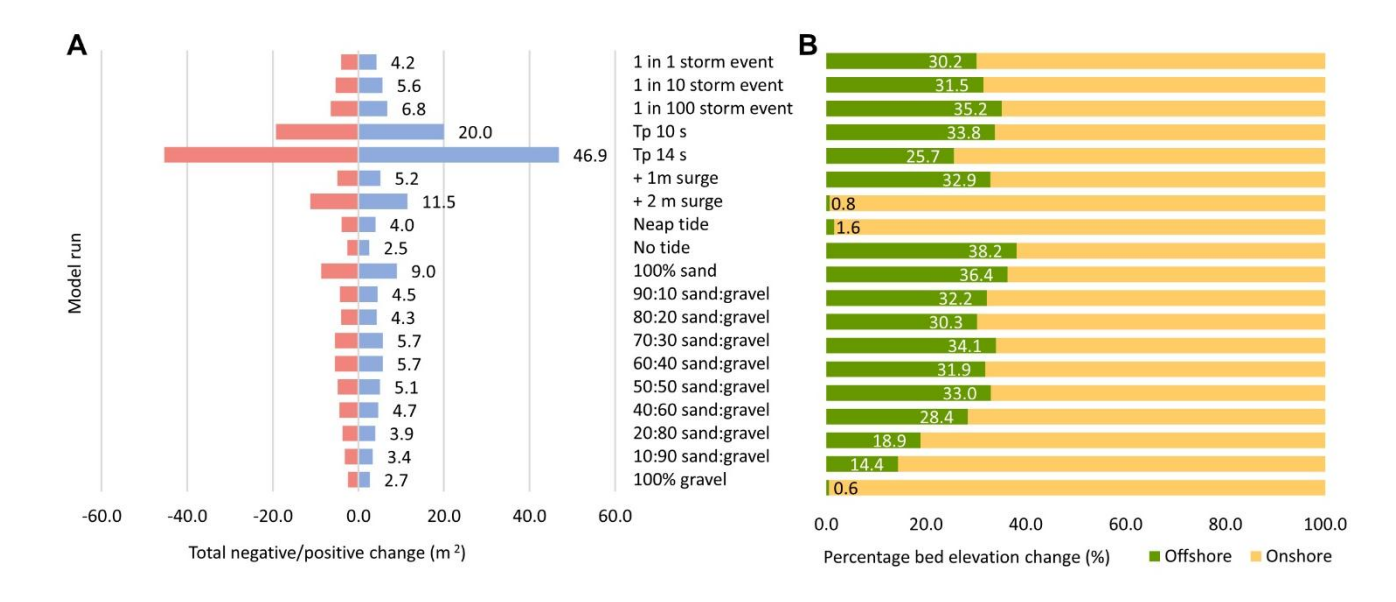


Figure 4.7 – A) Volumetric bed elevation change across the different model runs; B) relative percentage change onshore and offshore where the boundary used is the initial position of change in bed slope (beach toe). a chainage 3680 m.

4.5 Discussion

Overall, the model largely agreed with previous observations in the field. A key control on bed elevation change appears to be bed slope, as the upper beach was the most morphodynamically active region. From the offshore boundary to shore, the majority of the wave energy was attenuated by the gently sloping seabed. Additionally, the tidal levels were essential

in driving morphological change (Masselink and Short, 1993), as only during peak tide times was the water deep enough to allow larger waves to reach the upper beach. This reflects the findings of an Empirical Orthogonal Function analysis of observation data at the composite beach Milford-on-Sea through, which found the upper beach to be the most morphodynamically active zone (Karunarathna et al., 2012). In the model runs with varying sand content, it was shown that as the sand content increased the resultant post storm beach profile became flatter, and as this model cannot replicate onshore movement of gravel, the findings are thought to agree with Bujan et al. (2019) and Woodruff et al. (2021) where bed slope corresponds to the bulk median grain size. For Woodruff et al. 's work, this relationship broke down when the bulk median grain size exceeded 1 mm, which we postulate was due to the importance of numerous site specific factors influencing mixed beach sediment transport, however, in the model, as we are only able to model draw down of sediment (as the ground water effects which are needed to achieve the velocities for onshore gravel transport are not met)this relationship is preserved.

Under all scenarios, the majority of the upper beach profile became coarser. Sand was deposited at the very upper reaches of the swash limit, and also on the front face of the new berm which formed. The deposition of fine sand at the very top of the beach following stormy conditions has been reported at Pevensey (Ian Thomas, pers. comms), although this has also been reported in the wider literature (Ciavola and Castiglione, 2009). The time plots suggest that this is due to the uprush being stronger than the backwash on the rising tide, and weaker on the falling tide; depositing finer material which was suspended in the water column at the top of the beach, but not having enough energy to mobilise larger sediment from this region (Figure 4.4). As the tide receded and the newly formed berm, or 'beach step' (Bauer and Allen, 1995), migrated down the beach, the surface sediments became increasingly coarse (Figure 4.4). Observational data from Pevensey showed that following storm events, the section of beach between the beach crest and MSL was typically finer than the material between MSL and the beach toe (Watt et al., 2006). The model has shown that this response is linked to the draw down of sediments, with coarsening peaking at the location of the beach step. The fining at the toe of the beach occurs between the crest of the newly formed 'drawdown' bar, and the beach toe, which suggests a depositional environment as the tidal stage progresses to low water, transitioning between upper 'reflective' to the lower 'dissipative' wave conditions. No evidence of a 'plunge pool' style scour on the foreshore was found, as with modelling carried out on a composite beach (Phillips, Brown and Plater, 2020), and there are likely two main reasons for this. Firstly, the work by Phillips et al. used a non-erodible upper beach which would have had a stronger associated reflection in the absence of beach drawdown in the upper beach. Secondly, in our model the sediment is mixed throughout and therefore, for all the runs containing a fraction of

gravel, would be more stable than for a pure sand bed, as modelled by Phillips *et al.*. However, in reality following storms, the beach is usually very well sorted at the toe (Ian Thomas, *pers. comm*), which at a MSG in Teignmouth, UK, was shown to be attributed to an increasing in groundwater flow as the tide level fell below the groundwater table (Kulkarni *et al.*, 2004).

The modelling of mixed sediment beaches is currently limited due to the over-simplification of porosity and exclusion of ground water effects. Firstly, a uniform application of porosity across the model domain is not realistic for mixed sediment beaches. Porosity affects the attenuation and dispersion of wave energy and therefore controls the amount of energy available to mobilise sediment. As a function of void space between grains, porosity is lower for 'well-packed' mixed sediments but is higher for 'underfilled' or 'overfilled' more uniform sediments (She, Horn and Canning, 2006). Incorrect representation across a heterogeneous beach profile can therefore lead to under or over estimation of sediment transport. The inverse of porosity, the hydraulic conductivity, describes how quickly fluid can move through a matrix, and depends on both the permeability of the medium, grain size and viscosity of the fluid. A recent numerical modelling study using XBeach-G, showed that for gravel beaches the hydraulic conductivity was a key control on the morphodynamic response of a beach profile to storm waves, where high values led to berm formation whilst low values resulted in erosion (Soloy et al., 2024). This leads onto the second fundamental limitation. It is not currently possible to include groundwater effects when modelling multiple sediment fractions, although these have been implemented within XBeach-G as these effects are especially important for the mobilization of coarse material (McCall et al., 2014). As with the porosity, if adaptations can be made to enable the XBeach-G settings to be used for multi-fraction sediment modelling, it would also be necessary to have spatially varying values for hydraulic conductivity. To help accommodate this, dynamic values for hydraulic conductivity and porosity could be calculated from the sediment composition at each grid point, however it is unknown how computationally expensive this would be to implement.

4.6 Conclusion

The process based, XBeach-X model was used to examine changes in bed elevation and sediment composition of a mixed sand gravel beach for 21 scenarios with independent hydrodynamic, bed slope and initial sediment mixture configurations. The overall aim of this paper was to improve our understanding of how MSG beach sediment sorting and morphology respond to storm waves under varying conditions. We learnt:

- Hydrodynamics: wave power controlled the magnitude of change across the beach
 profile, although increased elevation change was a function of decreased tidal range.
 The rising and falling tide were also important in terms of the development of the
 fining:coarsening:fining change seen across the beach profile in response to all model
 runs, with the exception of the no tide run, which only became coarser above the
 waterline and finer below the waterline.
- Bed slope gradients: Two artificial slopes, with a grade of 1 in 5 and 1 in 12, were
 modelled in comparison to the natural analogue, and both exhibited much larger
 volumetric change, most likely as they were significantly out of equilibrium with the
 given wave conditions. As a result of the large draw down for both artificial slopes, no
 fining was seen at the top of the beach, unlike other test cases.
- Sediment composition: model runs with a higher sand content were more dynamic and had a larger berm form than those with a greater proportion of gravel, however, the changes at the upper reaches of the swash zone were greatest for beaches with a higher proportion of gravel. Berm formation was associated with finer/coarser bed material than the initial bed for sediment compositions >=60% sand/gravel, respectively.

Overall, the swash zone was shown to experience the largest changes in bed elevation, although the gently sloping foreshore was responsible for dissipating much of the incoming wave energy. All responses involved drawdown of the beach. Sorting patterns reflected largely those observed in the field, although exclusion of groundwater effects are thought to have allowed deposition of fine sediments at the toe of the beach. The study has highlighted the need for improved methods for modelling mixed sediment beaches in the future, namely through the inclusion of groundwater and variable permeability which is critical in highly heterogenous environments such as MSG beaches.

4.7 Acknowledgements

This work was supported by the Environment Agency through the project: "Delivering Legacy from the Pevensey Bay Coastal Defence Scheme (PI: Kassem, H.; Contract: 201-09-SD10). The lead author undertook this work as part of their PhD studentship, funded by NERC INSPIRE DTP (NE/S007210/1), the Graduate School of the National Oceanography Centre, Southampton, and the Environment Agency. Further thanks go to Connor McCarron, Kristian Ions, Ollie Foss and Jenny Brown for help and advice and Robert McCall for sharing archived versions of XBeach.

Chapter 5 Synthesis and Conclusion

The purpose of this chapter is to provide a comprehensive synthesis of the research carried out as part of this thesis, answering the three research questions and bring the work together to build a conceptual model (Section 5.1). The conceptual model summarises the significant original contributions to knowledge. Recommendations for further research are outlined (Section 5.2), and the conclusions of the thesis are given in Section 5.3.

5.1 Synthesis

5.1.1 Research Question I

What is the cross-shore extent of the geomorphologically active zone within a mixed sediment environment?

This question was addressed by Paper 1 which aimed to investigate depth of closure at a mixed sediment beach as virtually no information had been sourced from the literature. We follow Kraus et al.'s (1998) definition that the depth of closure marks the edge of the geomorphologically active zone, *i.e.* observed bed level change, over a given time-scale, and recognise that this is not the seaward limit to sediment transport (Valiente et al., 2019). Observational data of the nearshore was scrutinised over short (days-months) to medium (years) time scales to find 1) how the observed depth of closure compared to numerical estimations which have a basis in sandy sediments; and 2) a method for interpreting observed variations in the depth of closure.

In a bay wide assessment of the limit of seasonal bed elevation change (Paper 1), nearly every beach profile inspected had a shallower depth of closure than predicted from wave parameters (Hallermeier, 1978; Birkemeier, 1985). This is a common finding associated with comparisons between observation derived depth of closure, and the predictive equations (Hinton and Nicholls, 1998; Robertson *et al.*, 2008; Hartman and Kennedy, 2016; López *et al.*, 2020; Udo, Ranasinghe and Takeda, 2020; Barrineau, Janmaat and Kana, 2021). Two main causes are attributed: 1) real-world conditions do not reach equilibrium as achieved in the numerous laboratory flume tests used to validate Hallermeier's (1978) energetics-based equations (Rector, 1954; Eagleson, Glenne and Dracup, 1961; Monroe, 1969; Paul, Kamphuis and Brebner, 1972; Raman and Earattupuzha, 1972; Sunamura and Horikawa, 1974); 2) observational data does not capture a maximum geomorphic change which would occurs during the peak of a

storm event, rather it captures the seabed after it has had a chance to recover. The first point is difficult to address; the suggestion by Udo et al. (2020) to carry out a global reanalysis of existing datasets could potentially further our understanding of beach profile developments and the role of depth of closure, however was outside of the scope of research. Attempts to resolve the second issue were made using firstly the X-band radar derived bathymetry and secondly one of the X-band radar data flags - the depth saturation parameter (Figure 5.1). The depth saturation parameter is essentially a ratio between the wavelength detected and a pixel, and its deepwater equivalent (derived from the wave period using linear wave theory) and is a measure of how well the wave is touching the bottom (Paul Bell, pers. comms.).

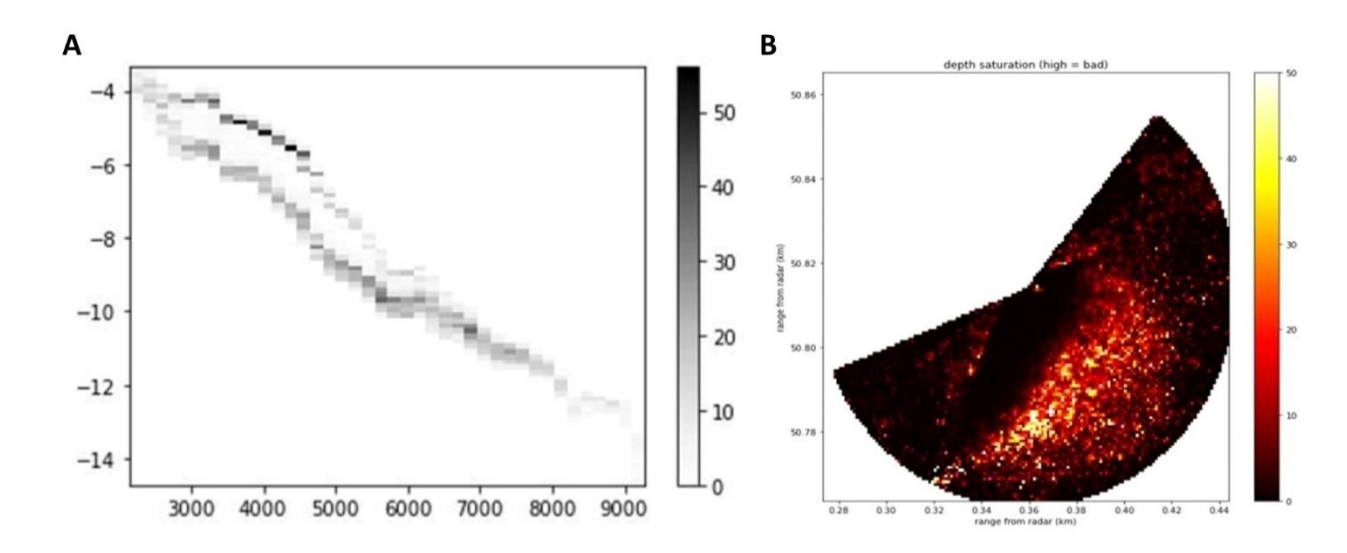


Figure 5.1 – Use of radar in detecting depth of closure taking a probabilistic approach, showing

A) a histogram of depth derived profiles, B) Depth saturation parameter.

The intended output of this research was to create a probabilistic depth of closure, taking advantage of the high-frequency temporal output (bathymetry produced ever fifteen minutes). However, the initial bathymetry elevations were highly variable and there were considerable differences between it and the conventionally surveyed data, and whilst revisions of the algorithm used to create the bathymetry from the raw data were subsequently improved, reanalysis of this dataset was not possible within the PhD timeline. Further development of this preliminary analysis may be an interesting research avenue, as the use of novel data sets to expand our knowledge of coastal morphodynamics and the depth of closure concept.

Reverting to more conventional methods of bathymetry collection, Paper 1 highlighted that the depth of closure was not constant within the bay. To help interpret local variations, the depth of closure conceptual model was designed to help scaffold a qualitative assessment of real site observations underpinned by existing coastal science theory (Paper 1, Figure 2.1). Following this

structure, grain size was not found to be as important as first thought. The image interpretation of the backscatter imagery showed that the nearshore area was a diverse array of sandy, mixed, gravel and rock outcrops, however, the local variation in the observed depth of closure did not correspond with grain size, *i.e.* some of the shallowest closure depths were associated with sandy beds. The mosaic of bed types, lack of widespread grain size distribution measurements, and even limited information on bed type (the surficial bed type interpretation was ten years old at the time) meant that it was not possible to create a new equation for a mixed/coarse sediment the depth of closure, as had been done at other sites to take into account local factors (Birkemeier, 1985; Aragonés, Pagán, I. López, *et al.*, 2019). Whilst this would have been highly useful for engineers and scientists, it brought to light the difficulty with working in complex environments with limited information, showcasing the importance of long-term nearshore datasets.

5.1.2 Research Question II

How does sediment move through and within a mixed sediment system and how does this contribute to change over different timescales?

As with many coastlines in the world, the gravel barrier at Pevensey Bay is constrained because of human intervention. The construction of Sovereign Harbour and its breakwaters in the 1990s interrupted the supply of sediment from the east to west and so ensued further active intervention along the coast. As a result, each year approximately 110 000 m³ of sediment is recycled (80 000 m³), renourished (20 000 m³) and bypassed (10 000 m³) to maintain what would have been the natural supply of sediment from the west (Townsend *et al.*, 2024). The increasing effort carried out by the contractor to maintain the beach volumes, despite no noticeable difference in storminess, has raised call for concern (Ian Thomas, *pers. comms.*). Active beach management data provided an insight into pinch points of erosion and volumes for total drift out of the study site each year, however, further work was required to understand how the sediment moved through and within the frontage, and what the impacts were.

Sediment transport modelling demonstrated that at Pevensey, longshore transport was considerably greater than cross-shore, at a ratio of approximately 25:1 for coarse gravel material and between 125 to 200:1 for fine sandy sediment (Paper 1, Figure 2.6). The dominant longshore drift direction was easterly, with cross-shore transport favouring offshore transport. The sediment transport modelling was based on application of sediment transport models to calculate long and cross-shore drift potential within the surf zone, using the wave and water level records, and geometry of the shoreline. These findings are supported by the study of

topographic and bathymetric change over time, which can be used to infer sediment transport pathways. Firstly, a regional sediment budget, calculated between Eastbourne and Rye, using the method of Rosati and Kraus (1999) showed that the frontage experienced net easterly transport, with transport rates ranging between 30 724 to 53 636 m³ per annum (Environment Agency, 2017). These values are in the same order of magnitude as those estimated for coarse grain littoral drift potential, using Damsgaard and Soulsby (1996), which estimated transport potential at 25 500 m³ pa in the west declining to around 15 300 m³ pa in the east (Paper 2, Figure 2.6).

In contrast, the Xbeach-X modelling indicated that over shorter timescales (days, months, years) cross-shore transport is limited at Pevensey. Over these small timescales high-tide berms, which migrate up and down the beach with the tidal cycle (Masselink *et al.*, 2010), are common across the frontage, normally with amplitudes of approximately half a metre, but are not present at the site all the time. Although not calibrated, Paper 3 explored the cross-shore storm response of a Pevensey analogue and found that the majority of change occurred in the upper beach. Overtopping was only observed in the model during a 2 m surge and under swell wave conditions, and therefore all sediment exchange was balanced (none exiting the system via roll-back processes). Of course, over longer timescales cross-shore transport and the reworking of sediments have played an important role at Pevensey; allowing the formation and landward migration of the shingle barrier over the course of thousands of years in response to sea level rise, as documented in the work by (Mellett *et al.*, 2012). Further description of cross-shore processes are described in RQ III.

In addition to the hightide berm (cross-shore process), a number of bedforms associated with longshore sediment transport were identified at Pevensey, namely; transverse finger bars, gravel ridges (Figure 5.2, subplot A) and large-scale surface undulations (Figure 5.2, subplot B). Migration rates were derived for the transverse finger bars and large-scale surface undulations, at weekly and annual scales, respectively, which were found to be comparable to each other, with a net easterly migration covering approximately 150 m per annum. Furthermore, a statistically significant (P < 0.001) relationship was found between the median weekly migration rate of the transverse finger bars and the average longshore drift potential ($R^2 = 0.38$), which takes into account both wave power and incident wave angle relative to the shore (Paper 2, Figure 3.7; Soulsby, 1997). Whilst this goes some way to explain the movement of the bars, further work is needed to uncover whether this accurately reflects the contributions of waves in mobilising the bars, or if other drivers are more important. Linear stability analysis (Ribas *et al.*, 2011, 2014) would be one potential avenue of further investigation that could potentially help

identify the conditions required for the formation of these features. Moreover, in Paper 3, the potential for extension of the 1-D multi-fraction XBeach-X modelling to a 2-D (quasi-3D) was discussed, and developments such as this could be used to investigate the formation of the transverse gravel ridges observed both at Pevensey (Figure 5.2) and on the Suffolk coast (Atkinson, 2019), which we suspect are related to longshore sorting processes and the more irregularly shaped gravel-runs described by (Lamarchina, Maenza and Isla, 2021).

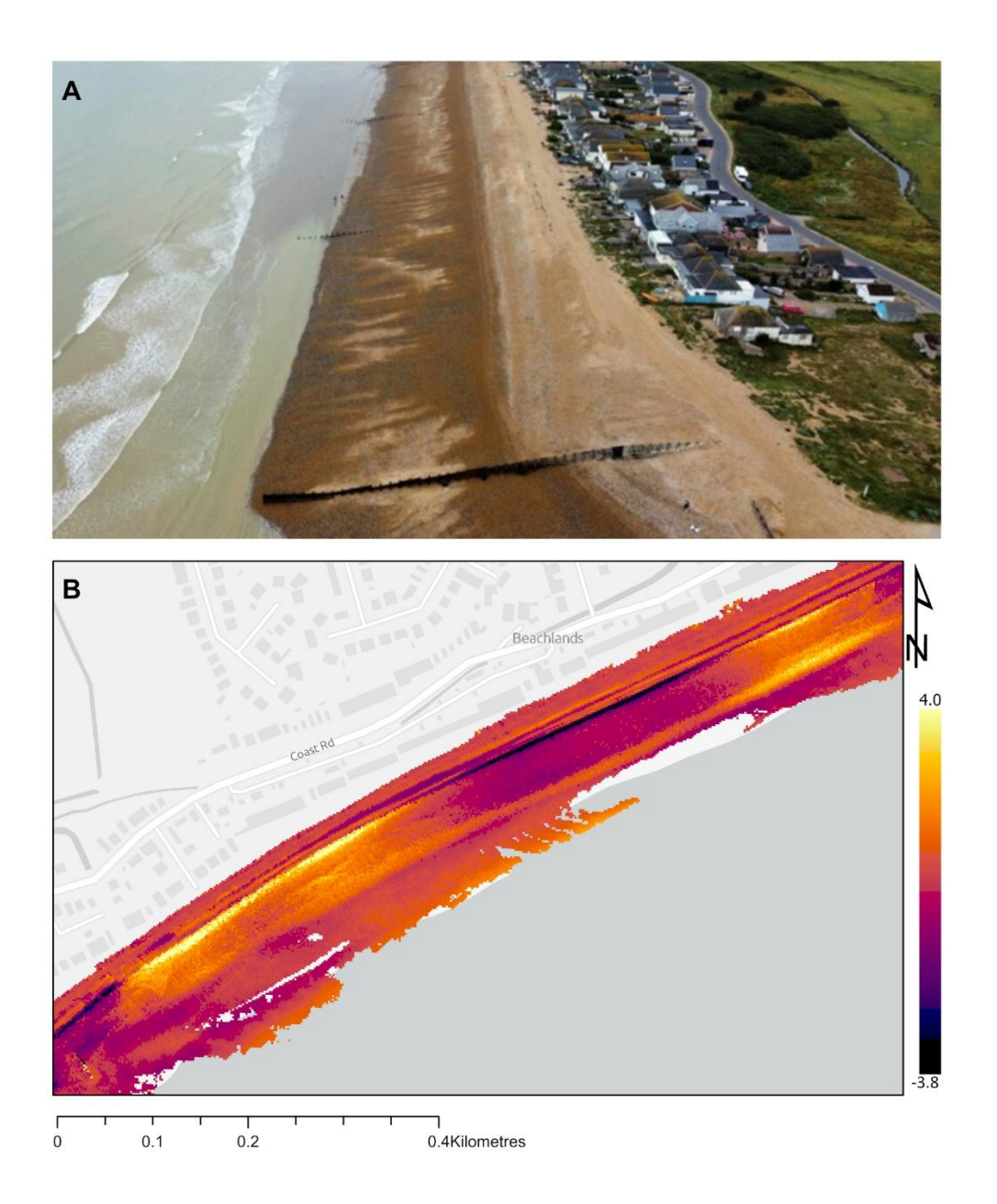


Figure 5.2 – Two examples of rhythmic bedforms found in the study site; A) small scale gravel ridges found alongshore (wavelength ~5-10 m); B) larger scale surface undulations as shown in difference model between 2018 and 2019 NNRCMP data (wavelength ~200 to ~400 m). Data from NNRCMP freely available from www.channelcoast.org.

Contains OS Data (c) Crown Copyright and database right 2023; contains data from OS Zoomstack.

Surficial sediments at points between 500 and 2300 m offshore were shown to change throughout the year in response to seasonal conditions. Sediment grab samples were taken from this area every four months over the course of 20 months (Paper 1, Table 2.2). Since the publication the work in Paper 1, the remaining samples have been analysed in the laboratory, and corresponding data collected (Table 5.1). The results show high variability in sediment textural groups both across time and between east and west, also onshore and offshore. Though this can partially be explained by seasonality and sediment suspension, and partially due to the presence of decaying transverse finger bars, neither offer a comprehensive explanation of what has occurred here. A standout finding is the significant proportion of mud within the system. It is still not understood what role this mud might play in sediment transport and the formation of bedforms, nor do we understand the mechanisms behind its wider complex distribution, which appears more complex than the picture painted from the 2013 backscatter inferred bed type.

Table 5.1 – Update to 'Mud, sand, gravel ratios by weight taken from samples at the instrumented array' as presented in Paper 1, Table 2.2, following additional samples being processed.

	West array			East array				
Metres offshore	% mud	% sand	% gravel	class	% mud	% sand	% gravel	class
	May sample							
500	5	95	0	sand	7	92	1	sand
1100	6	94	0	sand	30	70	0	sandy mud
1700	5	65	30	gravelly sand	27	73	0	sandy mud
2300	7	93	0	sand	8	78	14	gravelly sand
September sample								
500	31	69	0	muddy sand	35	65	0	muddy sand
1100	34	66	0	muddy sand	53	47	0	sandy mud
1700	64	36	0	sandy mud	73	27	0	sandy mud
2300	21	79	0	muddy sand	2	98	0	sand
	December sample							
500	11	64	25	gravelly muddy sand	24	74	2	muddy sand
1100	27	72	2	muddy sand	27	71	2	muddy sand
1700								
2300	15	61	24	gravelly muddy sand	28	54	18	gravelly muddy sand
February sample								

500	53	44	3	sandy mud	1	78	20	gravelly sand
1100	50	26	24	gravelly mud	19	77	5	muddy sand
1700	0	0	100	gravel	1	26	73	sandy gravel
2300	0	1	99	gravel	0	28	72	sandy gravel
	April sample							
500	42	56	2	muddy sand	24	74	1	muddy sand
1100	33	66	2	muddy sand	23	75	2	muddy sand
1700	39	59	3	muddy sand	38	59	3	muddy sand
2300	29	60	11	gravelly mud	24	67	10	gravelly mud

Change in the nearshore over medium timescales was quantified through the comparison of cross-sectional data, showing progressive loss of sediment over an 18-year period (between 2003 and 2021) (Paper 1, Figure 2.7). The finding, together with what we have learnt about sediment transport helps shed light on the loss of sediment to the upper beach as reported by Thomas (2015). We postulate that the nearshore is losing sediment overtime as the predominant south westerly waves drive sediment transport towards the east. Over time this is denuding the nearshore area at Pevensey, allowing larger waves to reach the shore. Changes to the upper beach are occurring too. The active beach management that is undertaken at Pevensey is effectively locking the shoreline in place, contributing to the steepening of the barrier overtime: as the nearshore, and sandy foreshore are losing sediment (Paper 1, Figure 2.7). This thesis does not attempt to model or predict change over longer timescales, nor does it examine historical change (Tyhurst, 1972; Jennings and Smyth, 1990) for clues of what may lay ahead at the site. However, the unique behaviour of mixed sediment beaches demonstrated over the short term brings into sharp focus the need to better understand the potential for long-term evolution: how resilient are mixed sediment beaches in the face of climate change?

5.1.3 Research Question III

How does cross-shore sediment exchange vary under a variety of hydrodynamic, morphodynamic and sedimentological conditions?

Paper 3 directly address this question by performing a series of experiments in the process-based 1-D model XBeach-X. The depth of closure framework was used to help develop a set of controlled tests whereby a beach profile could evolve in response to storm waves, under the three test headings of hydrodynamics, bed slope and sediment composition. The model grid and boundary conditions were based on an analogue of Pevensey Bay to give a robust physical basis for a model that could then be used as a toolbox to understand mixed sediment beach dynamics. During high-energy storm events, barrier beaches undergo rapid morphodynamic transformation; ranging from beach draw-down, storm crest building (on coarse clastic coasts),

hinterland inundation, barrier roll-over, and in extreme cases, catastrophic breakdown of the barrier (Bradbury and Powell, 1992; Sallenger, 2000). Because of the potential for destructive behaviour which threatens those living on the coast, the focus of modelling efforts to date has been simulating this behaviour. XBeach, for example, was created following the devastating impacts of hurricanes on the US East coast (2004-2005) (Roelvink *et al.*, 2009). However, there has been a recent shift towards modelling fair weather conditions, which are now being recognised as highly important in capability of coastal systems to bounce back after such erosive events (Grossmann *et al.*, 2023). These developments are promising, and would be worth exploring for mixed sediment beaches, especially following the recent attention on 'seasonal composite beaches' (Casamayor *et al.*, 2022; Soloy *et al.*, 2024). This thesis does not focus on the morphological response of fair weather forcing; however, this is a clear future avenue for research.

The modelling study concluded that the key response of the modelled mixed sediment beach was the drawdown of sediment and the formation of a 'beach step' with a distinctive pattern of sediment sorting across the upper beach. The beach step was shown to develop in the steeper upper section of the beach, tracking the waterline of the changing tide. Stronger uprush and weaker backrush on the rising tide drove fine sediment up the beach face, however on the falling tide, this relationship reversed, and fine material was drawn offshore, resulting in the distinctive finer:coarser:finer sediment composition distribution (Paper 3, Figure 4.3). These results reflect existing field work (Kulkarni et al., 2004; Watt et al., 2008), giving credence to the model behaviour. A key difference between field and modelled observations was the (modelled) deposition of fine material at the toe of the beach. This was attributed to the lack of groundwater effects within the model which would in reality, flush out fines from this area (Kulkarni et al., 2004). Additionally, the model provided a mechanism deposition of fine material at the tops of mixed sediment beaches after storm events both at the site and more widely (Figure 5.3; Ian Thomas, pers. comms., 2022; Ciavola and Castiglione, 2009).

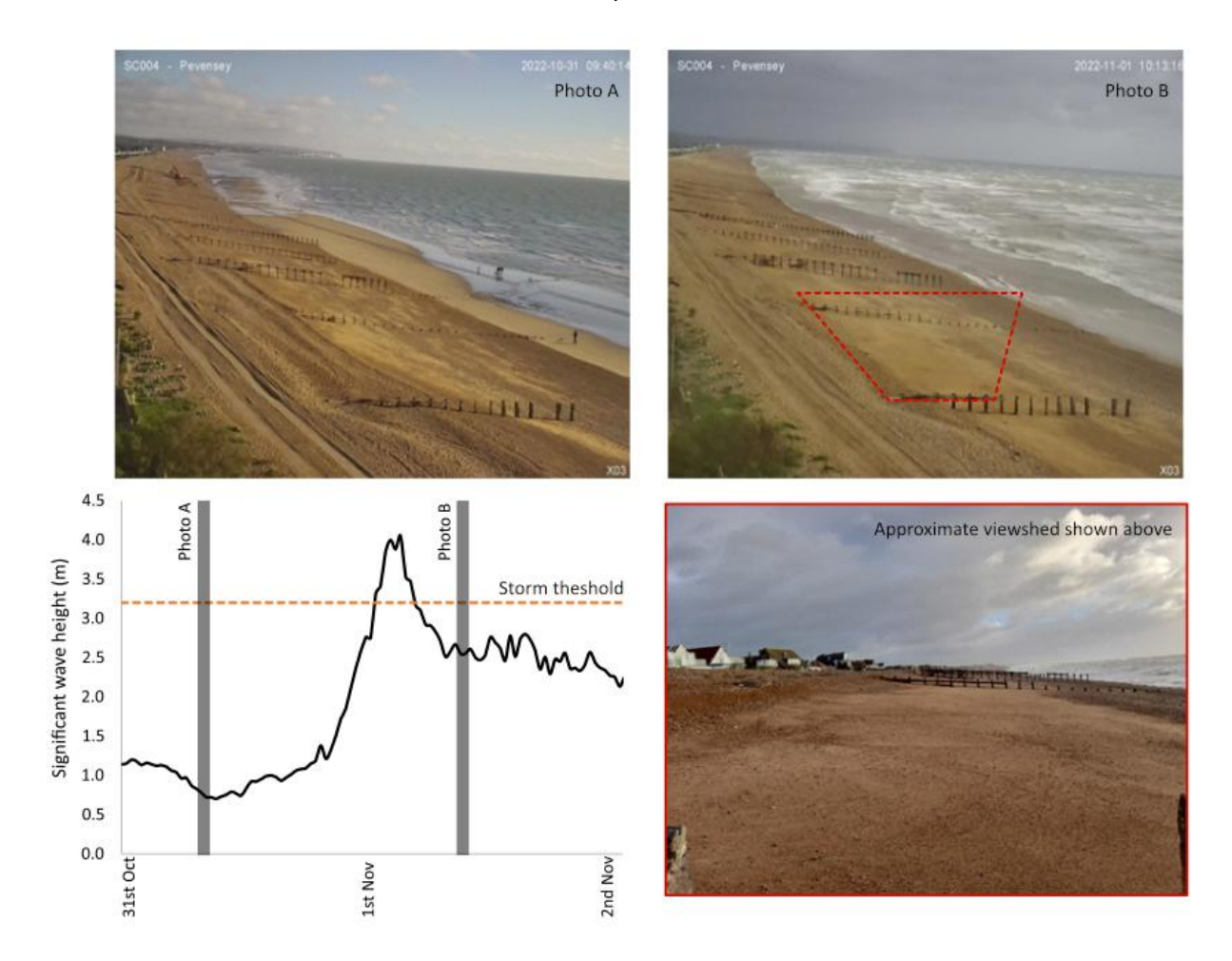


Figure 5.3 – Photos taken at low tide before and after a storm event on the 1st of Nov 2022, highlighting the change in surficial sediment composition and reduction in beach levels. Wave data pictured taken from the Pevensey wave buoy, part of the NNRCMP (freely available from www.channelcoast.org).

In Paper 1, the location of the 'Landward Minimum Morphological Change', defined as the most landward point to reach Kraus' definition of the depth of closure, brought to attention a morphologically stable point between larger changes on the steeper upper beach face, and larger still changes to the subtidal region. In Paper 3, this point was again observed for those scenarios with a strong basis in reality, *i.e.* those derived from the extremes analysis/ignoring those 10 s and 14 s Tp scenarios (Figure 5.4). Paper 1 showed this point to be widespread within the frontage, and the appearance of a stable zone in the shallow nearshore is an attractive explain all, as engineers typically treat the upper gravel-rich beach as a distinct entity from the sandy nearshore. The XBeach-X model in Paper 3 is strictly cross shore, and so therefore it is likely that this 'null point' is associated with cross-shore, or lack of, processes. Close inspection of the area that the null point appears (3550 m chainage, Figure 5.4) coincides with a very flat part of the shallow nearshore. This could mean that the inactivity in this region is due to

the lack of slope and suggests that the offshore slope term is highly important in the generation of bed elevation change, and sediment connectivity between the steeper upper beach and the lower flatter beach. This is an interesting area for further research, raising many questions: Is this feature found at other composite beaches, is there a sediment exchange above and below this point and does this point move over time? An initial study could focus on better quantification of this point, and the sediment balance/exchanges occurring around it, either through observations made in the field or through modelling.

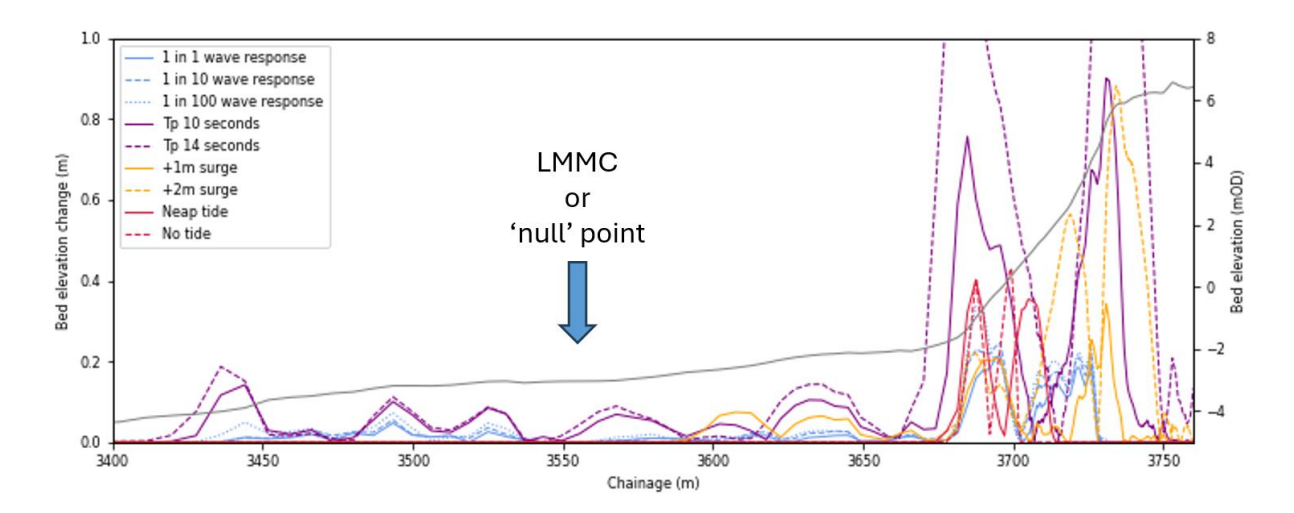


Figure 5.4 – Finding the 'null point,' or Landward Minimum Morphological Change (LMMC) on a modelled mixed sediment composite beach (Paper 3).

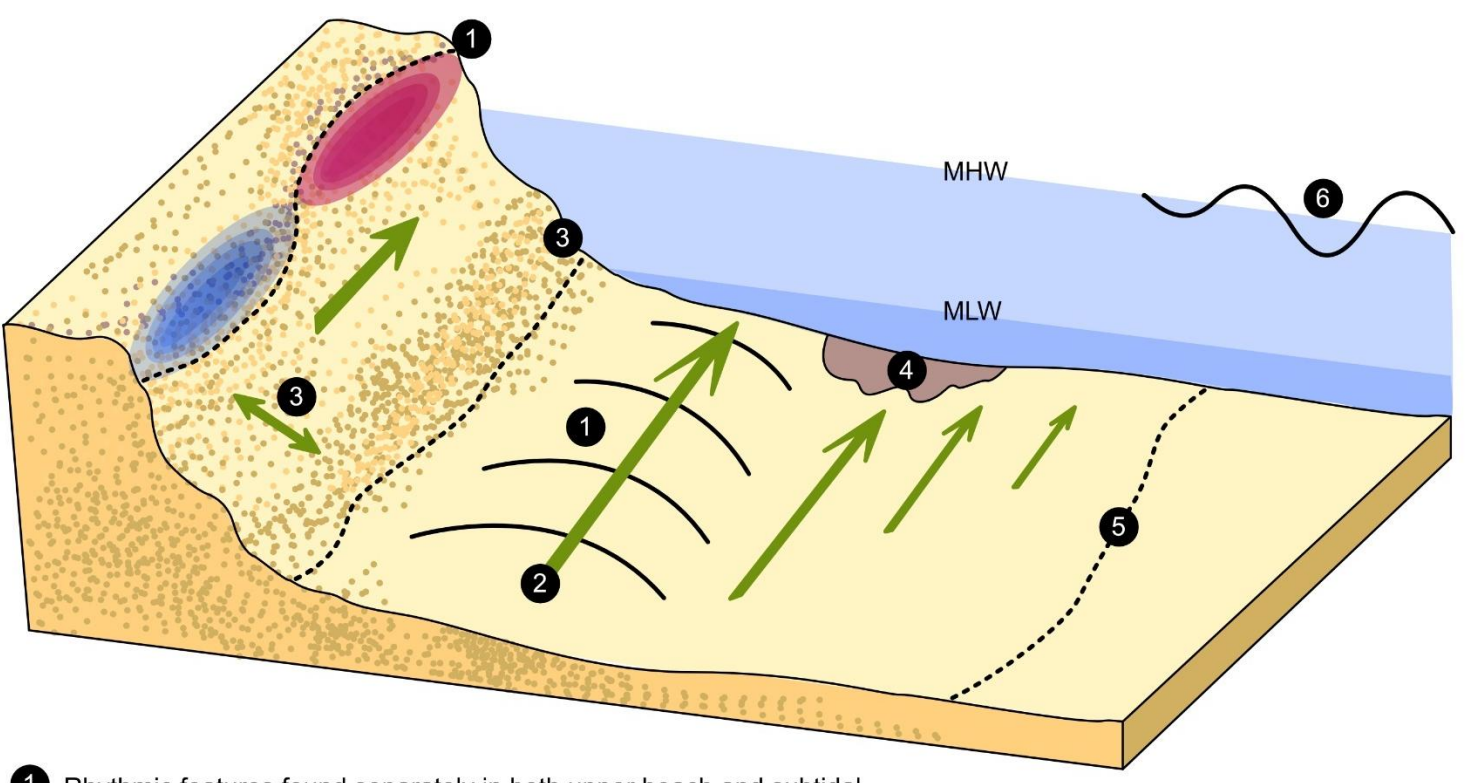
A final note should be made on the timescales considered in answering this chapter, which are all event focused. To investigate meaningful change at longer timescales, e.g. those useful to engineers, a different modelling approach may need to be taken either through the truncation of active time, such as that used by Broaddus and Foufoula-Georgiou (2024) in their representation of delta development over the scale of thousands of years using a process based model.

5.1.4 From swash to the depth of closure; a conceptual model for a mixed sediment beach

Six key findings were made as part of the research investigating nearshore change at Pevensey, which may be applicable to other mixed sediment beaches. Figure 5.5 summaries each finding, and here each finding is expanded, and its *significance* and *originality* demonstrated.

 Rhythmic features found separately both in upper beach and subtidal. Rhythmic bedforms in the upper beach and transverse finger bars shallow nearshore indicate shoreline instability driven by high angle waves. Transverse finger bars have not previously been reported associated with coarse clastic cuspate forelands, however, here we present a detailed analysis of the bars at Pevensey and report the presence of a larger system off Dungeness, Kent. Bar mobility was inferred from sea surface roughness images which were generated from X-band radar data to provide relatively high temporal resolution (weekly) records, for 16 months capturing two winter periods. The mobility of the transverse finger bars was found to relate to the littoral drift potential, and the bars were observed to move at similar rates to the rhythmic bedforms in the upper beach. These findings have practical applications for the beach managers that may be able to use the information to better manage their beach recycling operations.

- 2. Environment is strongly longshore dominant (between 1:25 to 1:250 crosshore:longshore sediment transport ratio). The sediment transport estimates (Paper 1, Figure 2.6) showed that this drift aligned coastal system is very strongly shaped by longshore transport. Whilst records of beach management activities, sediment budgets and bedforms supported the notion of a longshore dominant system, the modelling allowed the relative change to be quantified. This finding is important in interpreting long-term change at the site, namely the ongoing loss of nearshore sediments, which was highlighted in Paper 1, Figure 2.7. The ongoing loss of beach sediments below 0mOD was highlighted as a key management concern by Thomas (2015) and resulted in steepening of the upper beach (Paper 1, Figure 2.7).
- 3. Cross-shore transport causes formation of beach step and sediment sorting. The process-based modelling demonstrated realistic behaviour, namely the formation and mobilisation of a berm (beach step) associated with swash processes. The modelling is one of the few initial attempts to model coarse grained sediments using multi-fraction modelling(McCall, 2015; Rijper, 2018; McCarron, 2020), and the first to report on sediment sorting. The success of the model has helped us to better understand the observations reported by (Watt et al., 2006) and highlights the need for further improvements to the model.
- 4. Gravel outcrops may play a role in the termination of rhythmic features. The easterly migrating transverse finger bars did not progress into the area with gravel outcrops. This suggests that the resistant gravel bed may have played a role in their dissipation, possibly either through increased friction effects (and slowing of the current) or by preventing the propagation of the surface undulations through a medium requiring higher bed shear stress for sediment mobilisation than was available. This is a key area for further research and would potentially benefit from a linear stability analysis to compare the bar region under homogenous conditions.



- 1 Rhythmic features found separately in both upper beach and subtidal
- 2 Environment is strongly longshore dominant (between 1:25 to 1:250 crosshore:longshore ratio)
- 3 Cross shore transport causes formation of beach step and sediment sorting
- 4 Gravel outcrops may play a role in the termination of rhythmic features
- **5** The depth of closure is dependent on a number of interrelated drivers: hydrodynamics, geomorphology and sediment composition.
- 6 Majority of wave energy dissipated by shoaling waves, before waves reach land

Figure 5.5 – Conceptual model outlining key findings of PhD research.

- 5. The depth of closure is dependent on a number of interrelated drivers:
 hydrodynamics, geomorphology and sediment composition. The work completed as
 - part of Paper 1 showed that a highly spatially variable depth of closure, and the depth of closure conceptual model (Figure 2.1) was used to critically assess these variations and the likelihood of their origins. This work was significant in terms of it being the first study to explore the depth of closure for a mixed sand-gravel environment. The depth of closure is often used by engineers to understand the extent of the nearshore to inform scheme design, and this knowledge was previously based only on sandy environments.
- 6. Majority of wave energy dissipated by shoaling waves, before waves reach land. The cross-shore modelling showed large reductions in wave height across the dissipative sandy nearshore, and that the majority of bed change (due to cross-shore processes only) was to the steeper upper beach. Whilst the modelling found cross-shore change was focused over the upper beach, observational change showed that much larger volumes of change were occurring in the subtidal zone, which is likely due to the longshore current. High-angle waves approaching the coast from the south-west refract and the resultant longshore current, which is generated by radiative stresses, reaches a maximum in the shallow nearshore.

5.2 Further research

The research conducted as part of this thesis is a window into the nearshore zone of mixed sediment beaches. As part of this work, multiple opportunities for further research arose, which were not explored further due to limitations on time, data availability or model capability. These knowledge gaps are compiled here:

- There is a global lack of detailed data on the nearshore zone, especially in complex mixed sediment environments such as Pevensey Bay, UK. Further exploration of this zone may bring to light new discoveries, and more importantly long-term systematic measurement of the nearshore should be carried out at key sites, to help understand how this area is changing overtime, as there is currently only limited data available.
- Development of a probabilistic depth of closure using novel X-band radar datasets with high temporal and spatial frequency. More realistic than a 'line in the sand' approach, this exploratory approach may shed light on not only areas of geomorphological inactivity, but also the peak geomorphic change (Section 4.1.3 RQ II).

- Linear stability analysis could be used to examine the development of rhythmic features on coasts more complex than those already studied (Section 4.1.3 RQ II). Paper 2 attempted to redefine the existing classification system using coastal configuration, and it is likely that nearshore slope also plays a highly important role in the self-organisation of these features, which could be examined using this modelling technique.
- Multiple series of elongate transverse gravel ridges, approximately 5-10 m wide spanning the width of the upper beach, were found across the frontage Pevensey Bay on occasion. As far as the authors are aware the formation and mobilisation of these ephemeral features are not documented in the current literature.
- The surface samples of the sea bed taken between 500 to 2 300 m offshore showed that the bed is comprised of a complex mosaic of diverse sediments that responsd to hydrodynamic forcing throughout the year and are influenced by local variations in morphology. A significant component of the surface sediments was mud (up to 53%, Table 5.1). This thesis has not explored the importance of cohesive sediments in shaping the nearshore and is a clear avenue for further research.
- This thesis has exclusively focused on the short- and medium-term timescales, for which data was available. A very different, equally important study could examine the development of mixed sediment beaches over longer time scales to see if their behaviour varies from gravel or sandy coasts. Predictive modelling of historic formations (such as the growth and decline of The Crumbles) could provide an opportunity to do this, in the absence of suitably detailed datasets.
- Recent research by Casamayor et al. (2022) and Soloy et al. (2024) has shown that pure gravel beaches develop into 'composite' beaches during summer months when low-energy waves deposit fine material across the shore. Developments in modelling the effects of fair weather waves onto the beach profile (Grossmann et al., 2023) could be used to examine the different coarse clastic morphologies, and their resilience to changing conditions.
- The research conducted as part of Paper 3 highlighted the need for improvements to modelling mixed sediment beaches in the process-based model XBeach-X. Three items of particular importance are: 1) inclusion of ground water effects for multi-fraction modelling; 2) a 2-D application of the model for both coarse (XBeach-G) uni- and bi-, poly- modal sediment compositions, and 3) further development of the effects on the morphology of depositional, rather than erosive, wave conditions.

5.3 Conclusion

The current research aimed to develop a conceptual model of the behaviour and drivers of morphodynamic change across the nearshore zone for a mixed sediment beach. To engage with the construction of this model, three questions had to be answered:

- 1. What is the cross-shore extent of the geomorphologically active zone within a mixed sediment environment?
- 2. How does sediment move through and within a mixed sediment system contribute to short-term and long-term change?
- 3. How does cross-shore sediment exchange vary under a variety of hydrodynamic, morphodynamic and sedimentological conditions?

Analysis of observational data alongside numerical simulations were used to address these questions and build the mixed sediment beach conceptual model. A study site on the South East coast of the UK was used as a field laboratory; it was here that a variety of field data were gathered and modelled scenarios were based on. Repeat bathymetric data provided an insight into the extent of the geomorphologically active zone, using the depth of closure concept, a first look at the nearshore zone of complex mixed sediment environments (Townsend *et al.*, 2024). Rhythmic bedforms detected in the subtidal and upper beach are symptomatic of a beach subject to high wave angle shoreline instability, although the subtidal bedforms has not been observed persisting on a coastline like this (macrotidal open coast intermediate-energy wave dominated, wider mixed sediment setting) before (Townsend et al. 2024b *in review*). Finally robust tests of the effects of changing hydrodynamics, bed slope and sediment composition on sediment sorting and beach profile response were undertaken, mimicking sorting patterns seen in the field (Townsend et al. *in prep*). Brought together, the results from the three chapters describe the workings (morphology, drivers and sediment pathways) of a mixed sediment beach as a conceptual model.

The mixed sediment beach conceptual model provides new insight into present day morphodynamics across the nearshore zone. This work can be considered an important first step to understanding longer-term change. With increasing coastal populations, disproportionate social inequality on the coast and rising sea levels, it is imperative that we understand how these unique mixed sediment coasts will evolve over time to understand how the anticipated changes will impact both the communities and fragile coastal ecosystems. Ultimately, we must understand the resilience of mixed sediment beaches to climate change if we want to live on the coast in the coming decades.

Appendix A Paper 1; Supplementary information

This supplementary information details the wave transformation used to generate nearshore waves and the long and cross-shore sediment transport equations used.

5.4 Wave transformation

The wave record from the Pevensey Bay wave buoy (Figure 2.2) and water levels from the Newhaven tide gauge, was transformed to give the breaking wave height at the edge of the surf zone. This was done using linear wave theory, with plane bed refraction and shoaling, together with Weggel's (1972) empirical work relating beach slope to breaking wave height as given in equations 2-92, 2-93 and 2-94 of the Shoreline Protection Manual (USACE, 1984). The breaking wave height at the edge of the surf zone is given:

$$H_{si} = k_r k_s k_f H_{so}$$
 Equation S1

Where Hs is the (inshore and offshore) significant wave height, k_r is the refraction coefficient, k_s is the shoaling coefficient, and k_f is the friction coefficient. The refraction coefficient is defined as:

$$k_r = \sqrt{\frac{\cos(\alpha_o)}{\cos(\alpha_i)}} \text{ and } \alpha_i = \sin^{-1}\left(\frac{c_i}{c_o}\sin\alpha_o\right)$$
 Equation S2

Where α is the wave angle and c is the wave celerity (both onshore and offshore respectively).

The shoaling coefficient is:

$$k_{\scriptscriptstyle S} = rac{\sqrt{c_{go}}}{c_{gi}}$$
 Equation S3

$$c_g = \frac{c}{2} \left(\frac{1 + \frac{4\pi d}{c \cdot T_p}}{\sinh\left(\frac{4\pi d}{c \cdot T_p}\right)} \right)$$
 Equation S4

Where c is the wave celerity, c_g is the wave group celerity, Tp is the peak period. The friction coefficient is defined by the user, in this instance no frictional dampening was applied (value 1). The inshore wave height is then tested for wave breaking using , using Weggel's (1972) empirical work relating beach slope to breaking wave height as given in equations 2-92, 2-93 and 2-94 of the Shoreline Protection Manual (USACE, 1984):

$$\frac{d_b}{H_b} = \frac{1}{b - \left(\frac{aH_b}{gT^2}\right)}$$
 Equation S5

$$a = 43.75(1 - e^{19m})$$
 Equation S6

$$b = \frac{1.56}{1 + e^{19.5m}}$$
 Equation S7

Where m is bed slope, calculated as a linear slope between the given beach crest elevation and Mean Sea Level (MSL) and below MSL at each increment as an equilibrium beach profile using the Dean equation(Dean, 1977):

$$h = A_y^{2/3}$$
 Equation S8

A is a function of sediment fall velocity in the Dean formulation, but here it is derived from the depth 1km out from the mean tide level, which is input by the user as a bed level.

5.5 Sediment transport

From this inshore transformation of the wave record, both littoral drift potential and cross-shore transport rates were calculated independently for both fine sand (159 – 164 μ m) and medium pebbles (12mm), using locally derived shoreline angles for each profile. The chosen grain sizes were based on the average of samples collected by Dornbusch et al. (2005) for the upper beach

Appendix A

and using samples of the sandy foreshore as described in Section 2.3.4. Cross-shore transport rates were estimated using Bailard and Inman (1981), accounting for both suspended and bed load:

$$Q_c = \rho C_d u_m^3 \left\{ \frac{\varepsilon_b}{tan\phi} \left(\Psi_1 + \frac{2}{3} \delta_u - \frac{tan\beta}{tan\phi} u_3^* \right) + \frac{u_m}{w_s} \varepsilon_s \left(\Psi + \delta_u u_3^* - \frac{u_m}{w_s} \varepsilon_s u_5^* tan\beta \right) \right\}$$

Equation S9

Whereby $\varepsilon_b=0.21, \varepsilon_s=0.025, C_d$ is the drag coefficient, w_s is the sediment fall velocity (ms⁻¹), ϕ is the angle of repose, β is the beach slope, u_m is the near bed velocity (ms⁻¹), ρ is the water density (kgm⁻³), ρ_s is the sediment density (kgm⁻³) and δ_u , Ψ_1 , Ψ_2 , u_m and u_3^* , u_5^* are cross-shore variables related to the significant wave height (H_s) (Alexandrakis and Poulos, 2014):

$\delta_u = 0.0 - 0.00157 H_s$	Equation S10
$\Psi_1 = 0.00303 - 0.00144 H_s$	Equation S11
$\Psi_2 = 0.00603 - 0.00510 H_s$	Equation S12
$u_m = 0.319 + 0.403 H_s$	Equation S13
$u_3^* = 0.00548 + 0.000733 H_s$	Equation S14
$u_5^* = 0.015 + 0.00346 H_S$	Equation S15

Longshore transport rates were estimated using Damsgaard and Soulsby (1996) for the medium pebbles, which is a physics based equation used to predict longshore bedload transport, calibrated against a 3 year field dataset of longshore sediment transport on a shingle beach in the south of the UK. Where:

$$Q_{LS} = maximum of Q_{LS1} and Q_{LS2}$$
 Equation S16

Where $\theta_{cr} > 1$:

$$Q_{LS1} = \frac{0.19(g \tan \beta)^{\frac{1}{2}} (\sin 2\alpha_b)^{\frac{3}{2}} H_b^{\frac{5}{2}} (1 - \theta_{cr})}{12(s - 1)}$$
 Equation S17

$$Q_{LS2} = \frac{0.24 f(\alpha_b) g^{\frac{3}{8}} d_{50}^{\frac{1}{4}} H_b^{\frac{19}{8}}}{12(s-1)T^{\frac{1}{4}}} \qquad \text{for } \theta_{wr} \ge \theta_{wsf}$$

Equation S18

$$Q_{LS2} = \frac{0.046 f(\alpha_b) g^{\frac{2}{5}} H_b^{\frac{13}{5}}}{12(s-1)^{\frac{6}{5}} (\pi T)^{\frac{1}{5}}} \qquad \qquad \text{for } \theta_{wr} < \theta_{wsf}$$

$$Equation S19$$

Where: $\theta_{cr} = \frac{16.\widehat{70_{cr}(s-1)}d_{50}}{H_h(sin2\alpha_h)(tan\beta)}$ Equation S20

$$f(\alpha_b) = (0.95 - 0.19\cos\alpha_b)(\sin 2\alpha_b)$$
 Equation S21

$$\theta_{wr} = \frac{0.15H_b^{\frac{3}{4}}}{(s-1)g^{\frac{1}{4}}(Td_{50})^{1/2}}$$
 Equation S22

$$\theta_{wsf} = \frac{0.0040H_b^{\frac{6}{5}}}{(s-1)^{7/5}g^{1/5}T^{2/5}d_{50}}$$
 Equation S23

Where $\theta_w = maximum \ of \ \theta_{wr}$ and θ_{wsf} , $H_b = wave \ height \ at \ breaker \ line, <math>T = wave \ period$, $d_{50} = median \ grain \ diameter \ and \ tan\beta = beach \ slope$. Finally, the simplified version of the CERC equation (which does not take into account bed slope nor grain size), i.e. the SANDS formula was utilised for the fine sand (Soulsby, 1997), where:

$$Q_{LS} = \frac{0.023g^{\frac{1}{2}}H_{sb}^{\frac{5}{2}}\sin(2\alpha_b)}{(s-1)}$$
 Equation S24

Appendix B Paper 2; Supplementary information



Figure B.1 - Image showing the 50m polygons used in the analysis of the upper beach topographic datasets. 50 m polygons produced by Canterbury City Council as part of the project 'Eastbourne to Rye Regional Shingle Beach Management Plan' completed in 2015 on behalf of the Environment Agency. Map data © OpenStreetMap contributors, Microsoft, Facebook, Inc. and its affiliates, Esri Community Maps contributors, Map layer by Esri.

Appendix C Paper 3; Supplementary information

Keyword	Description	Setting	Comment			
Model Time Parameters (units: seconds)						
tstop	Simulation stop time	46800	14 hours covering full tidal cycle.			
tint	Simulation time step	360				
tintg	Simulation output time step	360				
Physical proce	Physical processes (Switches: 0 = off, 1 = on)					
nonh	Non-hydrostatic wave model type	1				
swave	Short wave action balance	0	Recommended to turn off swave with nonh			
flow	Tidal flow calculation	0	Tidal currents not calculated.			
sedtrans	Sediment transport	1				
mophology	Morphological processes	1				
wind	Wind stress	0	No wind forcing			
Grid set-up (S	witches: 0 = off, 1 = on)					
nx	Number of (x-direction) computational cells	1711#				
ny	Number of (y-direction) computational cells	0	1D model			
alfa	X-axis angle (relative to East)	0	Default			
xori	X origin point	0	Default			
yori	Y origin point	0	Default			
vardx	Variable grid spacing	1				
Posdwn	Bathymetry depths (positive down(1)) of heights (positive up(-1)).	-1				
xfile	Name of x-grid file	xfile.grd				
yfile	Name of y-grid file	yfile.grd				
dep.file	Name of bed depth file	bed.dep				
Boundary conditions						

Acknowledgements

front	Boundary condition at the seaward boundary	nonh_1d	1D Non-hydrostatic				
back	Boundary condition at the landward/bayside boundary	abs_1d	Absorbing-generating (weakly- reflective) boundary in 1D				
left	Boundary condition at the left lateral boundary	neumann	Neumann boundary condition (constant water level gradient)				
right	Boundary condition at the right lateral boundary	neumann	Neumann boundary condition (constant water level gradient)				
Waves							
instat	Wave boundary condition type	jons	Jonswap spectrum				
bcfile	Name of wave spectrum file	H2.txt					
Tm0switch	Switch to enable tm01, rather than tm-10	1	Recommended for nonh waves				
Tides	Tides						
tideloc	Number of tide specification points	1	Time varying tide, water levels given every 1200 seconds.				
zs0file	Name of tide boundary condition file	S1.txt					
Flow parame	ters						
bedfriction Bed friction formula		whitecolebrook	White-Colebrook formulation; constant roughness				
Sediment tra	nsport parameters						
form	Sediment transport formula	vanrijn1993					
Bed compos	ition						
nd	Number of bed layers	3					
ngd	Number of sediment fractions	2					
D50	Median grain size of all grain classes (ngd1; ngd2)	0.0004; 0.0042					
D90	90 th percentile grain size of all grain classes (ngd1; ngd2)	0.0005; 0.0054					
dzg1	Thickness of variable sediment bed layer	0.1	Default				

Acknowledgements

dzg2	Thickness of bottom sediment bed layer	1.0	Depth of maximum expected erosion.			
dzg3		0.1	Default			
Morphology pa	Morphology parameters					
morfac	Morphological acceleration Factor	1	seconds			
morstart	Morphological start time	0	seconds			
CFL	Maximum courant-friedrich- lewys number	0.9				
XBeach outputs						
outputformat	Output format file type	netcdf				
nglobalvar	Number of global (all grid points) outputs	4	zb, zb0, zs, pbbed			

Alexandrakis, G. and Poulos, S. E. (2014) 'An holistic approach to beach erosion vulnerability assessment', *Scientific Reports*, 4(i), pp. 1–8. doi: 10.1038/srep06078.

Almeida, L. P. *et al.* (2015) 'Observations of gravel beach dynamics during high energy wave conditions using a laser scanner', *Geomorphology*. Elsevier B.V., 228(1), pp. 15–27. doi: 10.1016/j.geomorph.2014.08.019.

Alpers, W. and Hennings, I. (1984) 'Theory of the Imaging Mechanism of Underwater Bottom Topography By Real and Synthetic Aperture Radar.', *Journal of Geophysical Research*, 89(C6), pp. 10529–10546. doi: 10.1029/JC089iC06p10529.

Amos, C. L. and King, E. L. (1984) 'Bedforms of the Canadian eastern seaboard: A comparison with global occurrences', *Marine Geology*, 57(1–4), pp. 167–208. doi: 10.1016/0025-3227(84)90199-3.

Anthony, E. J. and Aagaard, T. (2020) 'The lower shoreface: Morphodynamics and sediment connectivity with the upper shoreface and beach', *Earth-Science Reviews*. Elsevier, 210(March), p. 103334. doi: 10.1016/j.earscirev.2020.103334.

Aragonés, L. *et al.* (2015) 'New Methodology for the Classification of Gravel Beaches: Adjusted on Alicante (Spain)', *Journal of Coastal Research*, 314, pp. 1023–1034. doi: 10.2112/jcoastres-d-14-00140.1.

Aragonés, L. *et al.* (2018) 'Depth of closure: New calculation method based on sediment data', *International Journal of Sediment Research*. Elsevier B.V., 33(2), pp. 198–207. doi: 10.1016/j.ijsrc.2017.12.001.

Aragonés, L., Pagán, J. I., López, M. P., *et al.* (2019) 'Cross-shore sediment transport quantification on depth of closure calculation from profile surveys', *Coastal Engineering*. Elsevier, 151(March 2017), pp. 64–77. doi: 10.1016/j.coastaleng.2019.04.002.

Aragonés, L., Pagán, J. I., López, I., *et al.* (2019) 'Galerkin's formulation of the finite elements method to obtain the depth of closure', *Science of the Total Environment*. Elsevier B.V., 660, pp. 1256–1263. doi: 10.1016/j.scitotenv.2019.01.017.

Arriaga, J. et al. (2017) 'Formation and destruction of shoreline sand waves: observations and modelling.', in *Coastal Dynamics 2017*, pp. 9–15.

Ashton, A. D. and Murray, A. B. (2006) 'High-Angle Wave Instability and Emergent Shoreline Shapes: 2. Wave Climate Analysis and Comparisons to Nature High-angle wave instability and emergent shoreline shapes: 2. Wave climate analysis and comparisons to nature', *Journal of Geophysical Research Atmospheres*, (May 2014). doi: 10.1029/2005JF000423.

Atkinson, J. *et al.* (2017) 'Monitoring Nearshore Processes and Understanding Significant Coastal', *Coastal Dynamics*, (In: Coastal Dynamics 2017), pp. 1506–1517. Available at: http://eprints.bournemouth.ac.uk/29431/1/176_Atkinson_John.pdf.

Atkinson, J. (2019) *Understanding the Dynamics of a Mixed Sand and Gravel Coastline : A Multi-Method Approach*. University of Bournemouth.

Atkinson, J. and Esteves, L. S. (2018) 'Alongshore variability in the response of a mixed sand and gravel beach to bimodal wave direction', *Geosciences (Switzerland)*, 8(12). doi: 10.3390/geosciences8120488.

Austin, M. J. and Masselink, G. (2006) 'Observations of morphological change and sediment transport on a steep gravel beach', *Marine Geology*, 229(1–2), pp. 59–77. doi: 10.1016/j.margeo.2006.02.003.

Backstrom, J. et al. (2015) 'Contrasting geomorphological storm response from two adjacent shorefaces', *Earth Surface Processes and Landforms*, 40(15), pp. 2112–2120. doi: 10.1002/esp.3788.

Bailard, J. A. and Inman, D. L. (1981) 'An energetics total load sediment transport model for a plane sloping beach: Local transport.', *Journal of Geophysical Research: Oceans*, 86(C3), pp. 2035–2043.

Barrineau, P., Janmaat, R. and Kana, T. (2021) 'Empirical depths of closure along the US East coast', *Coastal Engineering*. Elsevier B.V., 170(February), p. 104009. doi: 10.1016/j.coastaleng.2021.104009.

Barton, C. *et al.* (2022) 'The future of coastal communities', *House of Commons Library*, (September), p. 26pp. Available at: https://commonslibrary.parliament.uk/research-briefings/cdp-2022-0153/.

Bauer, B. O. and Allen, J. R. (1995) 'Beach steps: an evolutionary perspective', *Marine Geology*, 123(3–4), pp. 143–166. doi: 10.1016/0025-3227(95)00011-M.

Beakawi Al-Hashemi, H. M. and Baghabra Al-Amoudi, O. S. (2018) 'A review on the angle of

repose of granular materials', *Powder Technology*. The Authors, 330, pp. 397–417. doi: 10.1016/j.powtec.2018.02.003.

Bell, P. S. *et al.* (2015) 'Remote detection of sea surface roughness signatures related to subsurface bathymetry, structures and tidal stream turbine wakes', in *Proceedings of the 11th European Wave and Tidal Energy Conference*. Nantes.

Bergillos, R. J., Masselink, G., *et al.* (2016) 'Modelling overwash vulnerability along mixed sand-gravel coasts with xbeach-g: Case study of playa granada, southern Spain', *Proceedings of the Coastal Engineering Conference*, 35, pp. 1–9.

Bergillos, R. J., Ortega-Sánchez, M., *et al.* (2016) 'Morpho-sedimentary dynamics of a micro-tidal mixed sand and gravel beach, Playa Granada, southern Spain', *Marine Geology*. Elsevier B.V., 379, pp. 28–38. doi: 10.1016/j.margeo.2016.05.003.

Birkemeier, W. A. (1985) 'Field Data on Seaward Limit of Profile Change', *Journal of Waterway, Port, Coastal, and Ocean Engineering*, 111(3), pp. 598–602. doi: 10.1061/(asce)0733-950x(1985)111:3(598).

Blott, S. J. and Pye, K. (2001) 'Gradistat: A grain size distribution and statistics package for the analysis of unconsolidated sediments', *Earth Surface Processes and Landforms*, 26(11), pp. 1237–1248. doi: 10.1002/esp.261.

Bocharov, G. (2021) *Pyextremes extreme value analysis (EVA) in Python*. Available at: https://georgebv.github.io/pyextremes/.

Boczar-Karakiewicz, B. and Bona, J. L. (1986) *Shelf Sands and Sandstones. Wave-dominated shelves: a model of sand-ridge formation by progressive, infragravity waves*. Edited by R. J. Knight and J. R. McLean. Can. Soc. Petr. Geol.

Bradbury, A. P., Mason, T. and Barter, P. (2005) 'Large-scale multi-agency strategic beach monitoring of the South-East Coast of England – provision of data and analytical tools', Proceedings of the 2005 National Conference on Beach Preservation Technology, 44(0), pp. 1–16.

Bradbury, A. P. and Powell, K. A. (1992) 'Short-term profile response of shingle spits to storm wave action', *Proceedings of the Coastal Engineering Conference*, 3, pp. 2694–2707. doi: 10.1061/9780872629332.205.

Brakenhoff, L., Ruessink, G. and van der Vegt, M. (2019) 'Characteristics of saw-tooth bars on

the ebb-tidal deltas of the Wadden Islands', *Ocean Dynamics*. Ocean Dynamics, 69(11–12), pp. 1273–1285. doi: 10.1007/s10236-019-01315-w.

Broaddus, C. and Foufoula-Georgiou, E. (2024) 'Controls on the growth of wave-influenced river deltas: The roles of fluvial sediment composition and basin depth', in *EGU General Assembly*. Vienna, Austria. doi: https://doi.org/10.5194/egusphere-egu24-21037.

Bruner, K. R. and Smosna, R. A. (1989) 'The movement and stabilization of beach sand on transverse bars, Assateague Island, Virginia', *Journal of Coastal Research*, 5(3), pp. 593–601.

Brutsché, K. E., Iii, J. R. and Pollock, C. E. (2015) 'Calculating Depth of Closure Using WIS Hindcast Data', *Erdc/Chl Chetn*, VI(45), p. 11. Available at: http://cirp.usace.army.mil/products/depth-of.

Buffington, J. M., Dietrich, W. E. and Kirchner, J. W. (1992) 'Friction angle measurements on a naturally formed gravel streambed: Implications for critical boundary shear stress', *Water Resources Research*, 28(2), pp. 411–425. doi: 10.1029/91WR02529.

Bujan, N., Cox, R. and Masselink, G. (2019) 'From fine sand to boulders: Examining the relationship between beach-face slope and sediment size', *Marine Geology*. Elsevier, 417(August), p. 106012. doi: 10.1016/j.margeo.2019.106012.

Burcharth, H. F., Lykke Andersen, T. and Lara, J. L. (2014) 'Upgrade of coastal defence structures against increased loadings caused by climate change: A first methodological approach', *Coastal Engineering*. Elsevier B.V., 87, pp. 112–121. doi: 10.1016/j.coastaleng.2013.12.006.

Burningham, H. and French, J. (2017) 'Understanding coastal change using shoreline trend analysis supported by cluster-based segmentation', *Geomorphology*. The Authors, 282, pp. 131–149. doi: 10.1016/j.geomorph.2016.12.029.

Buscombe, D. and Masselink, G. (2006) 'Concepts in gravel beach dynamics', *Earth-Science Reviews*, 79(1–2), pp. 33–52. doi: 10.1016/j.earscirev.2006.06.003.

Carter, R. W. G. (1978) 'Small-Scale Transverse Bars in Lough Neagh, Northern Ireland', *Journal of Earth Sciences*, 1(2), pp. 205–209.

Casamayor, M. et al. (2022) 'Seasonal response of a composite beach in relation to wave climate', *Geomorphology*, 408(July 2021). doi: 10.1016/j.geomorph.2022.108245.

Channel Coastal Observatory (2003) Metadata for Hydrographic Survey, ID: 64856. Available at:

coastalmonitoring.org.

Channel Coastal Observatory (2006) *Metadata for Hydrographic Survey, ID*: 91125. Available at: coastalmonitoring.org.

Channel Coastal Observatory (2014) Seabed Mapping. Dungeness to Selsey.

Chen, Q., Madsen, P. A. and Basco, D. R. (1999) 'Current effects on nonlinear interactions of shallow-water waves', *Journal of Waterway, Port, Coastal, and Ocean Engineering*, 125(August), pp. 176–186.

Chlachula, J. and Mychko, E. V. (2023) 'Geoheritage of the Kaliningrad Region, SE Baltic Coast', *Geoheritage*. Springer Berlin Heidelberg, 15(4). doi: 10.1007/s12371-023-00899-6.

Ciavola, P. and Castiglione, E. (2009) 'Sediment dynamics of mixed sand and gravel beaches at short timescales', *Journal of Coastal Research*, 2009(SPEC. ISSUE 56), pp. 1751–1755.

Coco, G. et al. (2007) 'Sorted bed forms as self-organized patterns: 2. Complex forcing scenarios', *Journal of Geophysical Research: Earth Surface*, 112(3). doi: 10.1029/2006JF000666.

Coco, G. and Murray, A. B. (2007) 'Patterns in the sand: From forcing templates to self-organization', *Geomorphology*, 91(3–4), pp. 271–290. doi: 10.1016/j.geomorph.2007.04.023.

Coco, G., Murray, A. B. and Green, M. O. (2007) 'Sorted bed forms as self-organized patterns: 1. Model development', *Journal of Geophysical Research: Earth Surface*, 112(3), pp. 1–18. doi: 10.1029/2006JF000665.

Costa, S. *et al.* (2008) 'Impact of sand content and cross-shore transport on the morphodynamics of macrotidalgravel beaches (Haute-Normandie, English channel)', *Zeitschrift fur Geomorphologie*, 52(SUPPL. 3), pp. 41–62. doi: 10.1127/0372-8854/2008/0052S3-0041.

Curoy, J. et al. (2009) 'Profile evolution and active layer measurements on a macrotidal composite gravel beach, Somme Estuary, France', *Zeitschrift fur Geomorphologie*, 53(3), pp. 387–409. doi: 10.1127/0372-8854/2009/0053-0387.

Damsgaard, J. S. and Soulsby, R. L. (1996) 'Longshore bed-load transport', in 25th International Conference on Coastal Engineering, pp. 3614–3627.

Dean, R. G. (1977) Equilibrium beach profiles: U.S. Atlantic and Gulf Coasts. Newark, Delaware.

Dhoop, T. and Mason, T. (2018) 'Method for Extremes Analysis of Coastal Wave Data, TN01', (May).

Dickson, M. E., Kench, P. S. and Kantor, M. S. (2011) 'Longshore transport of cobbles on a mixed sand and gravel beach, southern Hawke Bay, New Zealand', *Marine Geology*. Elsevier B.V., 287(1–4), pp. 31–42. doi: 10.1016/j.margeo.2011.06.009.

Dolphin, T. et al. (2020) 'Mixed Sand/Gravel Beach Response to the Beast from the East Storms', Journal of Coastal Research, 95(sp1), pp. 463–467. doi: 10.2112/SI95-090.1.

Dornbusch, U. (2017) 'Design requirement for mixed sand and gravel beach defences under scenarios of sea level rise', *Coastal Engineering*. Elsevier, 124(April), pp. 12–24. doi: 10.1016/j.coastaleng.2017.03.006.

Dornbusch, U. (2021) 'Destabilisation and Accelerated Roll-Back of a Mixed Sediment Barrier in Response to a Managed Breach', *Journal of Marine Science and Engineering*, 9(374). doi: https://doi.org/10.3390/jmse9040374 Abstract:

Dornbusch, U. and Hardiman, N. (2020) 'Disappearing beaches? Examples of their increasing replacement in Great Britain by hard structures and Non-Cohesive Sediment Accumulations', in *Coastal Management 2019*, pp. 347–360. doi: 10.13140/RG.2.2.32554.77760.

Dornbusch, U., Watt, T. and Williams, R. B. G. (2005) 'Sedimentary structure of mixed sand and shingle beaches: preservation potential and environmental conditions', in *INQUA-IGCP 495*Meeting on Late quaternary coastal changes: sea level, sedimentary forcing and anthropogenic impacts, pp. 19–20.

Dornbusch, U., Williams, R. and Moses, C. (2005) *Beach Materials Properties; BAR Phase 1, Science Report*. Available at:

http://www.sussex.ac.uk/geography/researchprojects/BAR/publish/Phase-1-final-beach material properties.pdf.

Dumas, S. and Arnott, R. W. C. (2006) 'Origin of hummocky and swaley cross-stratification - The controlling influence of unidirectional current strength and aggradation rate', *Geology*, 34(12), pp. 1073–1076. doi: 10.1130/G22930A.1.

Eagleson, P. S., Glenne, B. and Dracup, J. A. (1961) *Equilibrium Characteristics of Sand Beaches in the Offshore Zone, U.S. Army, Corps of Engineers, Beach Erosion Board, Washington*. Washington DC.

Egiazaroff, I. V. (1965) 'Calculation of nonuniform sediment concentrations', *Journal of the Hydraulics Division*, 9(4), pp. 225–247.

Elgar, S. et al. (1997) 'Spectral evolution of shoaling and breaking waves on a barred beach', Journal of Geophysical Research: Oceans, 102(C7), pp. 15797–15805. doi: 10.1029/97JC01010.

Elsner, P. *et al.* (2015) 'Monitoring Mixed Sand and Gravel Beaches Using Unmanned Aerial Systems'. doi: 10.1142/9789814689977_0172.

Environment Agency (2017) Regional Beach Management Plan Eastbourne to Rye.

Falqués, A. (1989) 'Formación de topografía rítmica en el delta del ebro', *Revista de Geofísica*, 45(January 1989), pp. 143–156.

Falqués, A. *et al.* (2008) 'Rhythmic surf zone bars and morphodynamic self-organization', *Coastal Engineering*, 55(7–8), pp. 622–641. doi: 10.1016/j.coastaleng.2007.11.012.

Falqués, A. et al. (2021) 'A New Morphodynamic Instability Associated With Cross-Shore Transport in the Nearshore', *Geophysical Research Letters*, 48(13), pp. 1–9. doi: 10.1029/2020GL091722.

Fernandez, R. *et al.* (2022) 'Changes in Ripple Migration Rates and Hydraulic Resistance with Increasing Mud-to-Sand Ratios', in *IAHR World Congress*. Granada, Spain. doi: https://doi.org/10.3850/IAHR-39WC2521711920221870.

de Figueiredo, S. A., Goulart, E. S. and Calliari, L. J. (2020) 'Effects of closure depth changes on coastal response to sea level rise: Insights from model experiments in southern Brazil', Geomorphology. Elsevier B.V., 351, p. 106935. doi: 10.1016/j.geomorph.2019.106935.

Finkl, C. W. (2004) 'Leaky Valves in Littoral Sediment Budgets: Loss of Nearshore Sand to Deep Offshore Zones via Chutes in Barrier Reef Systems, Southeast Coast of Florida, USA', *Journal of Coastal Research*, 20(2), pp. 605–611. doi: https://doi.org/10.2112/1551-5036(2004)020[0605:LVILSB]2.0.CO;2.

Fitzgerald, D. M. and Van Heteren, S. (1999) 'Classification of paraglacial barrier systems: Coastal New England, USA', *Sedimentology*, 46(6), pp. 1083–1108. doi: 10.1046/j.1365-3091.1999.00266.x.

Folk, R. L. (1954) 'The Distinction between Grain Size and Mineral Composition in Sedimentary-Rock Nomenclature', *Journal of Geology*, 62(4), pp. 344–359.

Foss, O. et al. (2023) 'Comparison of dynamic cobble berm revetments with differing gravel characteristics', *Coastal Engineering*. Elsevier B.V., 183(April), p. 104312. doi: 10.1016/j.coastaleng.2023.104312.

Francois, S., Stive, M. J. F. and Pons, F. (2005) 'Longshore Variation of Depth of Closure on a Micro-Tidal Wave-Dominated Coast', (March 2014), pp. 2327–2339. doi: 10.1142/9789812701916_0187.

French, J. *et al.* (2016) 'Conceptualising and mapping coupled estuary, coast and inner shelf sediment systems', *Geomorphology*. The Authors, 256, pp. 17–35. doi: 10.1016/j.geomorph.2015.10.006.

Fugro Emu (2016) 'Pevensey Bay, South-east England - Hydrodynamic Study ADP Investigation Report', (August).

Gardner, E. and Burningham, H. (2013) 'Ecology and conservation of the rare annual Petrorhagia nanteuilii (Childing Pink) on the vegetated shingle spits of Pagham Harbour, West Sussex', *Journal of Coastal Conservation*, 17(3), pp. 589–600. doi: 10.1007/s11852-013-0257-0.

Gauci, M. J., Deidun, A. and Schembri, P. J. (2005) 'Faunistic diversity of Maltese pocket sandy and shingle beaches: Are these of conservation value?', *Oceanologia*, 47(2), pp. 219–241.

Gelfenbaum, G. and Brooks, G. R. (2003) 'The morphology and migration of transverse bars off the west-central Florida coast', *Marine Geology*, 200, pp. 273–289. doi: 10.1016/S0025-3227(03)00187-7.

Goud, M. R. and Aubrey, D. G. (1985) 'Theoretical and observational estimates of nearshore bedload transport rates', *Marine Geology*, 64, pp. 91–111.

Grabowski, R. C., Droppo, I. G. and Wharton, G. (2011) 'Erodibility of cohesive sediment: The importance of sediment properties', *Earth-Science Reviews*. Elsevier B.V., 105(3–4), pp. 101–120. doi: 10.1016/j.earscirev.2011.01.008.

Grossmann, F. et al. (2023) 'Near-Bed Sediment Transport Processes During Onshore Bar Migration in Large-Scale Experiments: Comparison With Offshore Bar Migration', *Journal of Geophysical Research: Oceans*, 128(3). doi: 10.1029/2022JC018998.

Guza, R. T. and Inman, D. L. (1975) 'Beach Cusps and Edge Waves.', *Journal of Geophysical Research*, 80(21), pp. 2997–3012. doi: 10.9753/icce.v16.81.

Halcrow (2000) Rye Harbour to Beachy Head Coastal Processes and Resources Study: Sediment Budget for Cuckmere Haven to Copt Point, Folkestone. (2 Volumes: Report to Environment Agency on Behalf of Eastbourne to River Rother Coastal Group).

Halcrow (2010) South Foreland to Beachy Head Shoreline Management Plan. Appendix C:

Baseline Process Understanding.

Hallermeier, R. J. (1977) Calculating a Yearly Limit Depth to the Active Beach Profile, Techical Paper Coastal Engineering Research Centre, Ft. Belvoir, Va.

Hallermeier, R. J. (1978) 'Uses for a Calculated Limit Depth To Beach Erosion.', *Proceedings of the Coastal Engineering Conference*, 2(1977), pp. 1493–1512. doi: 10.9753/icce.v16.88.

Hallermeier, R. J. (1981) Seaward limit of significant sand transport by waves: an annual zonation for seasonal profiles, Coastal Engineering Technical Aid No. CERC-CETA-81-2. FORT BELVOIR VA.

Hallermeier, R. J. (1983) 'Sand transport limits in coastal structure designs.', in *Conference on Design, Construction, Maintenance and Performance of Coastal Structures*. Arlington: ASCE, pp. 703–716.

Hamon-Kerivel, K. et al. (2020) 'Shoreface mesoscale morphodynamics: A review', *Earth-Science Reviews*, 209(February). doi: 10.1016/j.earscirev.2020.103330.

Hartman, M. and Kennedy, A. B. (2016) 'Depth of closure over large regions using airborne bathymetric lidar', *Marine Geology*. Elsevier B.V., 379, pp. 52–63. doi: 10.1016/j.margeo.2016.05.012.

Hartmann, S. S. (2017) Wetland Reclamation in England: Medieval Risk Culture and the 1396 Commission of Sewers for Pevensey Levels. University of Waterloo. Available at: chrome-extension://efaidnbmnnnibpcajpcglclefindmkaj/https://core.ac.uk/download/144151327.pdf.

Hay, A. E., Zedel, L. and Stark, N. (2014) 'Sediment dynamics on a steep, megatidal, mixed sand-gravel-cobble beach', *Earth Surface Dynamics*, 2(2), pp. 443–453. doi: 10.5194/esurf-2-443-2014.

Hemmingsen, M. A., Eikaas, H. S. and Marsden, D. C. J. (2019) 'A GIS approach to sediment displacement in mixed sand and gravel beach environments', *Journal of Environmental Management*. Elsevier, 249(December 2018), p. 109083. doi: 10.1016/j.jenvman.2019.05.141.

Herrling, G. and Winter, C. (2014) 'Morphological and sedimentological response of a mixed-energy barrier island tidal inlet to storm and fair-weather conditions', *Earth Surface Dynamics*, 2(1), pp. 363–382. doi: 10.5194/esurf-2-363-2014.

Hersen, P. (2004) 'On the crescentic shape of barchan dunes', *European Physical Journal B*, 37(4), pp. 507–514. doi: 10.1140/epjb/e2004-00087-y.

Hinton, C. and Nicholls, R. J. (1998) 'Spatial and temporal behaviour of depth of closure along the Holland coast', *Proceedings of the Coastal Engineering Conference*, 3, pp. 2913–2925. doi: 10.1061/9780784404119.221.

Holland, K. T. and Elmore, P. A. (2008) 'A review of heterogeneous sediments in coastal environments', *Earth-Science Reviews*, 89(3–4), pp. 116–134. doi: 10.1016/j.earscirev.2008.03.003.

Holman, R. (1995) 'Nearshore processes', *Reviews of Geophysics*, 33(2 S), pp. 1237–1247. doi: 10.1029/95RG00297.

Hoonhout, B. M. and Vries, S. de (2016) 'A process-based model for aeolian sediment transport and spatiotemporal varying sediment availability', *Journal of Geophysical Research: Earth Surface*, 121(8), pp. 1555–1575. doi: 10.1002/2015JF003692.

Horn, D. P. and Walton, S. M. (2007) 'Spatial and temporal variations of sediment size on a mixed sand and gravel beach', *Sedimentary Geology*, 202(3), pp. 509–528. doi: 10.1016/j.sedgeo.2007.03.023.

House of Lords (2023) Future of seaside towns: government response to the Select Committee report. Available at: https://www.gov.uk/government/publications/future-of-seaside-towns-government-response-to-the-select-committee-report.

Ivamy, M. C. and Kench, P. S. (2006) 'Hydrodynamics and morphological adjustment of a mixed sand and gravel beach, Torere, Bay of Plenty, New Zealand', *Marine Geology*, 228(1–4), pp. 137–152. doi: 10.1016/j.margeo.2006.01.002.

Jacobs, W. et al. (2011) 'Erosion threshold of sand-mud mixtures', Continental Shelf Research, 31(10 SUPPL.), pp. 14–25. doi: 10.1016/j.csr.2010.05.012.

Jamal, M. H., Simmonds, D. J. and Magar, V. (2014) 'Modelling gravel beach dynamics with XBeach', *Coastal Engineering*. Elsevier B.V., 89, pp. 20–29. doi: 10.1016/j.coastaleng.2014.03.006.

Jennings, R. and Shulmeister, J. (2002) 'A field based classification scheme for gravel beaches', *Marine Geology*, 186(3–4), pp. 211–228. doi: 10.1016/S0025-3227(02)00314-6.

Jennings, S. and Smyth, C. (1987) 'Coastal sedimentation in East Sussex during the Holocene', *Progress in Oceanography*, 18(1–4), pp. 205–241. doi: 10.1016/0079-6611(87)90034-6.

Jennings, S. and Smyth, C. (1990) 'Holocene evolution of the gravel coastline of East Sussex',

Proceedings of the Geologists' Association. The Geologists' Association, 101(3), pp. 213–224. doi: 10.1016/S0016-7878(08)80006-5.

Karunarathna, H. *et al.* (2012) 'An analysis of the cross-shore beach morphodynamics of a sandy and a composite gravel beach', *Marine Geology*. Elsevier B.V., 299–302, pp. 33–42. doi: 10.1016/j.margeo.2011.12.011.

Khabidov, A. (2001) 'Transverse bars formation on a tideless beach.', in *Coastal Dynamics*. Lund, Sweden, pp. 666–672. doi: https://doi.org/10.1061/40566(260)68.

Kirezci, E. et al. (2023) 'Global-scale analysis of socioeconomic impacts of coastal flooding over the 21st century', *Frontiers in Marine Science*, 9(January), pp. 1–21. doi: 10.3389/fmars.2022.1024111.

Konicki, K. M. and Holman, R. A. (2000) 'The statistics and kinematics of transverse sand bars on an open coast', *Marine Geology*, 169(1–2), pp. 69–101. doi: 10.1016/S0025-3227(00)00057-8.

Kraus, N. C., Larson, M. and Wise, R. A. (1998) *Depth of closure in beach fill design*, Coastal Engineering Technical Note CETN II-40. Vicksburg, MS, p.13.

Krumbein, W. C. and Pettijohn, F. J. (1938) *Manual of Sedimentary Petrography*. New York: Appleton-Century-Crofts.

Kulkarni, C. D. *et al.* (2004) 'Morphological variations of a mixed sediment beachface (Teignmouth, UK)', *Continental Shelf Research*, 24(11), pp. 1203–1218. doi: 10.1016/j.csr.2004.03.005.

Kummu, M. *et al.* (2016) 'Over the hills and further away from coast: Global geospatial patterns of human and environment over the 20th-21st centuries', *Environmental Research Letters*. IOP Publishing, 11(3), p. 34010. doi: 10.1088/1748-9326/11/3/034010.

Lamarchina, S., Maenza, R. A. and Isla, F. (2021) 'Mixed sand and gravel beaches of Buenos Aires, Argentina. Morphodynamics and stability', *Journal of Coastal Conservation*. Springer Netherlands, 25(4), pp. 1–11. doi: 10.1007/s11852-021-00830-7.

Lazarow, N. (2007) 'The value of coastal recreation resources: a case study approach to examine the value of recreaional surfing to specific locales', *Journal of Coastal Research*, 50(1), pp. 12–20. doi: https://doi.org/10.2112/JCR-SI50-003.1.

Levoy, F. et al. (2013) 'Formation and migration of transverse bars along a tidal sandy coast deduced from multi-temporal Lidar datasets', 342, pp. 39–52.

López De San, B. and Blanco, R. (2003) *Dynamics of gravel and mixed, sand and gravel, beaches, PhD Thesis (unpublished)*. Univeristy of London.

López, I. et al. (2020) 'Determination of the study period necessary for calculating the equilibrium beach profile and the depth of closure', *Applied Ocean Research*. Elsevier, 94(November 2019), p. 102005. doi: 10.1016/j.apor.2019.102005.

Martewicz, J., Kalińska, E. and Weckwerth, P. (2022) 'What hides in the beach sand? A multiproxy approach and new textural code to recognition of beach evolution on the southern and eastern Baltic Sea coast', *Sedimentary Geology*, 435. doi: 10.1016/j.sedgeo.2022.106154.

Martínez, M. L. *et al.* (2007) 'The coasts of our world: Ecological, economic and social importance', *Ecological Economics*, 63(2–3), pp. 254–272. doi: 10.1016/j.ecolecon.2006.10.022.

Mason, T. (1997) *Hydrodynamics and sediment transport on a macro-tidal, mixed (sand and shingle) beach*. University of Southampton. Available at: http://eprints.soton.ac.uk/id/eprint/467193.

Mason, T. and Coates, T. T. (2001) 'Sediment transport processes on mixed beaches: A review for shoreline management', *Journal of Coastal Research*, 17(3), pp. 645–657.

Masselink, G. *et al.* (2010) 'Swash zone sediment transport, step dynamics and morphological response on a gravel beach', *Marine Geology*. Elsevier B.V., 274(1–4), pp. 50–68. doi: 10.1016/j.margeo.2010.03.005.

Masselink, G. and Puleo, J. A. (2006) 'Swash-zone morphodynamics', *Continental Shelf Research*, 26(5), pp. 661–680. doi: 10.1016/j.csr.2006.01.015.

Masselink, G. and Short, A. D. (1993) 'The Effect of Tide Range on Beach Morphodynamics and Morphology: A Conceptual Beach Model', *Journal of Coastal Research*, 9(1984), pp. 785–800.

McCall, R. T. *et al.* (2014) 'Modelling storm hydrodynamics on gravel beaches with XBeach-G', *Coastal Engineering*. Elsevier B.V., 91, pp. 231–250. doi: 10.1016/j.coastaleng.2014.06.007.

McCall, R. T. (2015) *Process-based modelling of storm impacts on gravel coasts*. University of Plymouth. Available at: https://pearl.plymouth.ac.uk//handle/10026.1/3929.

McCarron, C. J. et al. (2019) 'The hiding-exposure effect revisited: A method to calculate the mobility of bimodal sediment mixtures', *Marine Geology*. Elsevier, 410(June 2018), pp. 22–31. doi: 10.1016/j.margeo.2018.12.001.

McCarron, C. J. (2020) Bedload Transport of Sand-Gravel Mixtures in Coastal and Shelf-Sea Environments Bedload Transport of Sand-Gravel Mixtures in Coastal and Shelf-Sea Environments.

McNinch, J. E. (2004) 'Geologic control in the nearshore: shore-oblique sandbars and shoreline erosional hotspots, Mid-Atlantic Bight, USA', 211, pp. 121–141. doi: 10.1016/j.margeo.2004.07.006.

Mellett, C. L. *et al.* (2012) 'Preservation of a drowned gravel barrier complex: A landscape evolution study from the north-eastern English Channel', *Marine Geology*, 315–318, pp. 115–131. doi: 10.1016/j.margeo.2012.04.008.

Mitchener, H. and Torfs, H. (1995) 'Erosion of mud sand mixtures', *Coastal Engineering*, 29(96), p. 223.

Monroe, F. F. (1969) *Oolitic Aragonite and Quartz Sand: Laboratory Comparison under Wave Action, Coastal Engineering Research Cente*. Washington D.C.

Mujal-Colilles, A., Grifoll, M. and Falqués, A. (2019) 'Rhythmic morphology in a microtidal low-energy beach', *Geomorphology*. Elsevier B.V., 334, pp. 151–164. doi: 10.1016/j.geomorph.2019.02.037.

Murray, A. B. and Thieler, E. R. (2004) 'A new hypothesis and exploratory model for the formation of large-scale inner-shelf sediment sorting and "rippled scour depressions", *Continental Shelf Research*, 24(3), pp. 295–315. doi: 10.1016/j.csr.2003.11.001.

National Network of Regional Coastal Monitoring Programmes. (no date) *Pevensey Bay wave buoy statistics: average values for all years*. Available at:

https://coastalmonitoring.org/realtimedata/?chart=77&tab=stats&disp_option=&data_type=tab le&year=All years (Accessed: 11 December 2023).

New Forest District Council (2020) 'Metadata for Hydrographic Survey 4cSU23_20200915'.

Nicholls, R. J. (1991) 'Holocene evolution of the gravel coastline of East Sussex: discussion', *Proceedings of the Geologists' Association*. The Geologists' Association, 102(4), pp. 301–306. doi: 10.1016/S0016-7878(08)80089-2.

Nicholls, R. J. et al. (1998) 'Depth of closure: Improving understanding and prediction', Proceedings of the Coastal Engineering Conference, 3, pp. 2888–2901. doi: 10.1061/9780784404119.219.

Nicholls, R. J. *et al.* (2013) 'Planning for long-term coastal change: Experiences from England and Wales', *Ocean Engineering*. Elsevier, 71, pp. 3–16. doi: 10.1016/j.oceaneng.2013.01.025.

Nicholls, R. J., Birkemeier, W. A. and Hallermeier, R. J. (1996) 'Application of the depth of closure concept', *Proceedings of the Coastal Engineering Conference*, 4, pp. 3874–3887. doi: 10.1061/9780784402429.299.

Nicholls, R. J., Birkemeier, W. A. and Lee, G. (1998) 'Evaluation of depth of closure using data from Duck, NC, USA', *Marine Geology*, 148, pp. 179–201.

Niedoroda, A. W. and Tanner, W. F. (1970) 'Preliminary study of transverse bars', *Marine Geology*, 9(26).

Nieto-Borge, J. C. *et al.* (2006) 'Estimation of ocean wave heights from temporal sequences of X-band marine radar images', *European Signal Processing Conference*, (January).

Nordstrom, K. F. and Jackson, N. L. (2012) 'Physical processes and landforms on beaches in short fetch environments in estuaries, small lakes and reservoirs: A review', *Earth-Science Reviews*. Elsevier B.V., 111(1–2), pp. 232–247. doi: 10.1016/j.earscirev.2011.12.004.

Orford, J. D. and Carter, R. W. G. (1982) 'Crestal overtop and washover sedimentation on a fringing sandy gravel barrier coast, Carnshore Point, southeastern Ireland.', *Journal of Sedimentary Petrology*, 52(1), pp. 265–278. doi: 10.1306/212F7F2C-2B24-11D7-8648000102C1865D.

Ortega-Sánchez, M. et al. (2017) Morpho-Sedimentary Dynamics of Mixed Sand and Gravel Coasts. doi: 10.1007/978-3-319-52440-5_5.

Ortiz, A. C. and Ashton, A. D. (2016) 'Exploring shoreface dynamics and a mechanistic explanation for a morphodynamic depth of closure', *Journal of Geophysical Research: Earth Surface*, 121, pp. 442–464. doi: 10.1002/2015JF003699.

Pagán, J. I. et al. (2017) 'A software application to obtain the depth of closure from beach profile data', *International Journal of Computational Methods and Experimental Measurements*, 5(5), pp. 750–759. doi: 10.2495/CMEM-V5-N5-750-759.

Panagiotopoulos, I., Sylaios, G. and Collins, M. B. (1994) 'Threshold studies of gravel size particles under the co-linear combined action of waves and currents', *Sedimentology*, 41(5), pp. 951–962. doi: 10.1111/j.1365-3091.1994.tb01434.x.

Parkinson, R. W. and Ogurcak, D. E. (2018) 'Beach nourishment is not a sustainable strategy to

mitigate climate change', *Estuarine, Coastal and Shelf Science*. Elsevier, 212(June), pp. 203–209. doi: 10.1016/j.ecss.2018.07.011.

Paul, M. J., Kamphuis, J. W. and Brebner, A. (1972) 'Similarity of Equilibrium Beach Profiles', in *Proceedings of the 13th Coastal Engineering Conference*, pp. 1217–1236.

Pellón, E., Garnier, R. and Medina, R. (2014) 'Intertidal finger bars at El Puntal, Bay of Santander, Spain: Observation and forcing analysis', *Earth Surface Dynamics*, 2(1), pp. 349–361. doi: 10.5194/esurf-2-349-2014.

Phillips, B. T., Brown, J. M. and Plater, A. J. (2020) 'Modeling impact of intertidal foreshore evolution on gravel barrier erosion and wave runup with xbeach-x', *Journal of Marine Science and Engineering*, 8(11), pp. 1–22. doi: 10.3390/jmse8110914.

Plater, A. J., Stupples, P. and Roberts, H. M. (2009) 'Evidence of episodic coastal change during the Late Holocene: The Dungeness barrier complex, SE England', *Geomorphology*. Elsevier B.V., 104(1–2), pp. 47–58. doi: 10.1016/j.geomorph.2008.05.014.

Poate, T. et al. (2013) 'High frequency in-situ field measurements of morphological response on a fine gravel beach during energetic wave conditions', *Marine Geology*. Elsevier B.V., 342, pp. 1–13. doi: 10.1016/j.margeo.2013.05.009.

Poate, T. G., McCall, R. T. and Masselink, G. (2016) 'A new parameterisation for runup on gravel beaches', *Coastal Engineering*. The Authors, 117, pp. 176–190. doi: 10.1016/j.coastaleng.2016.08.003.

Polidoro, A., Dornbusch, U. and Pullen, T. (2013) 'Improved maximum run-up formula for mixed beaches based on field data', in *Coasts, Marine Structures and Breakwaters: From Sea to Shore - Meeting the Challenges of the Sea*, pp. 389–398. doi: 10.1680/fsts.59757.0389.

Polska, L. *et al.* (2015) 'Bulletin of the Maritime Institute in Gdańsk Depth of closure in the multibar non-tidal nearshore zone of the Baltic Sea: Lubiatowo (Poland) case study Głębokość zamknięcia w wielorewowej bezpływowej strefie', (April 2016), pp. 180–188. doi: 10.5604/12307424.1185577.

Pontee, N. (2013) 'Defining coastal squeeze: A discussion', *Ocean and Coastal Management*, 84, pp. 204–207. doi: 10.1016/j.ocecoaman.2013.07.010.

Pontee, N. I. (2011) 'Reappraising coastal squeeze: A case study from North-West England', Proceedings of the Institution of Civil Engineers: Maritime Engineering, 164(3), pp. 127–138. doi: 10.1680/maen.2011.164.3.127.

Pontee, N. I., Pye, K. and Blott, S. J. (2004) 'Morphodynamic Behaviour and Sedimentary Variation of Mixed Sand and Gravel Beaches, Suffolk, UK', *Journal of Coastal Research*, 201, pp. 256–276. doi: 10.2112/1551-5036(2004)20[256:mbasvo]2.0.co;2.

Raman, H. and Earattupuzha, J. J. (1972) 'Equilibrium Conditions in Beach Wave Interaction', in *Proceedings of the 13th Coastal Engineering Conference*, pp. 1237–1256.

Ray, G. C. (1991) 'Coastal-zone biodiversity patterns.', *Bioscience*, 41, pp. 490–498.

Rector, R. L. (1954) Laboratory Study of Equilibrium Beach profiles, U.S. Army Corps of Engineers, Beach Erosion Board. Washington D.C.

Reniers, A. J. H. M. *et al.* (2013) 'Observations and modeling of steep-beach grain-size variability', *Journal of Geophysical Research: Oceans*, 118(2), pp. 577–591. doi: 10.1029/2012JC008073.

Ribas, F. et al. (2011) 'Modelling the formation of transverse sand bars: application to Duck beach, USA', *Proc. 7th IAHR Symposium on River, Coastal and Estuarine Morphodynamics*, (January 1994).

Ribas, F. et al. (2014) 'Observations and modeling of surf zone transverse finger bars at the Gold Coast, Australia', *Ocean Dynamics*, 64(8), pp. 1193–1207. doi: 10.1007/s10236-014-0719-4.

Ribas, F. *et al.* (2015) 'Understanding coastal morphodynamic patterns from depth-averaged sediment concentration', *Reviews of Geophysics*, 53(2), pp. 362–410. doi: 10.1002/2014RG000457.

Ribas, F., Falque, A. and Montoto, A. (2003) 'Nearshore oblique sand bars', *Journal of Geophysical Research*, 108, pp. 1–17. doi: 10.1029/2001JC000985.

Ribas, F. and Kroon, A. (2007) 'Characteristics and dynamics of surfzone transverse finger bars', Journal of Geophysical Research: Earth Surface, 112(3), pp. 1–13. doi: 10.1029/2006JF000685.

van Rijn, L. C. (1984) 'Sediment Transport, Part II: Suspended Load Transport', *Journal of Hydraulic Engineering*, 110, pp. 1613–1641.

van Rijn, L. C. (1993) *Principles of sediment transport in rivers, estuaries and coastal seas*. Amsterdam: Aqua publications.

van Rijn, L. C. and Sutherland, J. (2011) 'Erosion of Gravel Barriers and Beaches', in Coastal

Sediments, pp. 2019–2032. doi: 10.1142/9789814355537_0152.

Rijper, H. T. (2018) Morphological modelling of the gravel revetment on artificial composite beaches, MSc Thesis.

Roberts, T. M., Wang, P. and Puleo, J. A. (2013) 'Storm-driven cyclic beach morphodynamics of a mixed sand and gravel beach along the Mid-Atlantic Coast, USA', *Marine Geology*. Elsevier B.V., 346, pp. 403–421. doi: 10.1016/j.margeo.2013.08.001.

Robertson, W. V. *et al.* (2008) 'Hydrodynamic and geologic influence of event-dependent depth of closure along the South Florida Atlantic Coast', *Marine Geology*, 252(3–4), pp. 156–165. doi: 10.1016/j.margeo.2008.03.018.

Roelvink, D. *et al.* (2009) 'Modelling storm impacts on beaches, dunes and barrier islands', *Coastal Engineering*. Elsevier B.V., 56(11–12), pp. 1133–1152. doi: 10.1016/j.coastaleng.2009.08.006.

Roelvink, D. et al. (2010) XBeach model description and manual. Unesco-IHE Institute for Water Education, Deltares and Delft University of Technology.

Roelvink, D. J. A. (2015) 'XBeach Technical Reference: Kingsday Release XBeach Technical Reference: Kingsday Release Model description and reference guide to functionalities', (April). doi: 10.13140/RG.2.1.4025.6244.

Rosati, J. D. and Kraus, N. C. (1999) US Army Corps of Engineers Sediment Budget Analysis System (SBAS) Sediment Budget Analysis System. Coastal Engineering Technical Note IV-20.

Sallenger, J. (2000) 'Storm impact scale for barrier islands', *Journal of Coastal Research*, 16(3), pp. 890–895.

de Schipper, M. A. *et al.* (2021) 'Beach nourishment has complex implications for the future of sandy shores', *Nature Reviews Earth and Environment*. Springer US, 2(1), pp. 70–84. doi: 10.1038/s43017-020-00109-9.

Schupp, C. A., McNinch, J. E. and List, J. H. (2006) 'Nearshore shore-oblique bars, gravel outcrops, and their correlation to shoreline change', *Marine Geology*, 233(1–4), pp. 63–79. doi: 10.1016/j.margeo.2006.08.007.

She, K. et al. (2007) 'Recharge of mixed sand and gravel beaches', *Proceedings of the Coastal Engineering Conference*, pp. 4092–4102. doi: 10.1142/9789812709554_0344.

She, K., Horn, D. and Canning, P. (2006) 'Porosity and Hydraulic Conductivity of Mixed Sand-Gravel Sediment Key words Porosity versus Sand Percentage', pp. 1–16.

Shoreline Surveys Ltd (2021) J1877 - Data Collection Parameters.

Singh, U. K. and Ahmad, Z. (2019) 'Transport rate and bed profile computations for clay–silt–gravel mixture', *Environmental Earth Sciences*. Springer Berlin Heidelberg, 78(15), pp. 1–20. doi: 10.1007/s12665-019-8419-5.

Soloy, A. *et al.* (2024) 'Rapid Changes in Permeability: Numerical Investigation into Storm-Driven Pebble Beach Morphodynamics with XBeach-G', *Journal of Marine Science and Engineering*, 12(2). doi: 10.3390/jmse12020327.

Sonu, C. J. (1968) 'Collective Movement of Sediment in Littoral Environment', *Coastal Engineering*, 1, pp. 373–400. doi: 10.9753/icce.v11.24.

Soulsby, R. (1997) *Dynamics of Marine Sands*. London: Thomas Telford.

Soulsby, R., Sutherland, J. and Brampton, A. (1999) *Coastal Steepening - the UK view, Technical Report 91*.

Staudt, F. et al. (2021) 'The sustainability of beach nourishments: a review of nourishment and environmental monitoring practice', *Journal of Coastal Conservation*. Journal of Coastal Conservation, 25(2). doi: 10.1007/s11852-021-00801-y.

Sunamura, T. and Horikawa, T. (1974) 'Two-dimentsional Beach Changes due to Waves', in *Proceedings of the 14th Coastal Engineering Conference*, pp. 920–938.

Sutherland, J. and Thomas, I. (2011) 'The management of Pevensey shingle barrier', *Ocean and Coastal Management*, 54(12), pp. 919–929. doi: 10.1016/j.ocecoaman.2011.07.004.

Sutherland, J. and Wolf, J. (2002) Coastal Defence Vulnerability 2075. Report SR 590.

Swift, D. J. P. et al. (1978) 'Shoreface-connected sand ridges on American and European shelves: A comparison', *Estuarine and Coastal Marine Science*, 7(3), pp. 257–273. doi: 10.1016/0302-3524(78)90109-3.

Szczyrba, L. et al. (2023) 'Morphodynamic link between shore-oblique bars and erosional hotspots', in *Coastal Sediments*, pp. 1907–1922. doi: https://doi.org/10.1142/9789811275135_0175.

Taylor, J. A., Murdock, A. P. and Pontee, N. I. (2004) 'A macroscale analysis of coastal

steepening around the coast of England and Wales', *Geographical Journal*, 170(3), pp. 179–188. doi: 10.1111/j.0016-7398.2004.00119.x.

Thieler, R. E. *et al.* (2001) 'Modern sedimentation on the shoreface and inner continental shelf at wrightsville beach, North Carolina, U.S.A', *Journal of Sedimentary Research*, 71(6), pp. 958–970. doi: 10.1306/032101710958.

Thomas, I. (2015) 'Long-term loss of beach material from the Eastern English Channel', Proceedings of the Institution of Civil Engineers: Maritime Engineering, 168(4), pp. 174–181. doi: 10.1680/jmaen.15.00025.

Touboul, J., Morales-Marquez, V. and Belibassakis, K. (2024) 'A Weakly Nonlinear System for Waves and Sheared Currents over Variable Bathymetry', *Journal of Marine Science and Engineering*, 12(3). doi: 10.3390/jmse12030509.

Townsend, D. *et al.* (2023) 'Linking nearshore morphological change to long term observed sand loss from a mixed sediment beach', in *EGU General Assembly*. Vienna. doi: https://doi.org/10.5194/egusphere-egu23-8572.

Townsend, D. *et al.* (2024) 'Exploring nearshore bed dynamics of a mixed beach using the depth of closure conceptual model', *Geomorphology*. Elsevier B.V., 454(March), p. 109150. doi: 10.1016/j.geomorph.2024.109150.

Tyhurst, M. F. (1972) 'Eastbourne's sea defences', J. Soc. Cov. Eng. Tech, 2, pp. 3-8.

Udo, K., Ranasinghe, R. and Takeda, Y. (2020) 'An assessment of measured and computed depth of closure around Japan', *Scientific Reports*, 10(1), pp. 1–8. doi: 10.1038/s41598-020-59718-5.

USACE (1984) *Shore Protection Manual*. Vicksburg, USA. Available at: https://luk.staff.ugm.ac.id/USACE/USACE-ShoreProtectionManual1.pdf.

USACE (1998) 'Part III Coastal Processes, Chapter 1 Coastal Sediment Properties', in *Coastal Engineering Manual*. Washington DC: Usace, pp. 1–499.

Valiente, N. G. *et al.* (2017) 'Depth of Closure Along an Embayed , Macro-Tidal and Exposed Coast : a Multi-Criteria Approach', *Coastal Dynamics*, (June).

Valiente, N. G. *et al.* (2019) 'Role of waves and tides on depth of closure and potential for headland bypassing', *Marine Geology*. Elsevier, 407(June 2018), pp. 60–75. doi: 10.1016/j.margeo.2018.10.009.

Vitousek, S. et al. (2017) 'Doubling of coastal flooding frequency within decades due to sea-level rise', *Scientific Reports*, 7(1), pp. 1–9. doi: 10.1038/s41598-017-01362-7.

Wahl, T. *et al.* (2017) 'Understanding extreme sea levels for broad-scale coastal impact and adaptation analysis', *Nature Communications*. Nature Publishing Group, 8(May), pp. 1–12. doi: 10.1038/ncomms16075.

Walmsley, C. A. and Davy, A. J. (1997) 'The Restoration of Coastal Shingle Vegetation: Effects of Substrate Composition on the Establishment of Seedlings', *Journal of Applied Ecology*, 34(1), pp. 143–153.

Watt, T. et al. (2006) 'Surface sediment distribution patterns on mixed beaches in response to wave conditions', Coastal Dynamics 2005 - Proceedings of the Fifth Coastal Dynamics International Conference, 40855(August 2018). doi: 10.1061/40855(214)17.

Watt, T. et al. (2008) 'Patterns of surface sediment grain size distribution under the influence of varying wave conditions on a mixed sediment beach at Pevensey Bay, southeast England', *Zeitschrift fur Geomorphologie*, 52(SUPPL. 3), pp. 63–77. doi: 10.1127/0372-8854/2008/0052S3-0063.

Weggel, J. R. (1972) 'Maximum Breaker Height', *Journal of the Waterways, Harbors and Coastal Engineering Division*, 98(WW4).

Williams, A. M. and Shaw, G. (2009) 'Future play: tourism, recreation and land use', *Land Use Policy*, 26(SUPPL. 1), pp. 326–335. doi: 10.1016/j.landusepol.2009.10.003.

Woodruff, J. D. *et al.* (2021) 'Grain size and beach face slope on paraglacial beaches of New England, USA', *Marine Geology*. Elsevier B.V., 438(September 2020), p. 106527. doi: 10.1016/j.margeo.2021.106527.

Zarkogiannis, S. D. *et al.* (2018) 'Scarping of artificially-nourished mixed sand and gravel beaches: Sedimentological characteristics of Hayling Island beach, Southern England', *Coastal Engineering*. Elsevier Ltd, 133(September 2017), pp. 1–12. doi: 10.1016/j.coastaleng.2017.12.003.